

STUDY OF THE CORROSION RESISTANCE OF BENCHMARK COATINGS
USING ELECTROCHEMICAL IMPEDANCE SPECTROSCOPY

A Thesis

by

SAFWAN GHANNAM

Submitted to the Office of Graduate and Professional Studies of
Texas A&M University
in partial fulfillment of the requirements for the degree of

MASTER OF SCIENCE

Chair of Committee,
Co-Chair of Committee,
Committee Member,
Head of Department,

Ahmed Abdel-Wahab
Luc Véhot
Hussein Alnuweiri
Patrick Linke

May 2015

Major Subject: Chemical Engineering

Copyright 2015 Safwan Ghannam

ABSTRACT

The corrosion resistance of polymer-coated carbon steel exposed to corrosive environment of 3.5% NaCl solution (weight fraction) at ambient conditions was evaluated using electrochemical impedance spectroscopy (EIS) technique. The analysis of impedance models involved using suitable electrical equivalent circuit that consists of passive electrical components. The impedance results suggested that there were two types of impedance models are applicable to the tested samples, one for intact coating and the other one for damaged or non-existent coating.

Results of laboratory experiments indicated that water uptake for the intact coating was negligible and that polarization resistance was very high of orders higher than $10^{11} \Omega \text{ cm}^2$ which indicates excellent corrosion protection. The obtained values also indicated that the corrosion resistance depends on the coating thickness. On the other hand, for the damaged coatings and non-coated metal, impedance models suggested the existence of a Warburg element referring to the metal diffusion and lower polarization resistance of orders lower than $10^7 \Omega \text{ cm}^2$ which indicates that corrosion reactions took place. This conclusion was confirmed using microscopic observation of corrosion products and change in defect depth using 3D profile surface analysis. Experimental results for damaged coating indicated that the depth of the defect influences the corrosion rate but all damaged coatings follow the same impedance model.

DEDICATION

To my family

ACKNOWLEDGEMENTS

I am extremely grateful to my previous advisor, Dr. Bruce Palmer, for his continuous support and guidance throughout the course of this research. I would like to thank Dr. Ahmed Abdel-Wahab, my current advisor, for supervising my research work. I would like to acknowledge my committee members: Dr. Luc Véchet and Dr. Hussein Alnuweiri for their valuable advice and support. I would like to recognize Dr. Walid Khalfaoui and Mr. Nasser Al Jassem for sharing their experience and knowledge in this field. I would like to extend my gratitude to Dr. Barbara haw from Penn State University for collaborating with our team. I am also thankful to Texas A&M University at Qatar for supporting me in pursuing my Master degree. Finally, thanks to my parents for their encouragement.

NOMENCLATURE

A	exposed specimen area, cm^2
A_a	Anodic site area, cm^2
A_c	Cathodic site area, cm^2
B	Stern-Geary constant, V
ba	Slope of the anodic Tafel reaction, when plotted on base 10 logarithmic scale
bc	Slope of the cathodic Tafel reaction when plotted on base 10 logarithmic scale
C	Coating capacitance, μF
C_0	Capacitance at $t=0$, μF
C_{eff}	Effective capacitance, μF
C_{dl}	electric double-layer capacitance, μF
C_f	film (coating) capacitance, μF
CR	Penetration rate, mm/yr
C_t	Capacitance at an instant 't', μF
d	Coating thickness, μm
E	Difference in current for the general case, V
E'	Difference in potential when no current is passing the interface, V
E''	Difference in potential when corrosion current is passing the interface, V
\bar{f}_i	the mass fraction of the i^{th} element in the alloy
I	Current, μA
i	Current density at cathode site, $\mu\text{A}/\text{cm}^2$
I_a	Anodic current (equal to corrosion current), μA
i_a	Current density at anode site, $\mu\text{A}/\text{cm}^2$
I_c	Cathodic current (equal to corrosion current), μA

i_{cor}	Corrosion current density, $\mu\text{A}/\text{cm}^2$
I_{cor}	Total anodic current, μA
I_{corr}	Corrosion current, μA
K_1	3.27×10^{-3} , $\text{mm.g}/\mu\text{A cm yr}$
K_2	8.954×10^{-3} , $\text{g cm}^2/\mu\text{A m}^2 \text{ d}$
m	Amount of material deposited, g
M	Metal
MR	Mass loss rate, $\text{g}/\text{m}^2 \text{ d}$
n	Charge number of the electrochemical cell reaction
n_i	the valence of the i^{th} element of the alloy
Q	Amount of charge consumed during the transformation, C
R_M	Metal path resistance, Ω
R_p	Polarization resistance, $\Omega \text{ cm}^2$
R_s	solution resistance, Ω
R_f	film (coating) resistance, Ω
S	Solution phase
t	duration of the electrolysis, s
W	the atomic weight of the element, g/mol
W_i	the atomic weight of the i^{th} element in the alloy, g/mol
Y_o	Capacitance, μF
ω	Frequency, Hz
α	Exponent equals to 1 for a capacitor
ΔG_f^0	Standard Gibbs free energy of formation, J
$\Delta G_{\text{react}}^0$	Change in the Gibbs free energy, J
ϵ_0	Dielectric constant in vacuum ($8.8542 \times 10^{-12} \text{ F/m}$)
ϵ_r	Material dependent relative permittivity

ϵ_w	Dielectric constant of water
$\eta(i)$	Shift in potential resulting from the current density, V
ϕ	Water volume fraction
ϕ_a	Electric potential at the cathodic site, V
ϕ_c	Electric potential at the anodic site, V

TABLE OF CONTENTS

	Page
ABSTRACT	ii
DEDICATION	iii
ACKNOWLEDGEMENTS	iv
NOMENCLATURE.....	v
TABLE OF CONTENTS	viii
LIST OF FIGURES.....	x
LIST OF TABLES	xiii
1 INTRODUCTION	1
2 BACKGROUND	3
2.1 Corrosion	3
2.2 Metal corrosion	5
2.3 Protection methods	10
2.4 Polymer coating	12
2.5 Electrochemical testing	13
3 STUDIES OF COATING SYSTEMS USING EIS	18
3.1 EIS study of self-healing coatings	18
3.2 EIS study of corrosion behavior of organic coating/Dacromet composite systems	20
3.3 EIS study of corrosion behavior of organic coatings with zirconia films	21
3.4 EIS study of NiTi coating on AISI 1045 Steel	23
3.5 EIS study of PPE coating corrosion resistance	24
3.6 EIS study of polymer coating degradation.....	25
4 METHODOLOGY.....	27
4.1 Step 1: Material identification.....	31
4.2 Step 2: Samples preparation.....	32
4.3 Step 3: Samples characterization	34
4.4 Step 4: Experimental setup and cell design.....	36
4.5 Step 5: EIS results analysis	42
5 RESULTS	43
5.1 Intact coating behavior.....	43
5.2 Damaged coating behavior	55
6 CONCLUSION.....	65

	Page
7 FUTURE WORK.....	66
REFERENCES.....	67
APPENDIX.....	70

LIST OF FIGURES

	Page
Figure 2-1: The corrosion cycle of steel ⁵	5
Figure 2-2: The elementary electrochemical corrosion circuit ²	7
Figure 2-3: Uniform corrosion ² a- in acidic solution b-neutral or alkaline solution.....	10
Figure 2-4: The potentiostatic circuit ²	14
Figure 3-1: Nyquist plots of scratched specimens of coated substrate ⁹	19
Figure 3-2: Bode plots of Dacromated carbon steel after immersion in 3.5 wt. % NaCl solution for different times ²⁰	20
Figure 3-3: Impedance plots of different pretreatments after 2 h of immersion in a 0.3 wt. % Na ₂ SO ₄ solution ²¹	22
Figure 3-4: Simplified equivalent electrical circuit and Nyquist and Bode plots for defected coating ²¹	23
Figure 3-5: Equivalent circuit for AISI steel coated with intermetallic coating. a- after 1 h immersion, b- longer than 1 day immersion ²²	24
Figure 3-6: Nyquist spectra of PPE coating in period of immersion in 3.5 wt. % NaCl solution ²³	25
Figure 3-7: Cell for EIS measurements ⁸	26
Figure 3-8: Equivalent circuits for coating substrate systems. (a) non-deteriorated polymer-coated steel; (b) deteriorated-polymer-coated steel ⁸	26
Figure 4-1: Example of Randles circuit for the corrosion behavior of the polymer coated metal ²⁶	28
Figure 4-2: Relationship between circuit model, physical coating and corrosion properties ²⁶	28
Figure 4-3: EIS data-presentation formats ²⁴	29
Figure 4-4: Nyquist plots with Warburg impedance ³⁰	30
Figure 4-5: Photo of the sample in the tribometer (left) and schematic of the test (right)	33
Figure 4-6: Working electrode	34
Figure 4-7: ZeGage profiler ³¹	35
Figure 4-8: Optical profiler basics ³¹	36
Figure 4-9: Corrosion cell connected to Gamry potentiostat.....	38

	Page
Figure 4-10: Corrosion cell	40
Figure 4-11: Technical sketch of designed corrosion cell (unit is mm)	41
Figure 5-1: Legend for studied samples	43
Figure 5-2: 'A Alpha' before exposure	44
Figure 5-3: 'A Alpha' after exposure	44
Figure 5-4: 3D profile of 'A Alpha' before exposure	45
Figure 5-5: 3D profile of 'A Alpha' after exposure	45
Figure 5-6: 'A Alpha' - Bode plot continuous exposure over 88 days.....	46
Figure 5-7: 'A Alpha' -Nyquist plot for continuous exposure over 88 days	47
Figure 5-8: Circuit 'A'	48
Figure 5-9: Bode plot after 65 days of exposure fitted using circuit 'A'	49
Figure 5-10: Nyquist plot after 65 days of exposure fitted using circuit 'A'	49
Figure 5-11: Time dependence of resistance R_p for 'A Alpha'	51
Figure 5-12: Time dependence of relative permittivity ϵ_r for 'A Alpha'	52
Figure 5-13: Thickness dependence of polarization resistance for the different types of coating	53
Figure 5-14: 3D profile of 'C Beta'	54
Figure 5-15: 'C Beta' before exposure	54
Figure 5-16: 'C Beta' after exposure	54
Figure 5-17: 'A Gamma' before exposure	55
Figure 5-18: 'A Gamma' after exposure before cleaning.....	55
Figure 5-19: 'A Gamma' after exposure after cleaning	56
Figure 5-20: 3D profile of 'A Gamma' before exposure	57
Figure 5-21: 3D profile of 'A Gamma' after exposure.....	57
Figure 5-22: 'A Gamma' - Bode plot continuous exposure over 75 days	59
Figure 5-23: 'A Gamma' - Nyquist plot continuous exposure over 75 days	60

	Page
Figure 5-24: 'A Gamma' - Nyquist plot continuous exposure over 60 days (after the 15th day)	61
Figure 5-25: Bode plot after 83 days of exposure fitted using circuit 'B'	62
Figure 5-26: Nyquist plot after 63 days of exposure fitted using circuit 'B'	62
Figure 5-27: Time dependence of resistance R_p for 'A Gamma'	63
Figure 5-28: Circuit 'B'	63
Figure 5-29: Average polarization resistance for all the tested samples	64

LIST OF TABLES

	Page
Table 4-1: Chemical composition of the substrate	31
Table 4-2: Samples obtained from Penn State	31
Table 4-3: Defect type and applied force parameters	33
Table 4-4: Corrosion cell parts	39
Table 4-5: Open circuit potential test parameters	42
Table 4-6: Electrochemical impedance spectroscopy test parameters	42
Table 5-1: Kinetic parameters for ‘A Alpha’ over 88 days	50
Table 5-2: Results for intact samples	52

1 INTRODUCTION

The state of Qatar's economy is highly dependent on its natural gas production. The Qatar North Gas Field is considered to be the largest gas field in the world. The gas extracted from the North Field contains impurities such as carbon dioxide, hydrogen sulfide and chlorides. These impurities induce corrosion in pipelines.

Low cost carbon steels are considered as the main construction material used in oil and gas production and in transportation pipelines. This material is very susceptible to corrosion in aggressive environments in the presence of carbon dioxide and chlorides. This corrosive behavior is causing multiple failures in gas pipelines and plant equipment.¹ It is essential that the materials used in the oil and gas production facilities have the ability to endure the corrosive nature of the extracted gas. The substrate used in gas pipelines can be protected from material degradation resulting from corrosion by covering it with an appropriate coating. The use of coatings is considered an economical alternative since it will allow the use of low-cost substrates instead of high cost corrosion resistant alloys.

This solution is being applied in several Arabian Gulf countries in the oil and gas industry. The coating application is therefore common in the region which creates a suitable ground for research and development. Developing a coating that has a high corrosion resistance to Qatari oil and gas environment can extend the use of economical carbon steel materials and therefore support the oil and gas industry.

This research work is a first phase of the NPRP project "Development of New Multifunctional Coatings for Protection against Erosion and Corrosion in Qatar oil and Gas Production". The overall objective is to develop new materials that can simultaneously provide corrosion protection and erosion resistance in the extreme environment of gas pipeline. Developing such coatings will provide a longer time span for the pipeline with a lower cost. This research project is a collaboration between Texas A&M University at Qatar (TAMUQ) Chemical Engineering Program and The Pennsylvania State University's (PSU) Engineering Science and Mechanics Department.

The first step was to study the corrosion protection behavior of benchmark coatings in 3.5 wt. % NaCl solution to provide a basis for optimizing a competitive coating designed for oil and gas transportation in this region. To conduct this study, the different corrosion monitoring methods were investigated such as weight loss and electrochemical methods. Electrochemical Impedance Spectroscopy (EIS) was found to be the most adequate method for this application. It is widely used to study the corrosion behavior of coated metals since it allows a continuous monitoring of the corrosion process without experiment interruption. EIS generates impedance values that can be used to determine an equivalent circuit to the corrosion cell, which gives an understanding about the corrosion rate and mechanism. The commercial coatings were selected by the PSU team. Steel samples were coated with two different polymer coatings by NOV Tuboscope that are designed to withstand an environment similar to the one in the pipelines used for gas transportation in Qatar. An experimental setup was established that complies with the International Organization for Standardization (ISO) and the American Society for Testing and Materials (ASTM) guidelines and regulations.

2 BACKGROUND

2.1 Corrosion

Corrosion can be defined as the deterioration of materials due to reactions with their environment. These materials can be metals, polymers or ceramics. The environmental factors include pressure, temperature and pH. The transport process of atoms, molecules or ions is the basic mechanism of corrosion. This transport process takes place on the surface of the materials. The corrosion process usually follows a number of steps and the overall rate of the reaction is controlled by the slowest step which makes it the main studied step to determine the kinetics of corrosion.²

The changes can be monitored by examining the change in weight or dimensions, the formation of corrosion products and the changes that take place on the surface by conducting optical or electron microscopy. Changes in mechanical or physical properties such as hardness and shear stress also present valuable indicators.²

In the case of electrochemical corrosion, electrical potential and current can be used to investigate the corrosion mechanism. However, electrochemical corrosion only occurs in an environment that allows the transport of ions such as aqueous solution. In this case, atoms at the metal surface diffuse into the solution as metal ions while the electrons migrate to a site where they are consumed by other species that are in contact with the metal in order to sustain the reaction. In other cases, the released metal ions can form complex ions or combine with other species present in the solution to form compounds such as hydroxides, oxides or sulfides that will precipitate. Metals can also corrode in gases at high temperature, such corrosion is caused by oxygen that forms oxides. Electrochemical corrosion is generally absent in polymers and ceramics since these materials do not support electron conduction which limits the corrosion mechanism to chemical and physical.²

2.1.1 Economic impact

Corrosion has a great impact on the economy. Costs associated with corrosion are estimated to reach around 4% of the Gross National Product (GNP).³ This cost depends on many variables including:

- Direct losses by replacing the corroded materials and equipment
- Indirect losses including the cost of repairing damaged equipment and losses due to delays in production
- Corrosion protection cost due to the use of expensive corrosion-resistant materials or applying corrosion protection techniques
- Corrosion prevention cost due to maintenance and inspections

It is worth mentioning that the indirect costs usually exceed the direct cost. The cost of replacing a corroded equipment can be much higher than the cost of the equipment itself. For example, the replacement of a corroded heat exchanger in a nuclear power plant will cause lost production time which brings the total cost to a figure much higher than the cost of the heat exchanger itself.²

2.1.2 Safety concerns

Corrosion is considered one of the major causes of failures of processing facilities in the oil and gas industry. The main material used in offshore processes is carbon steel. Therefore, all offshore equipment are at risk from corrosion. In case of a corrosion related failure, hydrocarbon release is a major concern. This will lead not only to production losses but also to maintenance and repair costs. This is one of the main reasons that make management corrosion not only a safety concern but also an environmental and economic matter.

In 1999, The Offshore Safety Division of the Health and Safety Executive (HSE) conducted a study that deals with the development of high level risk based corrosion strategy for offshore processing facilities. This project determined the basic corrosion risk management and assessment approach required when dealing with oil field production and transportation equipment. The following is a developed comprehensive pack that was proposed after conducting the study:⁴

- Corrosion Management and Risk Assessment of Offshore Processing for Offshore Facilities guideline
- Oil Industry Corrosion Management
- Corrosion Risk Assessment
- Health and Safety Verification and Corrosion Management for Offshore Processing

2.2 Metal corrosion

During the corrosion process, metals tend to return to the lowest energy state. In the case of iron and steel, hydrated iron oxides which are similar to the original iron ore present the lowest possible energy state. Figure 2-1 illustrates the corrosion cycle of steel.

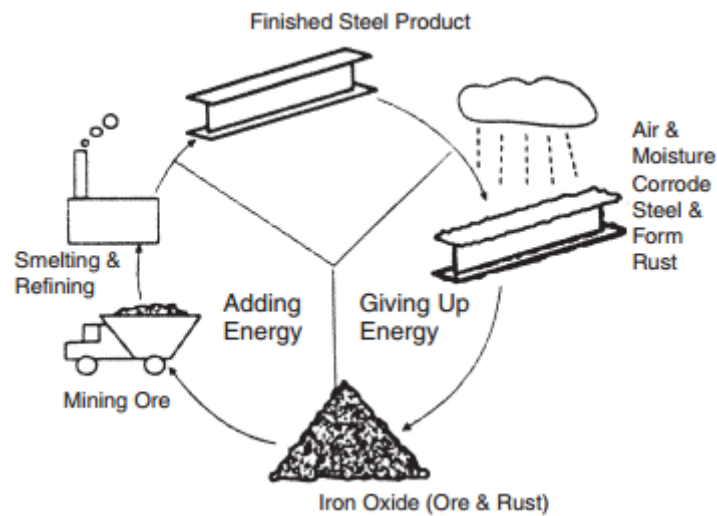


Figure 2-1: The corrosion cycle of steel⁵

In most cases, the corrosion of a metal results from the irreversible oxidation-reduction (redox) reaction taking place between a metal and an oxidizing agent.⁶

metal+ oxidizing agent → oxidized metal+ reducing agent

Equation 2-1

Different types of oxidizing agents exist. Corrosion taking place in aqueous solution can result from the following oxidizing agents:

- Solvated protons
- Dissolved oxygen
- Oxidizing metal cations: Cu^{2+} , Fe^{3+} ,
- Oxidizing anions: NO_2^- , NO_3^- , MnO_4^-
- Dissolved oxidizing gases: ozone (O_3), chlorine (Cl_2), Sulfur trioxide (SO_3)

Oxidizing agents also exist in dry conditions, at high temperatures. These agents include:

- Gaseous oxygen
- Carbon dioxide
- Water vapor
- Compounds containing sulfur: S_2 , SO_2

The corrosion reaction can be described as the transfer of metal atoms from the surface to the solution as metal ions with the release of electrons.²



During this process, the metal undergoes an oxidation reaction since the metal loses electrons, making the site where the metal was lost the anodic reaction site. The electrons are transferred through the metal, due to its conductivity, and are consumed by another reaction.²



A reduction reaction takes place at the site where the electrons are consumed making it the cathodic reaction site. The distance separating these two process can vary from few angstroms to hundreds of meters.² For example, in an aerated acid solution, iron corrodes following these reactions:



For the corrosion to actually occur, the change in the Gibbs free-energy has to be negative.² The change in the Gibbs free energy can be determined using the following equation:

$$\Delta G_{\text{react}}^0 = \sum \Delta G_f^0(\text{products}) - \sum \Delta G_f^0(\text{reactants}) \quad \text{Equation 2-7}$$

Aqueous corrosion can be represented as an electrochemical cell with two half cells as shown in Figure 2-2.

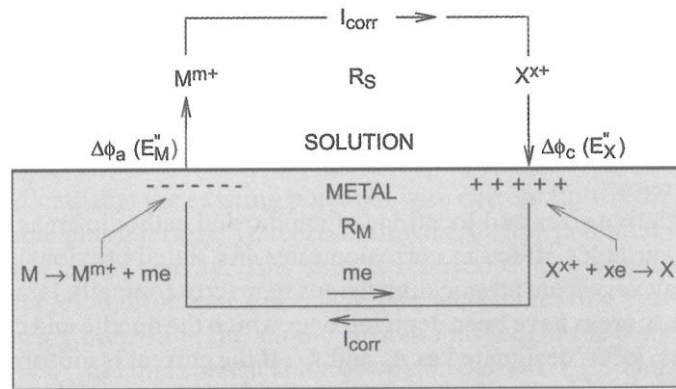


Figure 2-2: The elementary electrochemical corrosion circuit²

When compared to a battery, the electrolyte in contact with the corroding metal presents the battery fluid and the metallic path connecting the anodic site and the cathodic site presents the external circuit. Due to the ions transfer, differences in electrical potential (ϕ_a , ϕ_c) are developed between the metal (M) and solution (S) at both sites. These difference can be determined as follows:

$$\Delta \phi_a = \phi_{M,a} - \phi_{S,a} \quad \text{Equation 2-8}$$

$$\Delta \phi_c = \phi_{M,c} - \phi_{S,c} \quad \text{Equation 2-9}$$

Electrons flow from the anodic site to the cathodic site in the metal as the current flows in the opposite direction. Contrary, the current flows from the anodic to the cathodic site in the solution as explained in Figure 2-2. The corrosion current is as follows:

$$I_{\text{corr}} = (E''_X - E''_M) / (R_S + R_M) \quad \text{Equation 2-10}$$

For a known anode area and corrosion current the corrosion penetration rate can be determined. The corrosion also depends on the overall resistance. As the resistance increases, the corrosion current decreases and corrosion rate decreases. The total circuit resistance includes the solution resistance, metal path resistance and the resistance of the interface separating the anode from the solution (corrosion products or coatings for example).

Another important factors for the corrosion rate are sizes and location of the anode and cathode. For a given corrosion current that is uniformly distributed over these areas, the current densities can be determined.

$$i_a = I_a / A_a \quad \text{Equation 2-11}$$

$$i_c = I_c / A_c \quad \text{Equation 2-12}$$

The current density is considered an important parameter for two reasons. First, both the corrosion intensity and the corrosion penetration rate, are directly related to the anodic current density by following Faraday's law. The corrosion intensity is the mass loss per unit time per unit area and the corrosion penetration rate is the linear dimension loss per unit time. Second, it was determined that the interface potentials, E , are functions of the current density and given as follows:

$$E_X(i_c) = E'_X + \eta_X(i_c) = E'_X + \eta_X\left(\frac{I_c}{A_c}\right) \quad \text{Equation 2-13}$$

$$E_M(i_a) = E'_M + \eta_M(i_a) = E'_M + \eta_M\left(\frac{I_a}{A_a}\right) \quad \text{Equation 2-14}$$

When no current is passing the interface, the difference in potential will be equal the one for general case, i.e. E_X and E_M will be equal to E'_X and E'_M respectively, giving the potential difference across the interfaces at equilibrium. These potential present the equilibrium half-cell potentials.

The shift in potential from the current density presents the overpotential and is directly proportional to the current density.

When corrosion reaction is taking place, the cathodic current and anodic current must be equal to the corrosion current which is given by:

$$I_{\text{corr}} = \frac{E''_X - E''_M}{R_{\text{total}}} = \frac{\left[E'_X + \eta_X \left(\frac{I_{\text{corr}}}{A_c} \right) \right] - \left[E'_M + \eta_M \left(\frac{I_{\text{corr}}}{A_a} \right) \right]}{R_{\text{total}}} \quad \text{Equation 2-15}$$

The corrosion current presents the total loss of metal from the anodic site, and the corrosion current density is a presentation of the corrosion intensity which can be used to determine the corrosion penetration rate.

Faraday's law of electrolysis is used to precise magnitudes of electrolytic effect. The first law states that the amount of material dissolved or deposited during electrolysis is proportional to the electric charge that passed through. The second law states that the amounts of different materials dissolved or deposited due to the passage of the electric charge are proportional to their equivalent weight.³

The corrosion reaction for metals, with thermodynamic instability in water, can be presented as follows:



The corrosion reaction depends on the acidity of the solution. In an acidic solution, the metal reacts with hydrogen ions. As the pH increases, the metal starts reacting with water molecules when reaching neutral and basic conditions. Hydrogen gas is produced with the formation of metallic ions of valence m. Two processes occur in the corrosion reaction. The first is the formation of metallic ions from the metal and the second is the hydrogen gas production as illustrated in Figure 2-3.²

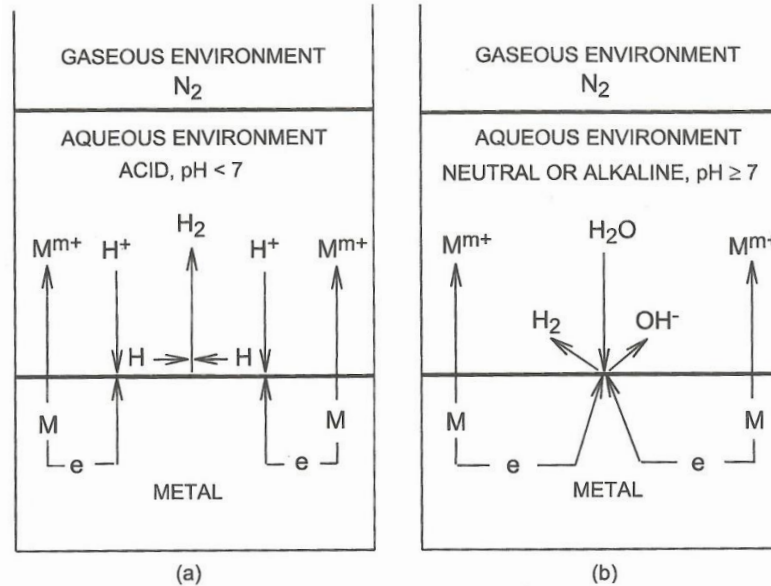


Figure 2-3: Uniform corrosion²
a- in acidic solution b-neutral or alkaline solution

The two processes takes place on separate sites of on the metal surface due to the metal conductivity, allowing the electrons transfer. Uniform corrosion occurs when the tow processes take place at a small distance, few atoms diameters, along with the change in the site location creating a uniform corrosion.

In the case of corrosion product formation, the corrosion mechanism follows s different path. For example, the rusting of iron in an aerated acidic solution with a pH greater than 4, two layers form. The first is a black layer containing Fe_3O_4 and $Fe(OH)_2$. The second is a red layer containing Fe_2O_3 or $FeOOH$. The formation of these layers introduce a barrier that influences the corrosion rate.²

2.3 Protection methods

Several protection methods are used to reduce corrosion and ensure durability for the material. The primary methods are summarized below.

2.3.1 *Material selection*

Metals and alloys have different corrosion behavior and their corrosion resistant varies from high for noble metals like gold to low for active metals like magnesium. The selection of the right material highly depends on the process environment, and the more economical metal or alloy is chosen depending on these factors.

2.3.2 *Coatings*

Two different types of coatings are usually used for corrosion protection: metallic and nonmetallic. Both types aim to isolate the substrate from the corrosive environment. Metallic coating uses more noble metal which have a higher corrosive resistance to protect the underlying metal, an example of that is tin-plated steel. Nonmetallic coatings also aims to isolate the substrate by forming a barrier between the metal and the environment.

2.3.3 *Inhibitors*

In several process, additives that function as corrosion inhibitors are added to the stream to protect the material from corroding. Different chemical species can be used as inhibitors such chromates, silicates and amines. Some inhibitors function by promoting the formation of protective films on the surface of the metal while other inhibitors are absorbed on the anodic and cathodic sites and hinders the corrosion current such as amines. Inhibitors are usually used in closed systems to maintain a stable concentration. They also can be incorporated in the coating or the primer that enhances the protection of the substrate in the case of defects.

2.3.4 *Cathodic protection*

Cathodic protection functions by forcing the current to flow to the structure that needs protection. This is achieved by either using a power source that forces the current to flow from the inert anode to the protected cathode or by the use of the sacrificial anode system in which a an active metal with a lower corrosion resistance in connected to the structure.

2.3.5 Design

Corrosion issues can be avoided by implementing a rational design that minimizes the possibility of corrosion or reduces the maintenance and repair costs. For example, during the design process, eliminating location where corrosion is favorable such as crevices will help reducing the corrosion effect. Furthermore, anticipating corrosion effects and providing an easy access for maintenance and repair will help reducing the cost.

2.4 Polymer coating

Phenolic resins are synthetic polymers that were first developed from thermosetting polymers. Today, they have several industrial applications including automotive, computing and building. The phenolic resin is produced through the condensation of a phenol with an aldehyde producing water as a by-product. Phenolic resin can be classified as novolac resins or resol resin.

The efficiency of polymer coatings against corrosion depends on two factors. The first is the intrinsic chemical stability of the polymer in a certain environment. The second is the absence of defects that can lead to the exposure of the metal surface to the corrosive environment.⁶ There are different types of organic coatings that provide corrosion protection.

Organic coatings are considered an important corrosion protection method for various reasons. Other than impeding corrodent ingress, this type of coating limits the electric transport between the anodic and cathodic sites on the metal surface.⁷

Polymer coatings are usually used as a barrier that protects the substrate metal from corrosion by separating it from the surrounding corrosion environment and isolating it from several factors such as UV light, temperature and humidity.⁸ Organic coatings with a high resistive protection characteristics have a high electrochemical impedance. For this kind of surfaces, Electrochemical Impedance Spectroscopy is the most suitable method to study the degradation of such material and determine the corrosion behavior of the underlying metal.⁷

One of the challenges that polymer coating has is the introduction of a defect through a mechanical damage. When a defect penetrates the coating and reaches the surface, the metal becomes vulnerable to

corrosive attacks. This problem can be solved through developing a coating with the ability to self-heal that allows the damaged area to be automatically repaired with the help of chemical components existent in the coating itself.⁹

2.5 Electrochemical testing

Electrochemical impedance spectroscopy present a new and promising method to study corrosion rates and behaviors. A potentiostatic circuit, shown in Figure 2-4, is used to perform these studies. It consists of:

- A working electrode (WE) which presents the studied corrosion sample,
- An auxiliary electrode (AE), also referred as the counter electrode. The counter electrode should be able to support oxidation and reduction reactions without undergoing corrosion to avoid electrolyte contamination. High density graphite or platinum are usually used as counter electrodes.
- A reference electrode is (RE) with a constant electrode potential is used to measure the potential of the working electrode.
- A potentiostat is used to maintain constant WE potential relative to the RE even with the change of the external circuit current. The potentiostat is a power supply with a rapid response direct-current (DC).

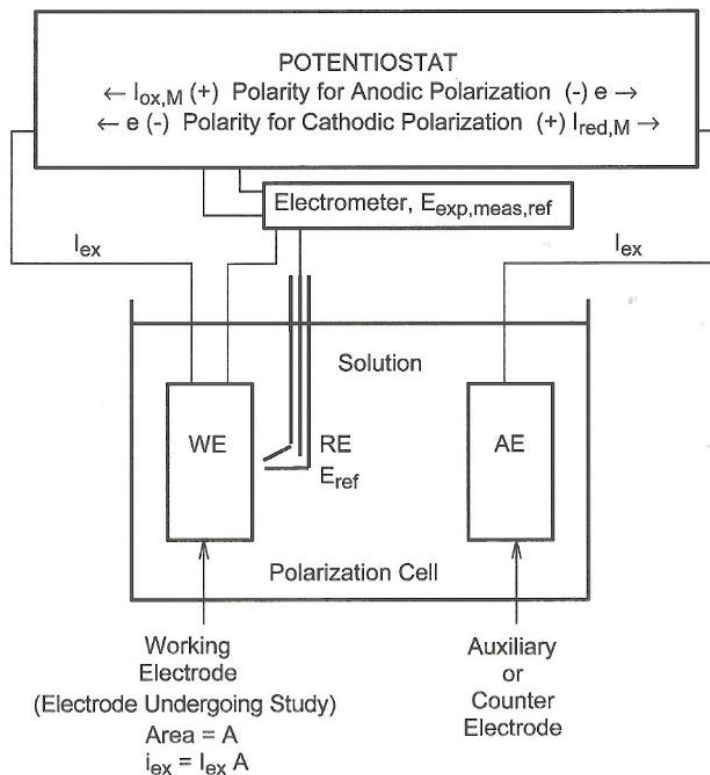


Figure 2-4: The potentiostatic circuit²

Measurements of alternating current (AC) impedance over a range of frequencies is the basis of the electrochemical impedance spectroscopy which is used to study the corrosion rate. Calculation of corrosion rates using electrochemical rate measurements are based on Faraday's electrolysis laws. The first law states that the amount of material deposited or evolved (m) during electrolysis is directly proportional to the current (I) and the time (t) which presents the quantity of electricity (Q) that passes through the solution. The second law states that the amount of the product depends on the equivalent mass of the substance electrolyzed. These laws are based on the conservation laws of matter and charge.¹⁰

$$m = \frac{MQ}{nF} = \frac{Mit}{nF}$$

Equation 2-18

2.5.1 Current density

The current density is obtained by dividing the total current by the exposed area of the electrode, assuming that the current is uniformly distributed across the area as shown in the equation below:

$$i_{\text{corr}} = \frac{I_{\text{corr}}}{A} \quad \text{Equation 2-19}$$

2.5.2 Equivalent weight

The equivalent weight can be defined as the mass of the metal that will be oxidized by the passage of one Faraday of electric charge. For alloys, the equivalent weight is obtained by the following equation:¹¹

$$EW = \frac{W}{n} \quad \text{Equation 2-20}$$

For pure elements, the equivalent weight is obtained by the following equation:¹¹

$$EW = \frac{1}{\sum \frac{n_i f_i}{W_i}} \quad \text{Equation 2-21}$$

2.5.3 Calculation of corrosion rate

Based on Faraday's law, the corrosion rate can be determined either in terms of penetration rate (CR) or mass loss rate (MR). Assuming a uniform corrosion, the rates can be calculated using the following equations:¹¹

$$CR = K_1 \frac{i_{\text{corr}}}{\rho} EW \quad \text{Equation 2-22}$$

$$MR = K_2 i_{\text{corr}} EW \quad \text{Equation 2-23}$$

2.5.4 Calculation of current density

In order to determine the current density, the Stern-Geary constant has to be determined from the Tafel slopes as indicated in the equation below:¹²

$$B = \frac{b_a b_c}{2.303 (b_a + b_c)} \quad \text{Equation 2-24}$$

The current density is then calculated using the following equation:

$$i_{\text{cor}} = \frac{B}{R_p}$$

Equation 2-25

In conclusion, the corrosion rate is inversely proportional to the polarization resistance which is one of main parameters obtained from the EIS experiments.

2.5.5 *Effective capacitance*

The impedance response of for coated metal in an electrochemical system is usually represented in an equivalent circuit as a constant-phase element (CPE) not a pure capacitance. The impedance associated with the constant phase element can be expressed as:

$$Z_{\text{CPE}} = \frac{1}{(j\omega)^\alpha Q}$$

Equation 2-26

Q can only represent the capacitance when $\alpha=1$ which is not usually the case.¹³ In order to determine the capacitance of the coating, Brug et al. developed a relationship between the CPE parameters and the interfacial capacitance expressed in the following equation:¹⁴

$$C_{\text{eff}} = Q \left(\frac{1}{\alpha} \right) \left(\frac{R_s R_p}{R_s + R_p} \right)^{\frac{(1-\alpha)}{\alpha}}$$

Equation 2-27

2.5.6 *Water uptakes in coatings*

One of the major factors affecting the corrosion protection of a coating is water absorption. As water penetrates the coating, internal stresses are induced. These stresses can be either contractive as the soluble components are extracted or expansive through swelling which will eventually lead to damaging the coating and promoting corrosion.¹⁵ Water penetration can also induce blister formation and delamination which affect the adhesion of the coating to the metal substrate.¹⁶ Weight measurements can be used to determine the water content in the coating by determining the weight gained after absorption or weight lost after drying. However, in corrosion electrochemical studies, capacitance determination is often used to study the water uptake since the presence of water in the coating increases its capacitance. The relative dielectric constant is related to the capacitance through the following equation:

$$C = \frac{\epsilon_0 \epsilon_r A}{d}$$

Equation 2-28

For a typical polymer coating, the dielectric constant ranges from 3 to 8 while for water it reaches 80 at ambient conditions. Therefore, a higher capacitance is obtained when water penetrates the coating.¹⁵

Brasher and Kingsbury proposed an equation that determines the water content in an organic coating using the capacitance measurements.¹⁷ Assuming a uniform distribution of water with a low volume fraction and that the change in coating capacitance is only due to the water uptake, the volume fraction of water can be determined from the following equation:

$$\phi = \frac{\log(C_t/C_0)}{\log(\epsilon_w)}$$

Equation 2-29

3 STUDIES OF COATING SYSTEMS USING EIS

3.1 EIS study of self-healing coatings

Yabuki et al. studied the self-healing properties of different multi-layer coatings when damaged.⁹ Several self-healing techniques can be applied to the different types of coatings. One of these techniques is encapsulating inhibiting compounds before being added to the corrosion-protection systems.¹⁸ Another method that was widely used is Chromate Conversion Coatings (CCCs) that are very effective against localized corrosion. The self-healing behavior manifest through the migration of soluble Cr species from the coating to the defected area. However, CCCs present an extreme health hazard and can cause environmental contaminations, which led to research alternative methods for self-healing.¹⁹ Another approach is the use of Superabsorbent polymers. Due to their water-absorbing and swelling behavior, these polymers are being used in diverse fields. They can be used for moisture preservation in the soil in agriculture, or protecting building from water drainage in construction.

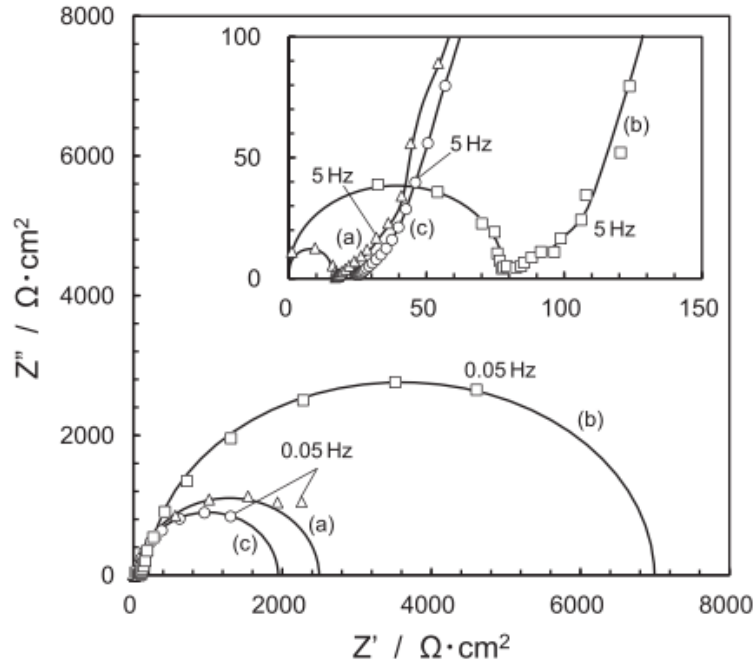


Figure 3-1: Nyquist plots of scratched specimens of coated substrate⁹
(a) VEP/SAP/VEP coatings after 1 h immersion
(b) VEP/SAP/VEP coatings after 6 h immersion
(c) Plain VEP coating after 1 h immersion

A superabsorbent polymer absorbs water and swells into the polymer network, filling the inside of the defected areas. The study conducted by Yabuki et al.⁹ focused on the use of superabsorbent polymer and a vinyl ester polymer in polymer coatings for carbon steel. Different types of multi-layer coatings were tested after using a knife to introduce a defect. The self-healing properties were monitored through performing Electrochemical Impedance Spectroscopy tests and obtaining polarization resistance values at different immersion exposure times of the sample to a 0.5 wt. % NaCl corrosive solution. It was determined that the tested 3-layer coating, which consists vinyl ester polymers at the base and top layers and superabsorbent polymer as middle layer, exhibits a self-healing capability since the polarization resistance increased with time as shown in Figure 3-1.⁹

3.2 EIS study of corrosion behavior of organic coating/Dacromet composite systems

Dacromet, an anti-corrosion coating that consists of zinc and aluminum flakes organized with a chromate matrix, has been studied by Jianguo et al.²⁰ This type of coating is broadly used in several fields due to its excellent corrosion resistance characteristics as well as its environmental friendly behavior. Electrochemical Impedance Spectroscopy was used to study the corrosion behavior of the Dacromet coating and the composite systems consisting of an organic film and a Dacromet layer. The coated samples were carbon steel sample. All tests were conducted in a 3.5 wt. % NaCl solution at atmospheric pressure and room temperature. The samples were immersed in the solution for nine months. For the Dacromet coating, the Bode plots with increased $|Z|$ values were obtained as the immersion time increased as shown in Figure 3-2. This was explained by the formation of a protective layer enhancing corrosion resistance with time.²⁰

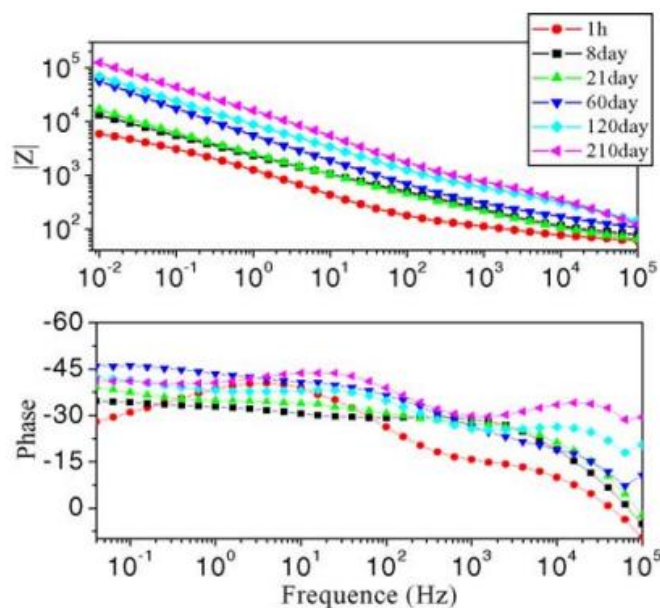


Figure 3-2: Bode plots of Dacromated carbon steel after immersion in 3.5 wt. % NaCl solution for different times²⁰

Three different types of organic films were used with the Dacromet for the thin organic film/Dacromet composite system. After a short period of immersion, the Nyquist plots showed a flat semicircle. It was shown that the thick organic/Dacromet system provide better protection than the thin organic/Dacromet system. Studying the Nyquist plots, it was shown that the circuit contained two capacitive loops with or without a Warburg tail for the polyurethane and alkyd while the styrene-acrylate system had two undistinguishable loops. It was also determined that the thin organic film/Dacromet composite system provides a better illustration of the corrosion kinetic process than the thick one. The polyurethane/Dacromet system showed an increase of R_p and C_p with immersion time. The increase in R_p and C_p was explained as the result of the formation of a passive layer and the accumulation of formed insoluble corrosion products of Dacromet sealing the pores in the polymer which inhibits the corrosion species diffusion. It was not possible to distinguish the two capacitive loops in the Nyquist plots.²⁰

The difference between thick and thin coating was studied before to study the corrosion kinetic process and it showed that the thick layer provide more details. On the other hand, the R_p for the thick coating was higher than the thin one by at least 2 orders of magnitude.²⁰

3.3 EIS study of corrosion behavior of organic coatings with zirconia films

One of the popular techniques in corrosion protection through coating was the use of chromates, which later on was restricted due to its high toxicity. One of the proposed alternatives was the deposition of a thin layers of zirconia by the sol-gel process on the metal surface. In order to study the corrosion behavior of this alternative, electrochemical techniques were used by Fedrizzi et al.²¹ using the dip-coating technique, low carbon steel sheets were coated with thin film of amorphous zirconia. Impedance results shown in Figure 3-3 from the coated samples after 2 hours of immersion has shown that the sol-gel does not have significant effects on the electrochemical behavior of the substrate, while the use of triatomic phosphate led to an impedance increase, which means better corrosion resistance. EIS was used to evaluate the trend of the electric parameter to the capacitance of the reactive metal interface in very short

times, which helped in eliminating several pretreated samples. The EIS results were fitted to an equivalent circuit to determine the double layer capacitance for the different pretreatment techniques.²¹

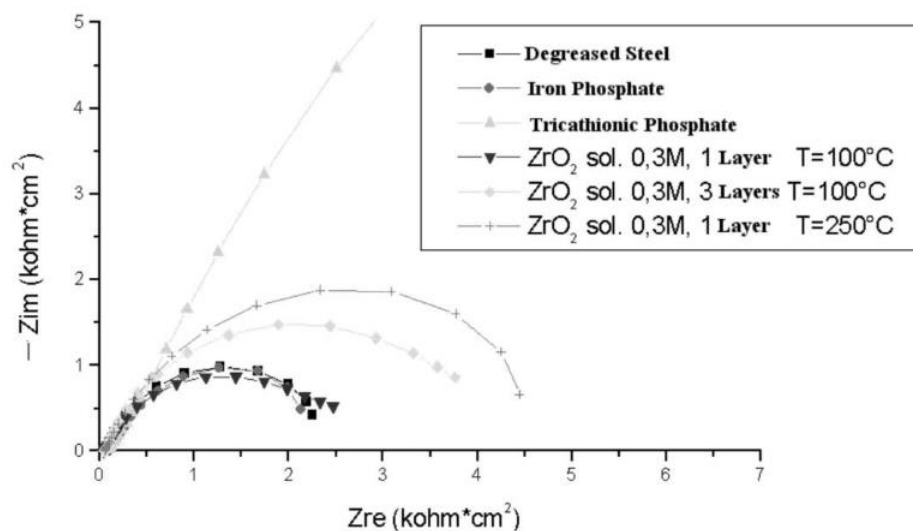


Figure 3-3: Impedance plots of different pretreatments after 2 h of immersion in a 0.3 wt. % Na_2SO_4 solution²¹

Samples with an artificial mechanical defect using drills were also studied. The impedances plots for the defected samples have shown several capacitive loops as demonstrated in Figure 3-4. It was also noticed that the defect dimension has a significant effect on the impedance data. The small defects had impedance results in the order of $\text{M}\Omega$ while larger defects had impedance values of lower orders which means that the corrosion resistance decreasing with larger defects.

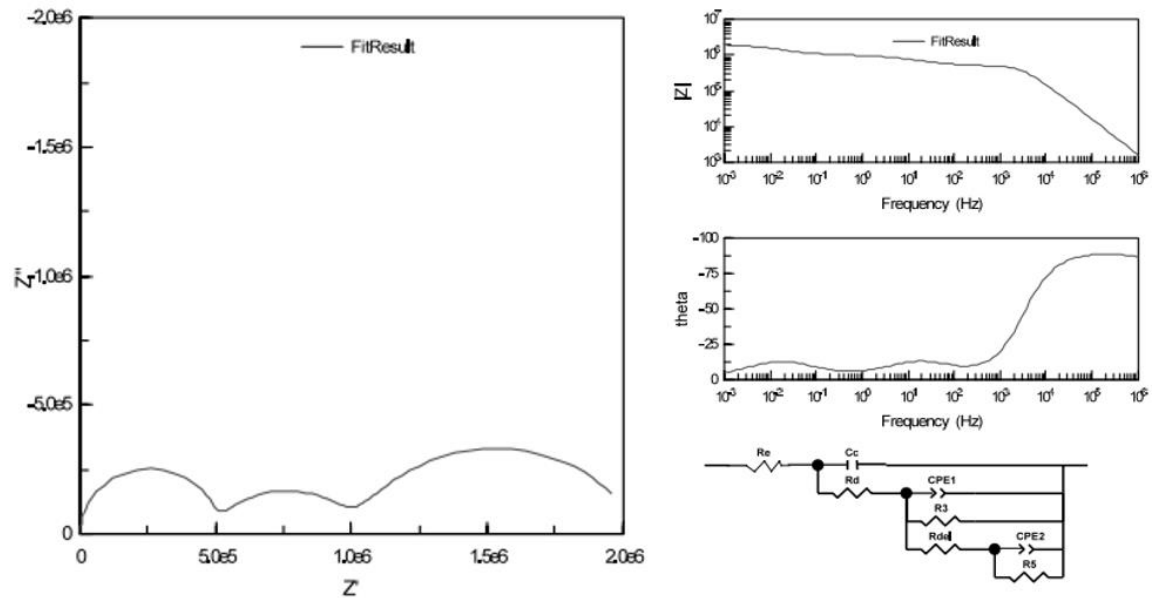


Figure 3-4: Simplified equivalent electrical circuit and Nyquist and Bode plots for defected coating²¹

3.4 EIS study of NiTi coating on AISI 1045 Steel

The equivalent circuit R.CPE-R was used by Verdian et al.²² to simulate the corrosion process of AISI 1045 Steel coated by NiTi intermetallic coating. As immersion time increased, a straight line at low frequencies in the Nyquist plots was observed indicating the existence of a Warburg impedance due to mass diffusion which led to adding the element in series with the R pore as shown Figure 3-5.²²

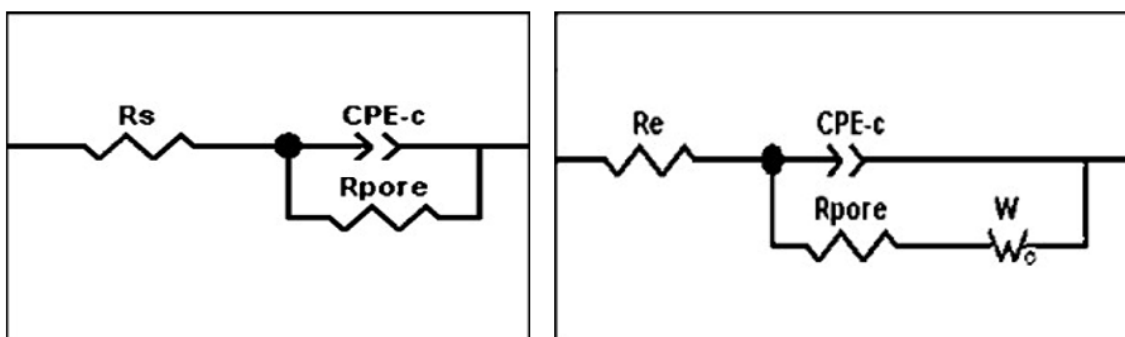


Figure 3-5: Equivalent circuit for AISI steel coated with intermetallic coating. a- after 1 h immersion, b-longer than 1 day immersion²²

3.5 EIS study of PPE coating corrosion resistance

Polyurea Polyaspartic Ester (PPE) coating is one of the polymer coatings that are used for metal protection due to its several advantages and characteristics including instant cure, high solid content, good weather resistance and excellent adhesion. Liu et al.²³ used electrochemical impedance spectroscopy to study the corrosion resistance of (PPE) Coating in 3.5 wt. % NaCl. Several impedance spectra were measured of the PPE during the immersion of the coated samples in the solution. The obtained EIS spectra showed that the corrosion resistance of the PPE coating was declining with time. This can be explained by the gradual penetration of the electrolyte solution. This degradation is clear through the Nyquist plots shown in Figure 3-6. It is clear how the diameters of the semi-circles were decreasing with time.²³

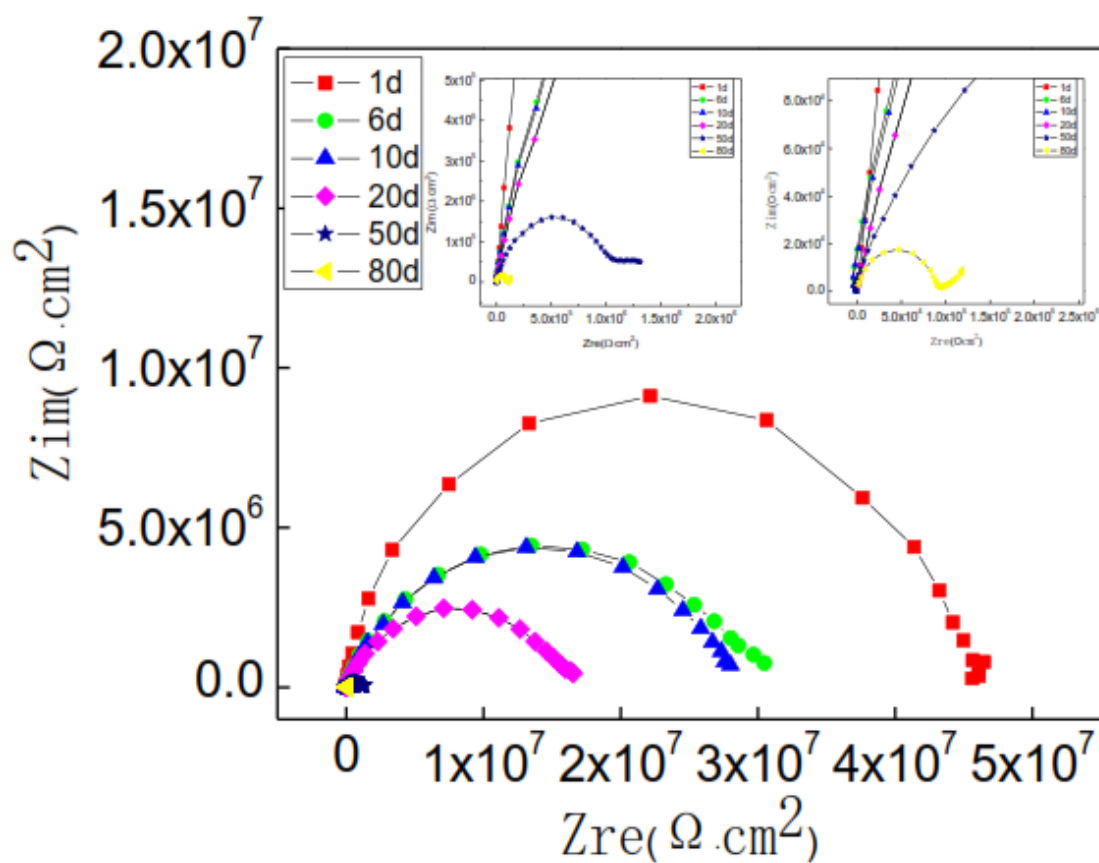


Figure 3-6: Nyquist spectra of PPE coating in period of immersion in 3.5 wt. % NaCl solution²³

3.6 EIS study of polymer coating degradation

A study of the degradation of polymer-coated steel under ultraviolet radiation in a 3% NaCl solution using EIS was conducted by Hattori et al. A three electrode cell was used as shown in Figure 3-7.⁸

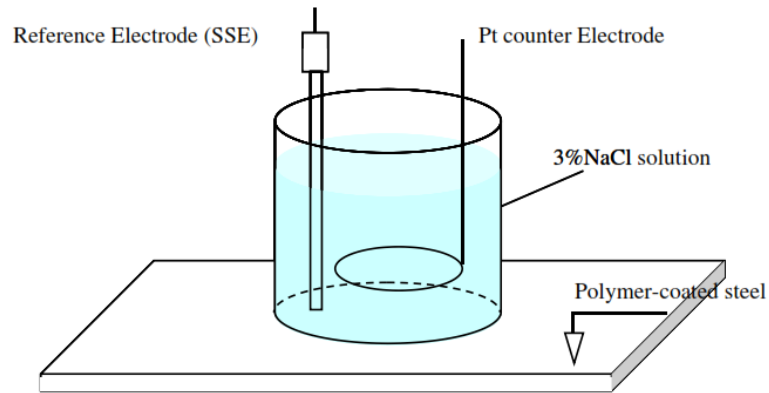


Figure 3-7: Cell for EIS measurements⁸

Based on the obtained results, a process of polymer coating degradation was proposed. This process goes through two main stages. The first stage presents the degradation of the polymer coating which can be caused by several factors such as sunlight or wet/dry cycles that causes a cyclic swelling/shrinking as a result of water absorption/desorption. As a result of polymer degradation, diffusion paths could be created which allows water and oxygen to reach the surface of the substrate which induces the corrosion of the steel leading to the following stage in the polymer degradation. During the second stage the substrate starts to corrode and induces delamination of the coating which causes further degradation of the polymer coating.⁸ Simple equivalent circuits were used to model the corrosion cell and shown in Figure 3-8.

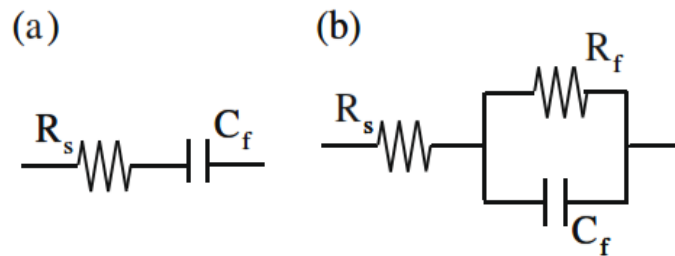


Figure 3-8: Equivalent circuits for coating substrate systems. (a) non-deteriorated polymer-coated steel; (b) deteriorated-polymer-coated steel⁸

4 METHODOLOGY

Coatings are used as a protective barrier separating the metal from corrosive environment which slows down the corrosion process. This work will focus on using electrochemical chemical methods to study the corrosion process of metals under the protection of polymer coatings.

Electrochemical methods are widely used to study the corrosion process for metals and other materials. The most used technique is the Electrochemical Impedance spectroscopy. It was proven that this method provides a good way to analyze the corrosion behavior of coatings. Different variables play a role in the electrochemical corrosion process. These variables include electrolyte solution, materials, interfacial geometry and others. The electrochemical corrosion also depends highly on the nature and characteristics of the corrosion layer.²⁴

One of the main advantages of the EIS techniques include the ability to monitor the progress of corrosion over a period of time without interrupting the experiment. The data obtained from this test provides information about the corrosion rate, mechanism and electrochemical deterioration. In order to interpret the impedance data, a proper model for an equivalent circuit has to be determined.²⁴ The equivalent circuit is usually modeled using passive circuit elements. A passive circuit element is component that does not generate current or potential. The passive elements that are usually used in electrochemical methods are the resistor and the capacitor.²⁵ One of the most used equivalent circuits to interpret electrochemical impedance data is the Randles circuit illustrated in Figure 4-1.^{26,27,28}

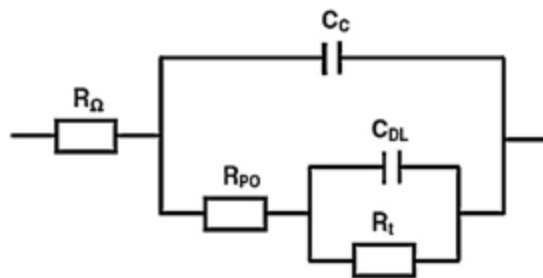


Figure 4-1: Example of Randles circuit for the corrosion behavior of the polymer coated metal²⁶

Each electrical element in the equivalent circuit corresponds to an electrochemical, chemical or physical process that is taking place in the corrosion cell.² An example of the analogy between the electrical circuit and the cell is shown in Figure 4-2. R_{Ω} stands for the solution resistance. This resistance depends on the electrolyte solution and the distance separating the reference electrode from the working electrode. The ionically conducting paths in the polymer, if existent, generate a resistance R_{po} . The coating capacitance is labeled by C_C . R_t stands for the charge transfer resistance at the surface of the metal and the double layer capacitance.

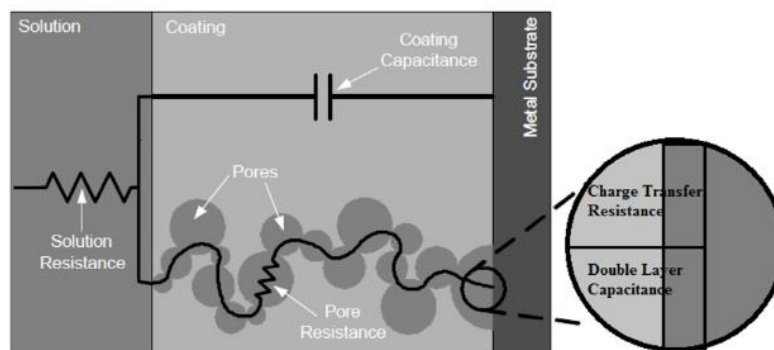


Figure 4-2: Relationship between circuit model, physical coating and corrosion properties²⁶

EIS data are commonly illustrated in two different formats as shown in Figure 4-3 below. The first is the Nyquist data-presentation format in which the impedance imaginary component Z'' is plotted versus the real component. The second representation is the Bode format which illustrates the impedance Z and phase angle as a function of frequency.

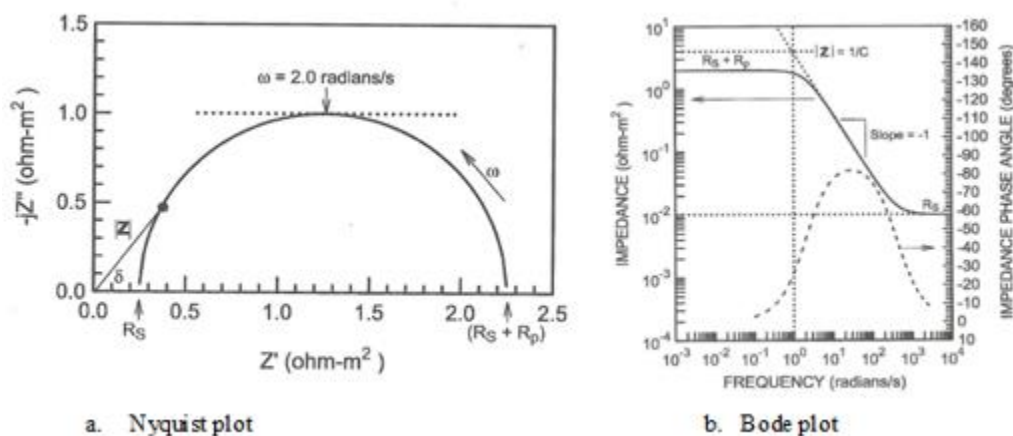


Figure 4-3: EIS data-presentation formats²⁴

Nyquist diagram exhibiting a semicircle matches a charge-transfer resistance in parallel with a capacitance.²⁴ However, in electrochemical corrosion, a perfect semicircle is never observed due to the distribution of physical properties on the surface and the non-homogeneity of the system.¹³ For this reason, a pure capacitance is replaced with a constant phase element which provides a better fit.²⁹

Another element, called the Warburg impedance element, is introduced in the equivalent circuit when a diffusion-controlled charge transfer is observed at low frequencies as illustrated in Figure 4-4.³⁰ The diffusion of reactive species is existent in most electrochemical corrosion cases.²⁴ The use of Warburg impedance raises a challenge in most cases since it is not possible to measure the Warburg coefficient because of the lack of control of the diffusion layer.

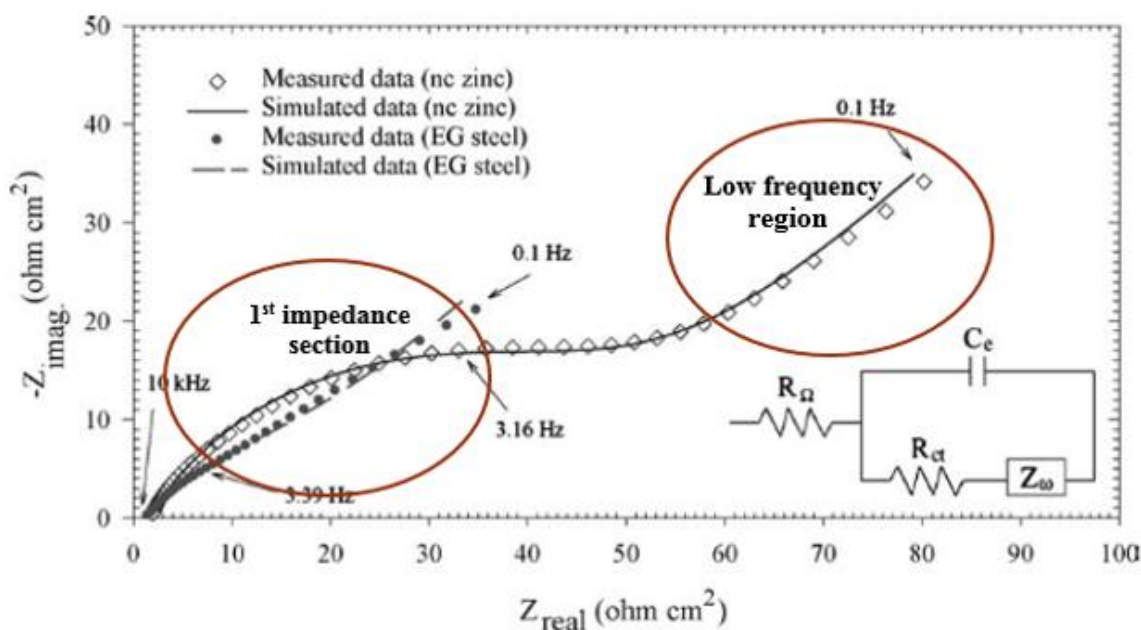


Figure 4-4: Nyquist plots with Warburg impedance³⁰

The first impedance section which includes a phase capacitance and a resistor in parallel can be attributed to the faradaic charge transfer process.²⁴ The third impedance parameter, including the Warburg term, can be attributed to the diffusion through the formed corrosion layer on the electrodes surface.

The high frequency region provides information about coating defects and changes in the surface of the coating. The low frequency region provides information about processes occurring near the metal surface.²⁶

The purpose of this research is to identify and test a benchmark corrosion resistant coating material for oil and gas applications. This commercial material is expected to resist the corrosive conditions in gas pipelines. The project focused on studying the corrosion resistant properties of the coating through electrochemical impedance method. This study will be used as a comparison when a new multifunctional material is developed. This goal was achieved through the methodology described below.

4.1 Step 1: Material identification

The first step was to identify coatings with the targeted properties and produce materials for the study. The coatings are aimed to provide a corrosion resistant layer for gas pipelines at critical conditions. The material should resist carbon dioxide and hydrogen sulfide corrosion at high temperatures and high pressures. It was also planned to investigate the best coating system that will fit the specifications. This part of the project was handled by the research team in Pennsylvania State University.

Two different types of polymer coatings were selected. The first is a liquid-epoxy phenolic (TK-805) and the second is powder-phenolic novolac (TK-34XT) both provided by NOV Tuboscope. These two materials were used to coat carbon steel slabs. The chemical composition of the carbon steel is shown in Table 4-1.

Table 4-1: Chemical composition of the substrate

Element	C	Mn	P	D	Di	Cu	Ni	Cr	Mo	Fe
percentage	0.17	1.05	0.012	0.003	0.22	0.14	0.09	0.09	0.02	balance

Prior to applying the polymer coating, a primer was applied to the metal surface. The primer is considered a preparatory coating that provides better adhesion between the coating and the surface. Five samples were received from the Pennsylvania State Research group as described in Table 4-2.

Table 4-2: Samples obtained from Penn State

Sample	coating	Thickness	Dimension (cm)
A	Primer + TK 805	Low	10x15
C	Primer + TK 805	High	10x15
H	Primer + TK 34XT	Low	10x15
I	Primer + TK 34XT	High	10x15
F	Primer	NA	10x15

Details about the chemical composition of the coating and the deposition technique were not provided by the supplier. These details will not be discussed in this study.

4.2 Step 2: Samples preparation

The second step was to define and prepare the samples that will be tested. The project did not only aim to test the coated samples; a Bruker tribometer was used to introduce measured and reproducible defects on some of the samples. The same tests on substrates without coating and substrates with defected coatings were also conducted. The purpose of these tests was to compare the results from different experiments to determine the efficiency and effectiveness of the coating.

4.2.1 Cutting

The coated slabs were cut using a mechanical saw. The desired tested area was 11.4 cm^2 . To obtain a circular surface area exposed to the solution with this dimension, the slabs of $10 \times 15 \text{ cm}^2$ were divided into 6 pieces with $5 \times 5 \text{ cm}^2$ each.

4.2.2 Introducing the defect

After cutting the slabs, a mechanical defect was introduced to one sample from each coating using the Bruker tribometer as shown in Figure 4-5. Two types of defects were suggested. However, it was not possible to introduce both defects for each coatings due to technical problems with the device. It was only possible to obtain one type of defect for each coating. Table 4-3 presents the two types of defect with the parameters of the applied force.

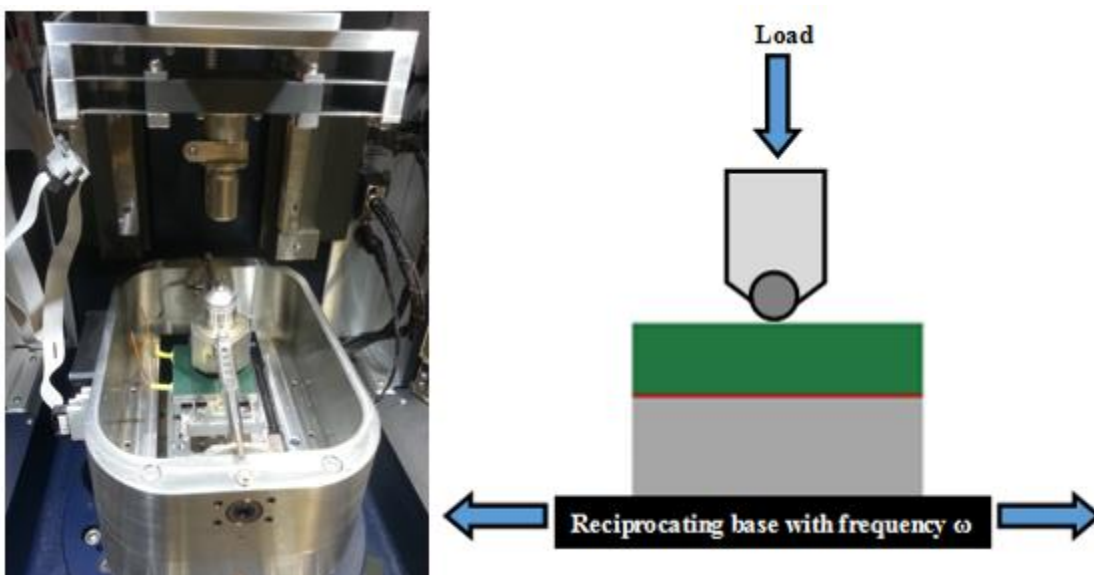


Figure 4-5: Photo of the sample in the tribometer (left) and schematic of the test (right)

Table 4-3: Defect type and applied force parameters

Defect type	Load (N)	Frequency (Hz)	Duration (s)
Beta	20	0.25	120
Gamma	41	0.25	120

4.2.3 Preparation for electrochemical test

In order to perform the electrochemical tests, it is essential to provide a conductive medium between the substrate and the potentiostat. A hole with 1 mm in diameter and 0.5 cm in depth was drilled on the sides of each samples. Each hole was filled with silver conductive epoxy and a 4 cm copper wire was then inserted in the hole. The gel was allowed to dry for 2 hours. After preparing all the samples, a mechanical engraver was used for labelling purposes. Figure 4-6 below shows an example of a working electrode.



Figure 4-6: Working electrode

4.3 Step 3: Samples characterization

The third step was to characterize the coating systems. This objective was achieved by determining the critical metrics such as surface morphology and coating thickness. A thickness gauge was used to determine the average thickness of each sample since the samples were not polished prior to coating which lead to variation in the thickness. The morphology was studied using an optical profilometer.

4.3.1 *Optical profilometer*

A ZeGage profilometer by Zygo Company, shown in Figure 4-7, was used to obtain a 3D profile for each sample surface. An optical profiler is an interference microscope that used to measure height variations with significant precision using light wavelength as a ruler. This method is widely used to obtain accurate measurements for different surfaces.

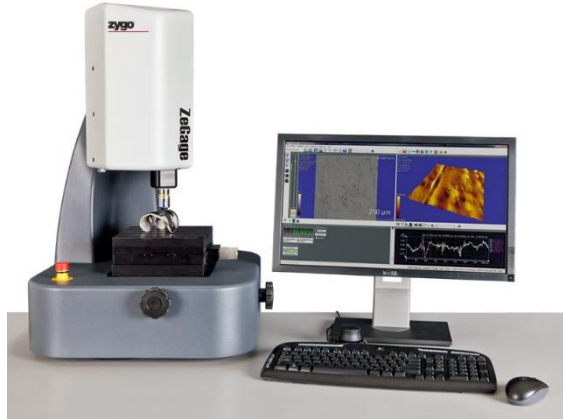


Figure 4-7: ZeGage profiler³¹

Optical profiling is carried by using the wave properties of light in order to compare the optical path difference between the tested surface and a reference surface. The light beam is split within the optical interference profiler into two beams. The first split beam passes through the focal plane of the microscope objective and reflects from the test material while the second beam is reflected from the reference mirror as shown in Figure 4-8. When the beam splitter is at an equal distance from the reference mirror and the test surface, the split beams are then recombined creating light and dark bands known as interference fringes. The reference mirror being of a known flatness, allows determining the optical path differences which are due to height variances in the test surface. The height differences are then used to obtain a 3D surface map.

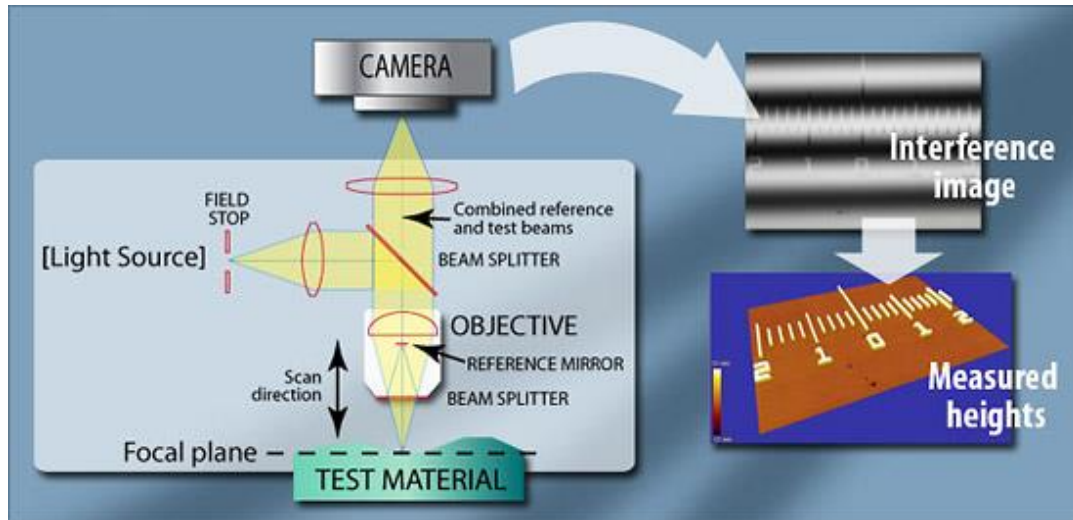


Figure 4-8: Optical profiler basics³¹

4.3.2 Thickness gauge

As previously mentioned, the substrate was well polished prior to the coatings which led to a variation in the thickness from one sample to another. Several measurements at different points were taken and then averaged for each sample using PosiTector 6000.

4.3.3 Stereo microscope

A Zeiss Stemi 2000-C Microscope was used to obtain magnified images of the samples surface ranging from 1x to 5x. This allowed studying any significant visible effects of the corrosion on the tested samples.

4.4 Step 4: Experimental setup and cell design

The fourth step was to establish an experimental setup to study to corrosion in a corrosive environment. After conducting literature review, an appropriate setup was identified. This setup will be used to conduct the necessary tests to study the corrosion of the coatings. These tests also followed the required standards proposed by NACE, The Corrosion Society (ISO).

The standard solution that was used as a corrosive environment is a 3.5 wt. % NaCl aqueous solution. The solution was prepared by dissolving solid sodium chloride in distilled water. A potentiostat was used to apply the AC excitation to the metal sample. An electrochemical cell was designed to accommodate for the potentiostatic circuit in order to perform the tests. The corrosion cell should be compliant with the ASTM standards and also have a reduced cost since such corrosion cell cost around \$1000 per unit. The following parameters should be taken into account when designing the corrosion cell:

- Material
 - The used material was Poly(methyl methacrylate) PMMA. This material is usually used for these application because of its durability and non-conductivity.
- Exposure surface area
 - The exposed surface area of the working electrode depends on surface material. For coatings, it is recommended that the surface area exceeds 10 cm^2 as mentioned in ISO standard.³² A surface area of 11.4 cm^2 was used to maximize the number of samples obtained from each slab.
- Distance separating the reference electrode for the working electrode surface
 - When conducting an electrochemical corrosion test, it is essential to reduce the distance separating the reference electrode from the working electrode. The solution exhibits a certain resistance that depends on the electrolyte and it is directly proportional to the distance separating the working electrode from the sample surface.
- Counter electrode
 - The counter electrode area exposed to the solution has to be larger than the working electrode area. A graphite rod will be used as a counter electrode. In order to obtain the required area, the counter electrode had to be immersed in 15 cm of solution. This parameter will also be used to define the height and the volume of the cell. A graphite rod of a 0.6 cm in diameter was used. To obtain a surface area that is equal to 1.2 times

the exposed surface area, the rod has to be immersed for 13 cm in order to get an area of 14.7 cm².

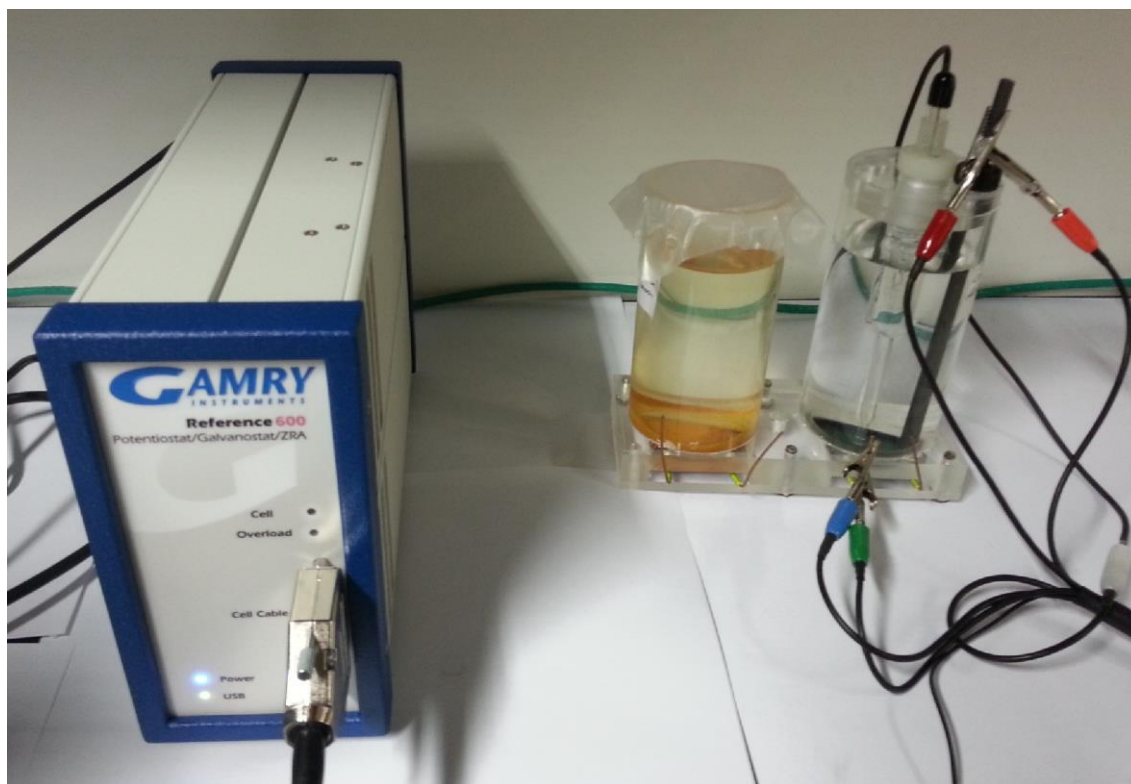


Figure 4-9: Corrosion cell connected to Gamry potentiostat

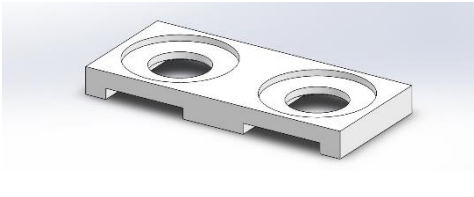
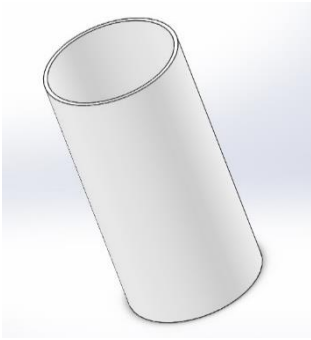
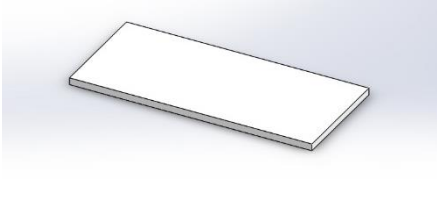
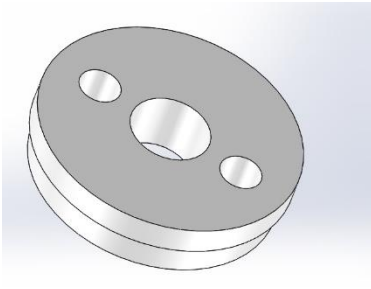
The following is a list of materials used to build the cells. Each cell could hold two samples at a time.

The overall cost of the materials was \$ 474.

- Optically cast acrylic rectangle bar, 3/4" thick, 3" width X 4' length, clear
- Optically clear cast acrylic tube, 2-3/4" OD X 2-1/2" ID, 3' length
- Optically cast acrylic rectangle bar, 1/4" thick, 3" width X 4' length, clear
- EPDM O-ring, 2-3/4" OD X 2-1/2" ID

These materials were used to construct the cell. Each cell consists of 4 parts. A 3D illustration was performed using solid works. The parts are listed in Table 4-4 .

Table 4-4: Corrosion cell parts

Part	3D illustration
Base	
Cylinder	
Lower base	
Cover	

The cylinder is inserted on the top of the base and glued using chloroform. The lower cover is connected to the base using bolts. It aims to apply a force on the sample that will inserted between the base and the lower cover in order to avoid any leak. An O-ring was inserted between the base and the sample. The top cover is only placed while conducting the test. It has three opening that are used to insert the following elements: the graphite rode, the reference electrode and the pH meter. Figure 4-10 below shows the assembled corrosion cell and technical sketch is illustrated in Figure 4-11.

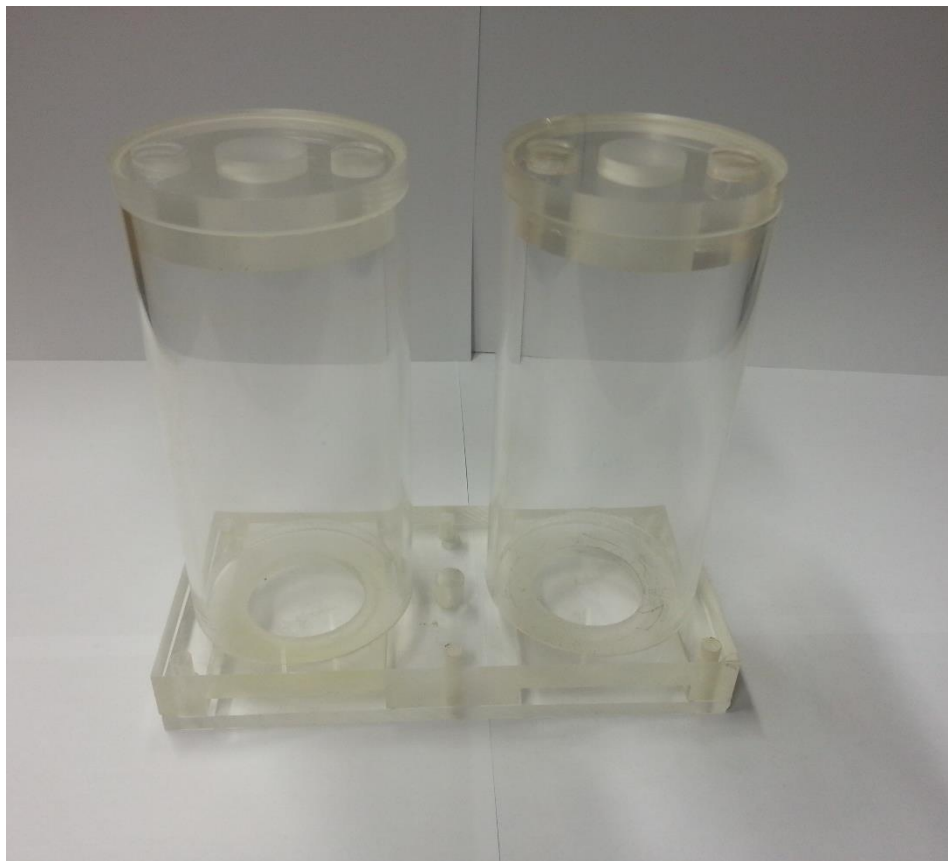


Figure 4-10: Corrosion cell

Once the cells are constructed and the samples were prepared for testing. Electrochemical measurement will be taken for each sample each few days. The Open Circuit Potential (OCP) and Electrochemical Impedance Spectroscopy (EIS) measurement will be performed using Reference 600 Potentiostat with the parameters listed in Table 4-5 and Table 4-6.

Table 4-5: Open circuit potential test parameters

Parameter	Value
Sample period	0.5 s
Total time	4800 s
Sample area	11.4 cm ²

Table 4-6: Electrochemical impedance spectroscopy test parameters

Parameter	Value
DC voltage	0 V vs Open circuit potential
AC voltage	20 mV rms
Initial Frequency	100000 Hz
Final Frequency	0.001 Hz
Points/decade	10
Sample area	11.4 cm ²

4.5 Step 5: EIS results analysis

The fifth step is to run simulations to determine the equivalent circuit for each EIS spectra obtained. Gamry Echem Analyst will be used. The first circuit that will be tested is the Randles circuit, then other circuits will be constructed and tested using the main elements that are commonly used which are: resistance, capacity, constant-phase element and Warburg impedance.

5 RESULTS

This study was divided into two sections depending on the integrity of the coating. The first part will discuss the behavior of the samples exposed to the corrosive environment of 3.5 wt. % NaCl solution at ambient conditions without introducing any defects which were labeled as Alpha samples. The second part will discuss the corrosion behavior of the samples exposed to the same conditions that were subjected to a minor or a major defect labeled as ‘Beta’ and ‘Gamma’ respectively.

5.1 Intact coating behavior

Four different samples labeled Alpha were studied. Since all the samples exhibited a similar behavior, only one of them will be discussed in this section. These four samples can be divided into two categories. The first category is the TK-805 which includes the powder phenolic-novolac thermoset coatings. In this category, two different thicknesses were applied, a low thickness of 150-162 μm , labeled ‘A’, and high thickness of 316-338 μm labeled ‘C’. The second category is the TK-34XT which includes the liquid novolac thermoset coating. Two different thicknesses were applied as well, a low thickness of 66-72 μm labeled ‘H’ and high thickness of 166-178 μm labeled ‘I’. The samples in this study are named based on the thickness label and the defect type. For example, the sample discussed in this section is ‘A Alpha’ which is a TK-805 coating with a low thickness that was not subjected to a defect. Figure 5-1 shows the studied samples.

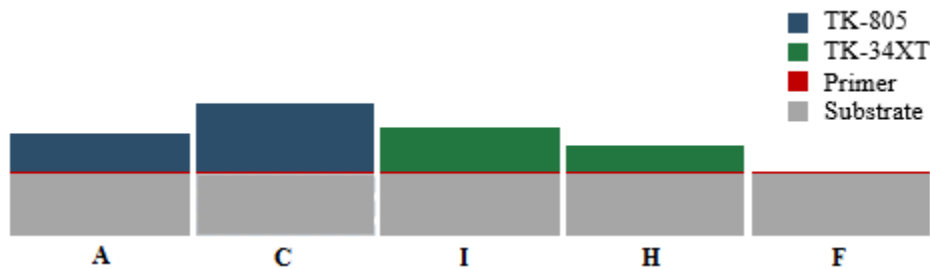


Figure 5-1: Legend for studied samples

5.1.1 ‘A Alpha’ case study

5.1.1.1 Imaging

No visible differences were noticed on the sample after 88 days of exposure to the corrosive environment as shown in Figure 5-2 and Figure 5-3. The coating is designed to withstand more aggressive corrosive environments. The difference in color is due to the different light parameters used when taking the photo.

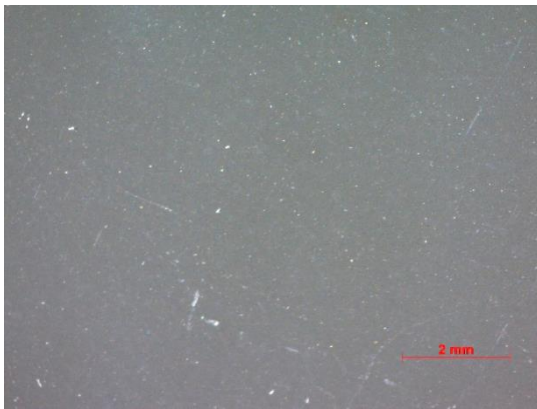


Figure 5-2: ‘A Alpha’ before exposure

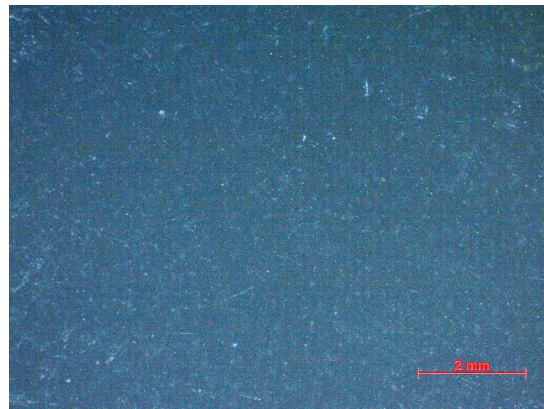


Figure 5-3: ‘A Alpha’ after exposure

5.1.1.2 3D profile

The 3D profile did not show any significant changes on the integrity of the coating as shown in Figure 5-4 and Figure 5-5. It was noticed that the surface is not completely plane. This can be explained by the fact that the metal surface was not polished prior to applying the coating.

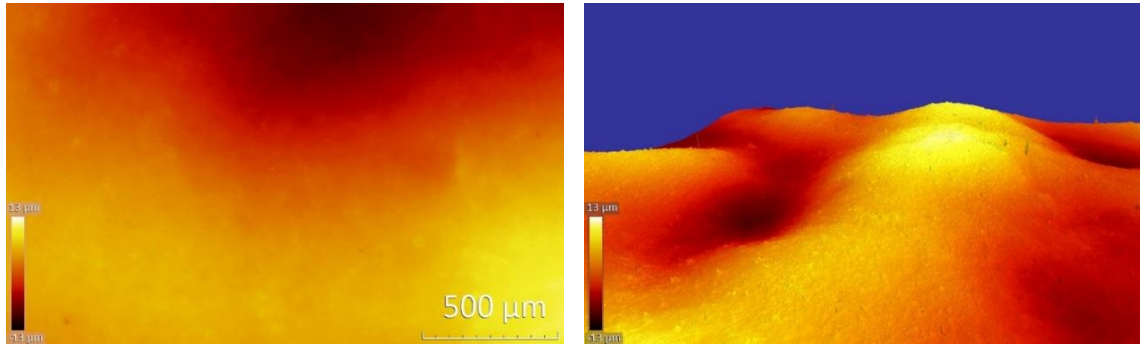


Figure 5-4: 3D profile of 'A Alpha' before exposure

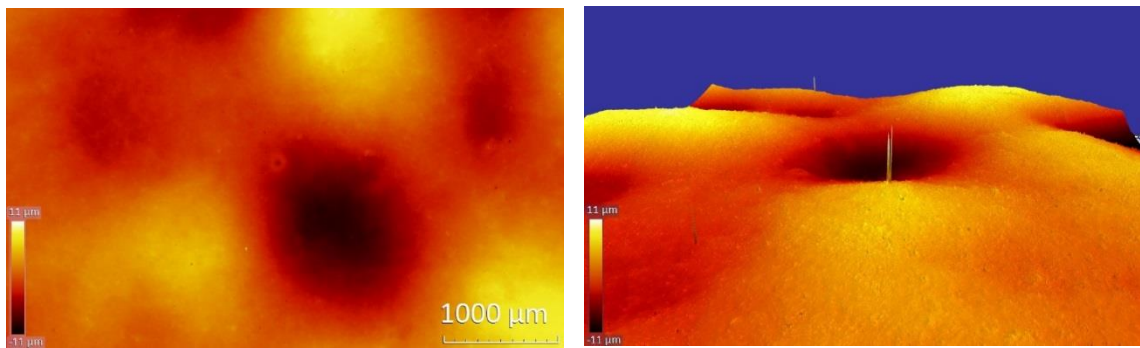


Figure 5-5: 3D profile of 'A Alpha' after exposure

5.1.1.3 *Electrochemical impedance spectroscopy*

The electrochemical impedance spectroscopic analysis of the coating exposed to 3.5 wt. % NaCl solution for selective times was performed on the basis of Bode and Nyquist plots as shown in Figure 5-6 and Figure 5-7 below. At the low-frequency limit, the impedance modulus $|Z|$ values obtained for all the tests conducted on the sample were in the range of $G\Omega$ ($>10^{11}\Omega$). This significant high resistance implies that the corrosion rate is very negligible and close to zero since the corrosion rate is inversely proportional to the polarization resistance. It is also noticed that all the tests exhibited a similar behavior of a one-time constant which is expected for organic coatings. The correspondent phase angle for all the test was ranging from 80 to 85 degrees at the high-frequency limit.

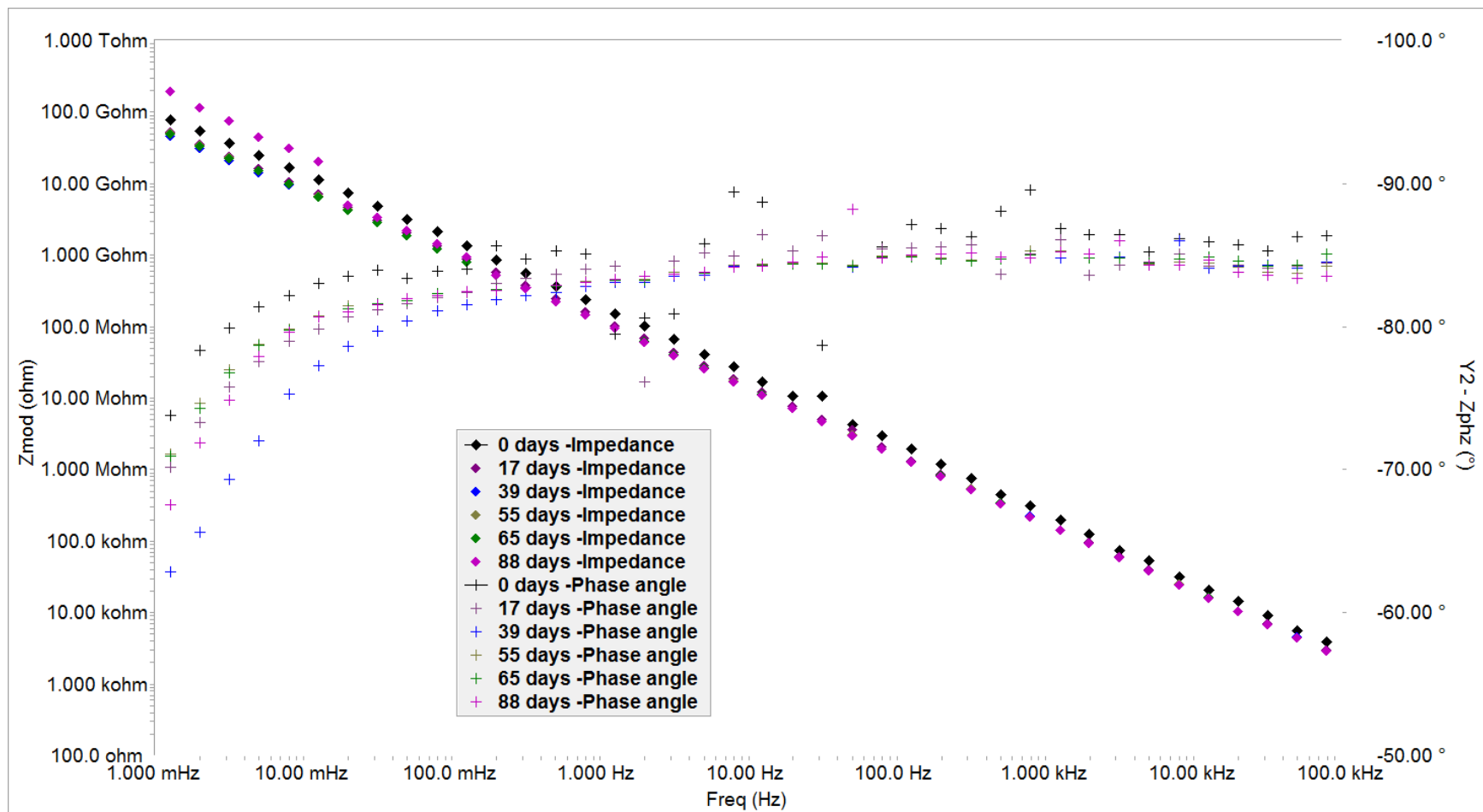


Figure 5-6: 'A Alpha' - Bode plot continuous exposure over 88 days

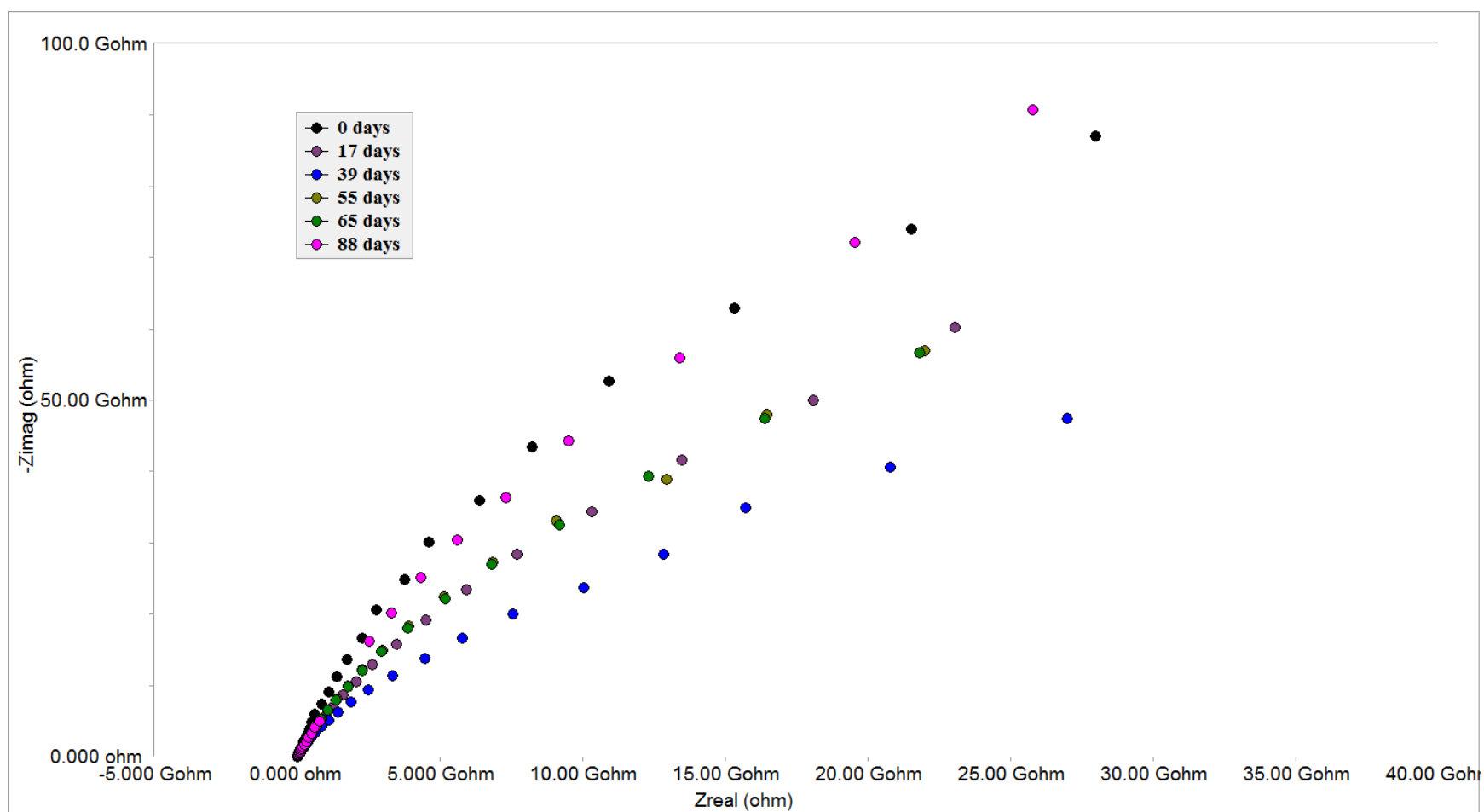


Figure 5-7: 'A Alpha' -Nyquist plot for continuous exposure over 88 days

In order to determine the kinetic parameters for this corrosion model it is essential to determine the right equivalent circuit. Most studies suggest that perfect coatings would behave as a pure capacitance and use a simple Randles circuit consisting of a resistance in series with a parallel combination of a capacitor and a resistor to simulate it. However, this model only applies for ideal cases. The morphology of the sample and its effect on the circuit can be taken into consideration through introducing a constant phase element (CPE). The circuit shown in Figure 5-8 is usually used for similar systems of coatings and provides a better fit than the typical Randles circuit. R.E and W.E refer to reference electrode and working electrode respectively. The equivalent impedance for the proposed circuit can be calculated from the equation below.

$$Z=R_s+\frac{R_p}{1+R_p(j\omega)^{\alpha}Y_0} \quad \text{Equation 5-1}$$

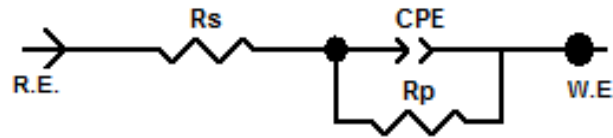


Figure 5-8: Circuit 'A'

Figure 5-9 and Figure 5-10 below illustrates the fitting of circuit A on the 65 days exposure time test using Gamry Echem.

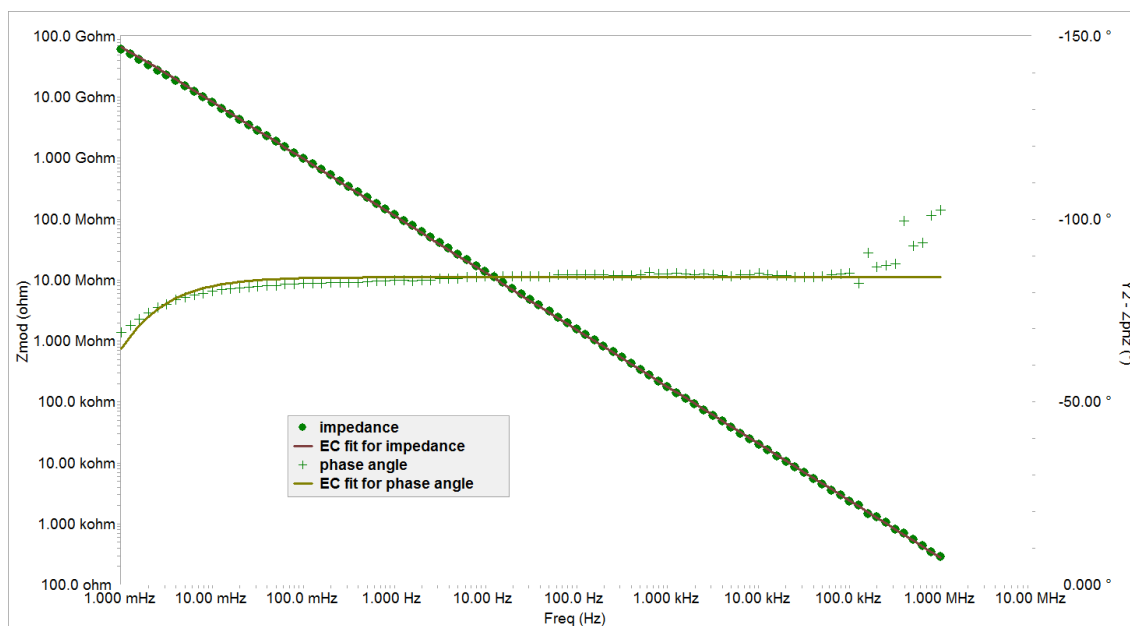


Figure 5-9: Bode plot after 65 days of exposure fitted using circuit 'A'

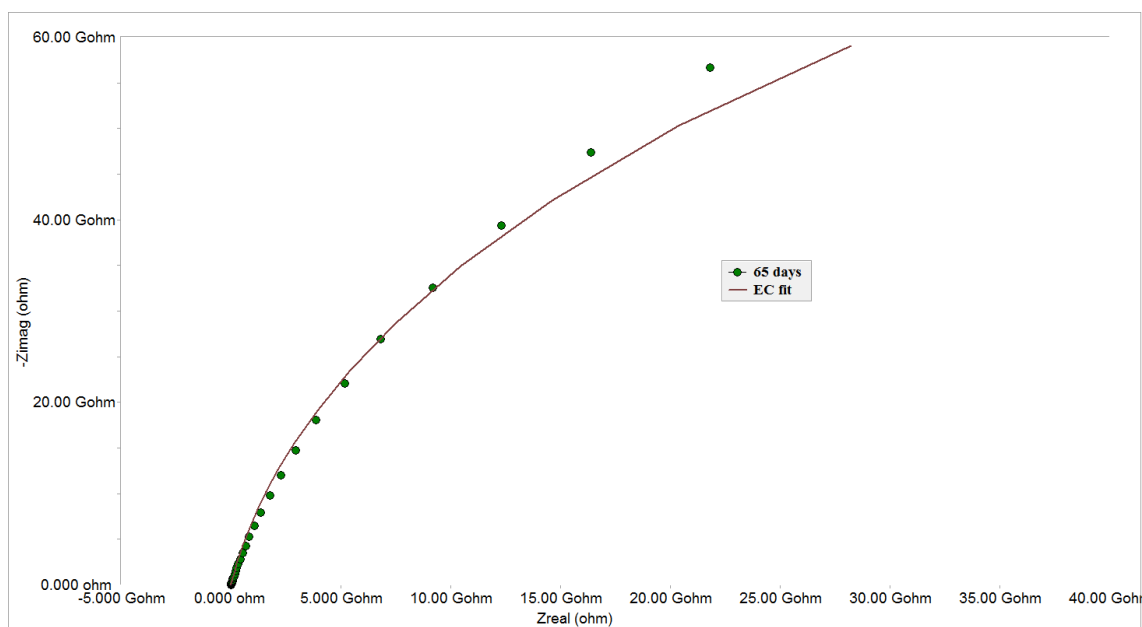


Figure 5-10: Nyquist plot after 65 days of exposure fitted using circuit 'A'

Using the circuit A, the polarization resistance and the constant phase element parameters were determined for each test as listed in Table 5-1. As the time elapsed, it was noticed from bode and Nyquist plots and the values in the table that the polarization resistance fluctuates around $2300 \text{ G}\Omega \text{ cm}^2$. There were no specific trend of increase or decrease in the values which means that the coating was not affected by the corrosive environment.

Table 5-1: Kinetic parameters for ‘A Alpha’ over 88 days

Exposure time (days)	$R_s (\Omega)$	$R_p (\Omega \text{ cm}^2)$	Q	α	$C_{\text{eff}} (\mu\text{F})$	ϵ
0	2.19×10^{-3}	3.92×10^{12}	1.01×10^{-9}	0.95	0.24	3.74
8	47.55	2.41×10^{11}	1.40×10^{-9}	0.95	0.54	8.28
17	3.34×10^{-3}	2.12×10^{12}	1.48×10^{-9}	0.94	0.26	4.05
33	1.19×10^{-3}	1.44×10^{12}	1.57×10^{-9}	0.93	0.24	3.67
39	1.54×10^{-1}	1.17×10^{12}	1.60×10^{-9}	0.93	0.34	5.16
41	4.95×10^{-1}	2.02×10^{12}	1.57×10^{-9}	0.94	0.37	5.64
55	2.21×10^{-1}	2.22×10^{12}	1.57×10^{-9}	0.93	0.34	5.21
57	1.33×10^{-1}	3.40×10^{12}	1.39×10^{-9}	0.95	0.40	6.18
65	1.79×10^{-3}	2.20×10^{12}	1.59×10^{-9}	0.93	0.25	3.80
70	1.78×10^{-4}	4.07×10^{12}	1.39×10^{-9}	0.95	0.29	4.43
74	5.77×10^{-4}	3.02×10^{12}	1.41×10^{-9}	0.95	0.31	4.73
88	3.15×10^{-2}	3.95×10^{12}	1.31×10^{-9}	0.96	0.43	6.65

The figures below illustrates the polarization resistance as a function of time on a logarithmic scale. It is evident that the variation of R_p per time is minor and fluctuates around an average value of $218 \text{ G}\Omega$ as shown in Figure 5-11. The log scale was used to better present the large scaled values.

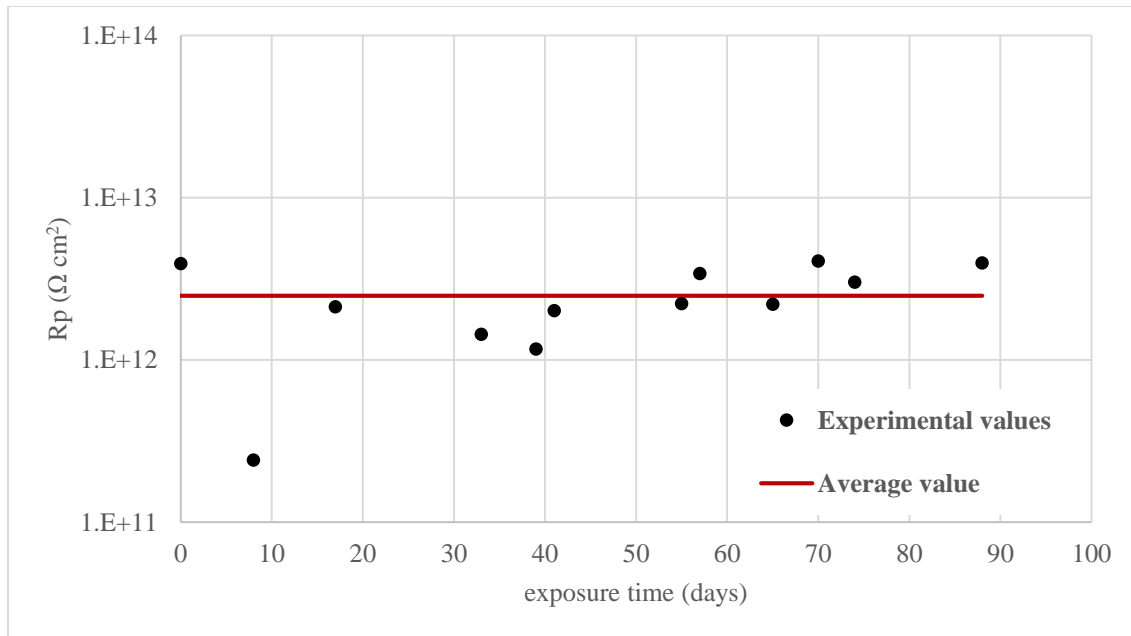


Figure 5-11: Time dependence of resistance R_p for 'A Alpha'

One of the studies suggested a method to determine the effective capacitance from the constant phase elements values. The dielectric permittivity was determined from the capacitance values using the following equations and listed in Table 5-1.

Figure 5-12 below shows that the relative permittivity fluctuates around an average value of 5. This result indicates two conclusions. First, the typical dielectric relative permittivity value of a polymer coating ranges from 3 to 8, obtaining a value that agrees with this statement supports the use of the suggested circuit as a simulation model. Second, the relative permittivity of water is 80.2 at ambient conditions. In case of water penetration, the relative permittivity of the coating is expected to increase drastically, leading to the conclusion that the coating is still intact.

Furthermore, by applying Brasher and Kingsbury theory of water uptake by organic coatings, it was determined that the volume fraction of water in the coating had an average of 0.076.

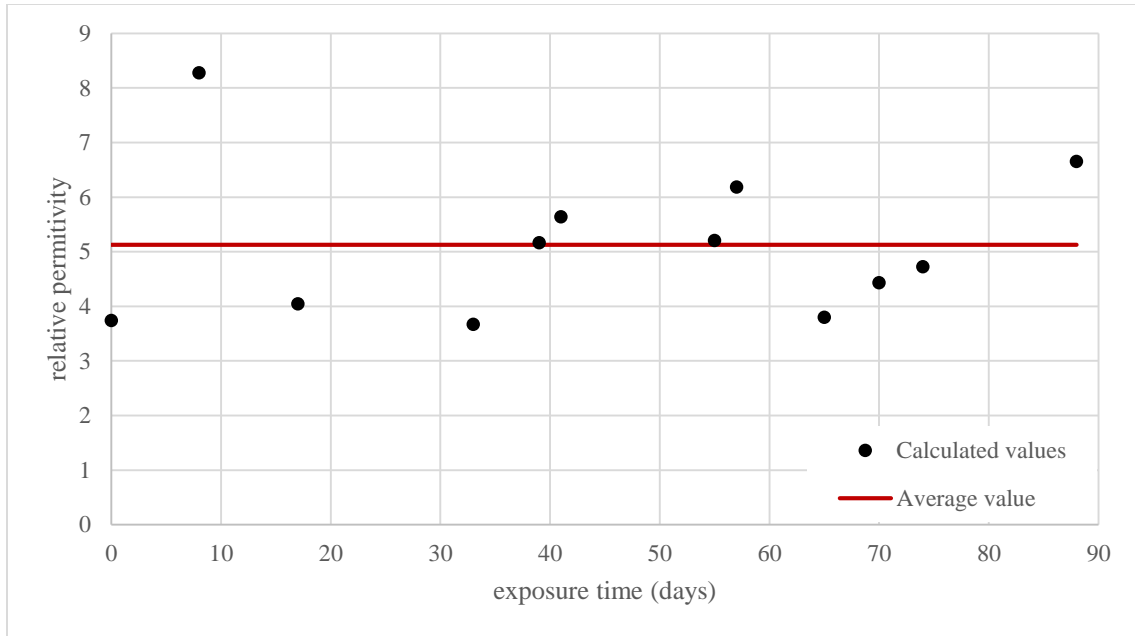


Figure 5-12: Time dependence of relative permittivity ϵ_r for 'A Alpha'

5.1.2 Summary

The same circuit was found to be applicable to the other three Alpha samples. Table 5-2 includes results obtained from all 'Alpha' samples. All the samples maintained a high polarization resistance during the exposure period, it was concluded from the values that the corrosion resistance of the coating depends on the thickness. All samples maintained an impedance over $10^{11} \Omega \cdot \text{cm}^2$ at the low frequency limit on the Bode plot which indicates an excellent corrosion protection values.

Table 5-2: Results for intact samples

Sample	Average R_p ($\text{G}\Omega \cdot \text{cm}^2$)	Average ϵ	Thickness (μm)
'A Alpha'	2481.78	5.12	150-162
'C Alpha'	5788.92	5.09	316-338
'I Alpha'	3790.5	3.02	166-178
'H Alpha'	242.82	3.26	66-72

The results also suggest that the effect of the thickness also depends on the type of coating. Assuming a liner relation between the polarization resistance and the thickness, it could be deduced that the powder coating is more effective since the obtained slope is higher than the slope for the liquid coating as shown in Figure 5-13.

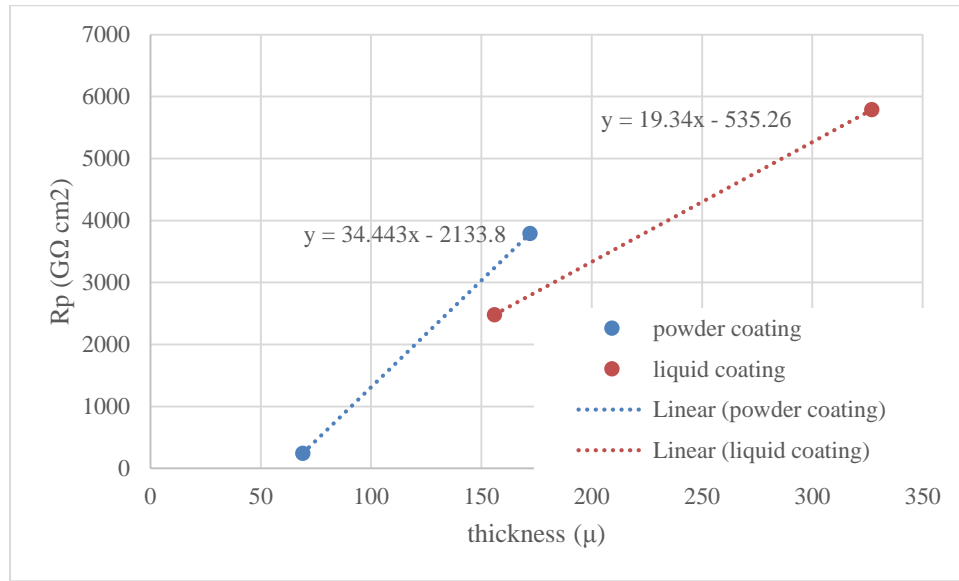


Figure 5-13: Thickness dependence of polarization resistance for the different types of coating

5.1.3 'C Beta' special case

Circuit 'A' was also applicable for the C Beta sample. 'C Beta' refers to the sample coated with TK-805 with a high thickness varying from 316 to 338 μm. The load applied on the sample didn't cause serious damage to the coating as illustrated in Figure 5-14. In others words, the cracks did not propagate to the metal surface and only reached a depth of 7 to 17 μm. After 80 days of exposure to the corrosive environment, no corrosion products were formed as shown in Figure 5-15 and Figure 5-16. The average polarization resistance obtained for this samples was 7427.1 GΩ cm² which is of the same order of the intact sample.

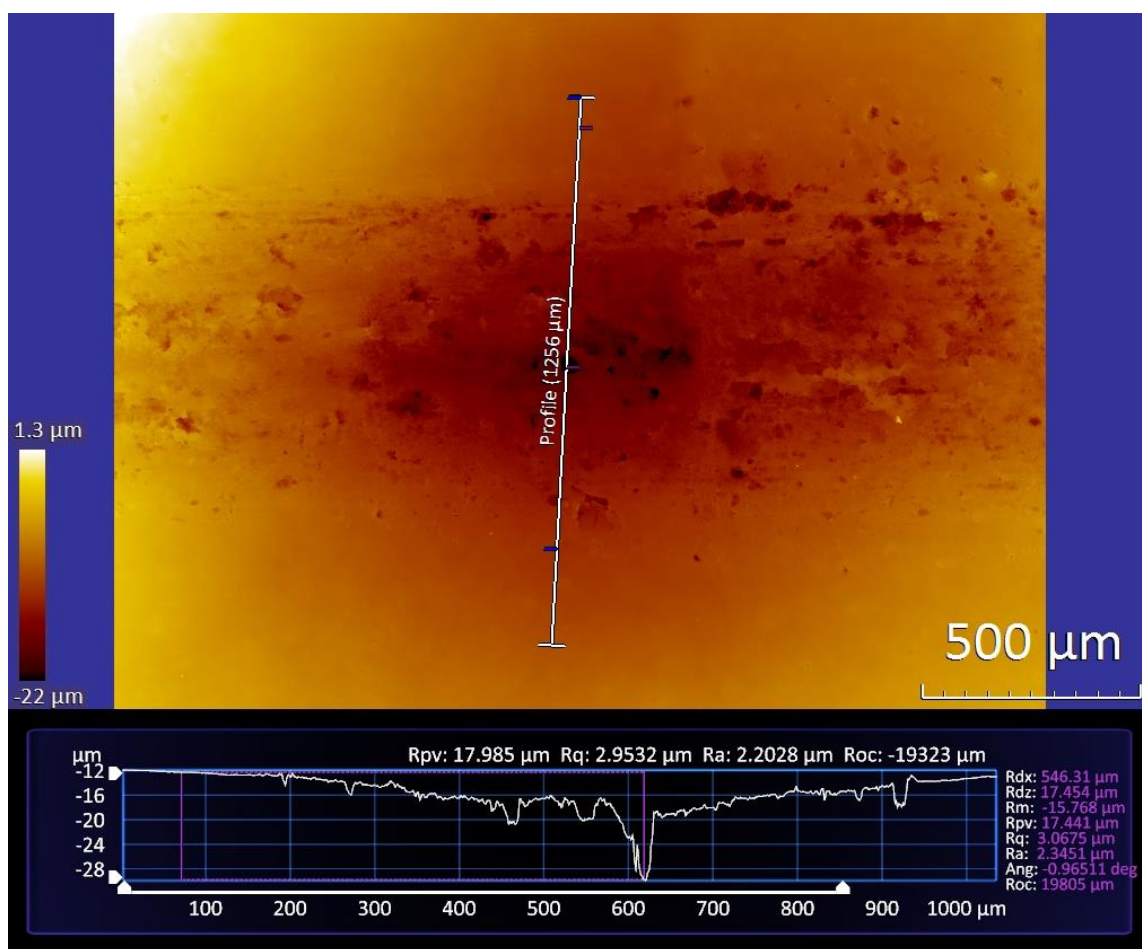


Figure 5-14: 3D profile of 'C Beta'



Figure 5-15: 'C Beta' before exposure

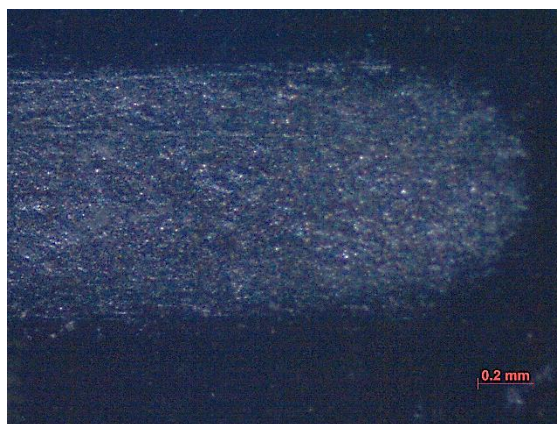


Figure 5-16: 'C Beta' after exposure

5.2 Damaged coating behavior

As previously mentioned, four different coating systems were studied. A different defect was introduced to each of the coating system. Two different behavior were observed for the defected sample. A load of 41N was applied on the surface of the sample coated with TK-805 with a thickness of 150 μm at a rate of 0.25 Hz for 120 seconds. This force severely damaged the coating and removed most of the top layer exposing the surface of the metal. This sample was referred was 'A Gamma'.

5.2.1 'A Gamma' case study

5.2.1.1 Imaging

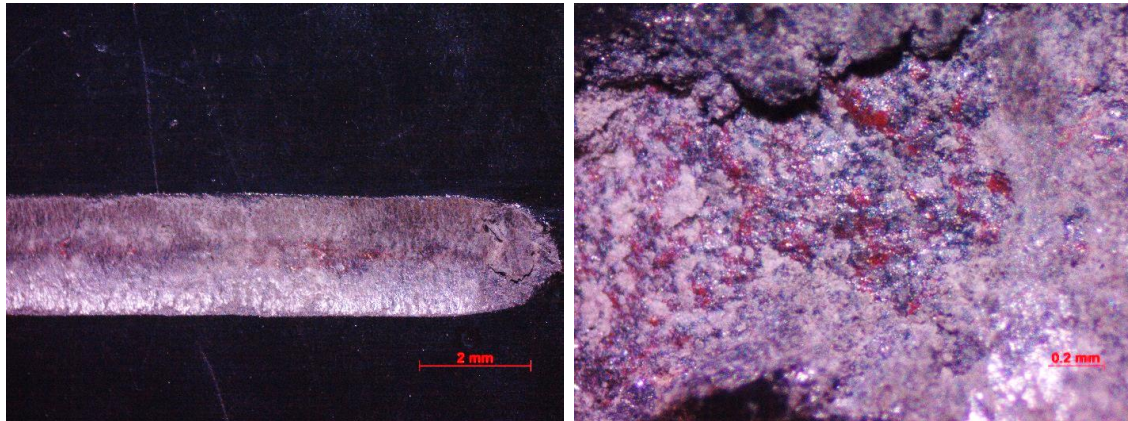


Figure 5-17: 'A Gamma' before exposure

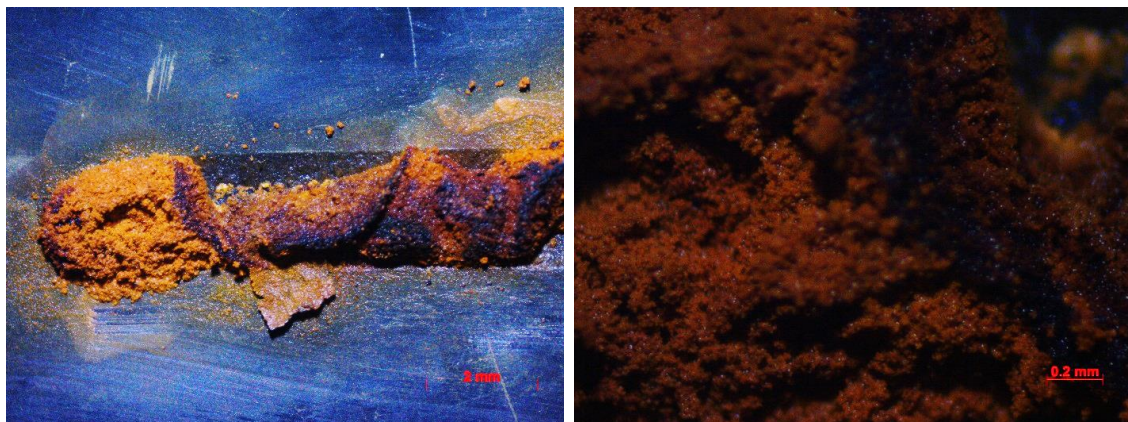


Figure 5-18: 'A Gamma' after exposure before cleaning

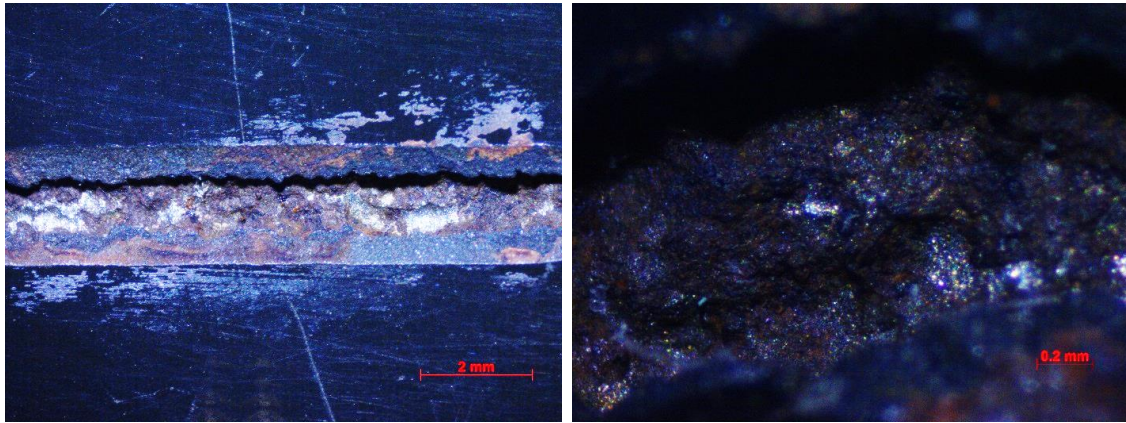


Figure 5-19: ‘A Gamma’ after exposure after cleaning

Figure 5-17 shows an image of the Gamma defect on the coating A. It is 1 cm in length and 2 mm in width. When looking at the magnified image in the same figure, red areas can be spotted. These areas refer to the primer on the metal substrate. The grey areas are the damaged coating products. These products are still covering a significant area of the defect. This implies that the defect was significant and that the metal surface was reached. It is expected that the coating will no longer protect these areas and a corrosion of the exposed metal was expected to occur. Figure 5-18 shows an image of the sample after 75 days of exposure to 3.5 wt. % NaCl solution at ambient conditions. Corrosion products has formed a thick layer and completely covered the defected area. Figure 5-19 shows images of the sample after cleaning, it was noticed that the coating was completely removed in the defected area and that the metal is completely exposed.

5.2.1.2 3D profile

To further investigate the corrosion effect on the sample, a 3D profile was acquired. Figure 5-20 and Figure 5-21 illustrate the 3D profile of the defect before and after exposure. The most important parameter in the change in the depth of the defect from a maximum of 170 μm before the test to a maximum of 320 μm . A layer of 150 μm corroded and turned into corrosion products taking with it the primer and the reminder of the coating that was covering the defected areas.

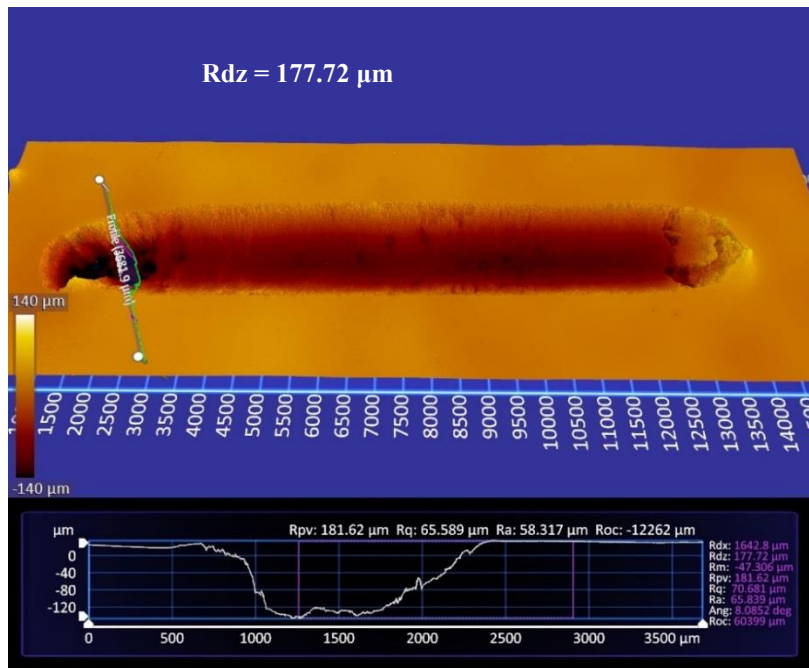


Figure 5-20: 3D profile of 'A Gamma' before exposure

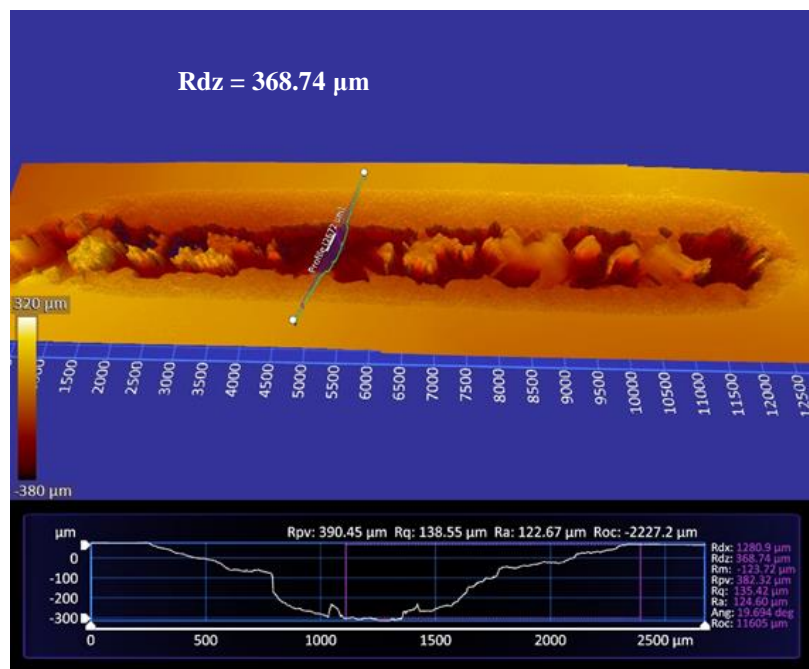


Figure 5-21: 3D profile of 'A Gamma' after exposure

5.2.1.3 *Electrochemical impedance spectroscopy*

The electrochemical impedance spectroscopic analysis of the coating exposed to 3.5 wt. % NaCl solution for selective times was performed on the basis of Bode and Nyquist plots as shown in Figure 5-22, Figure 5-23 and Figure 5-24 below. In the low frequency limit, significantly higher values of impedance in the order of 90 k Ω were observed for the first run and a phase angle close to 10° as shown in Figure 5-22. For the other runs, lower values of impedance in the order of 5 k Ω were observed and a phase angle was close to 0°. The significant difference between the EIS measurements of the first run and the following can be explained as follows. Certain areas of the defect were still covered by a thin layer of coating. After the first run, with the corrosion of metal covered by the thin film, more area was exposed to the corrosive solution. The polarization resistance then decreased slowly from 86.6 k Ω cm² to 57 k Ω cm² between day 15 and day 44. Afterwards, the R_p reached a steady value with an average of 60 k Ω cm². The consistence in the corrosion rate afterwards can be due to the corrosion products formed. The corrosion cell is vertical which allows the corrosion products to deposit on the metal surface. These products form a protective layer that inhibits the corrosion rate from further development.

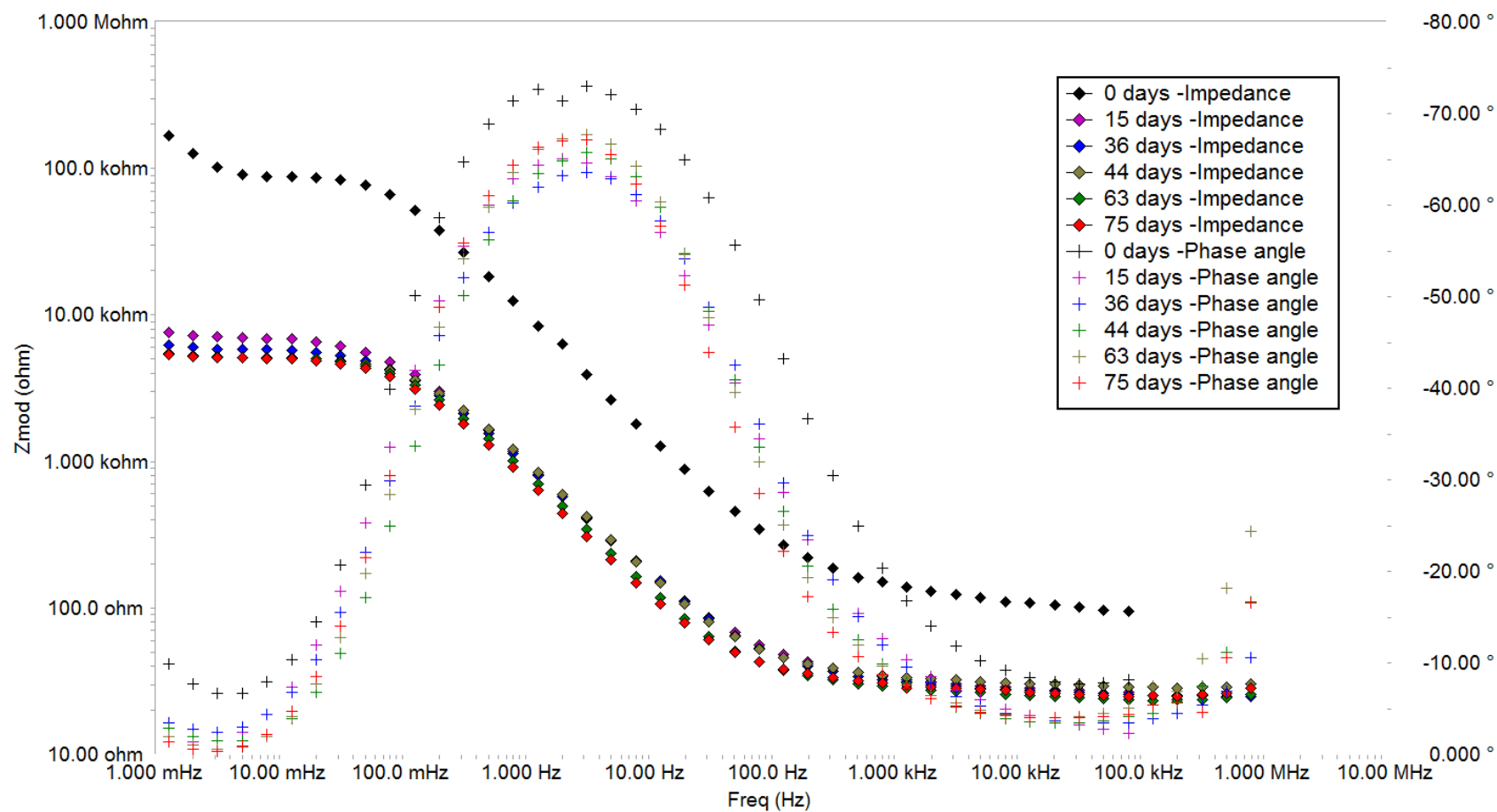


Figure 5-22: 'A Gamma' - Bode plot continuous exposure over 75 days

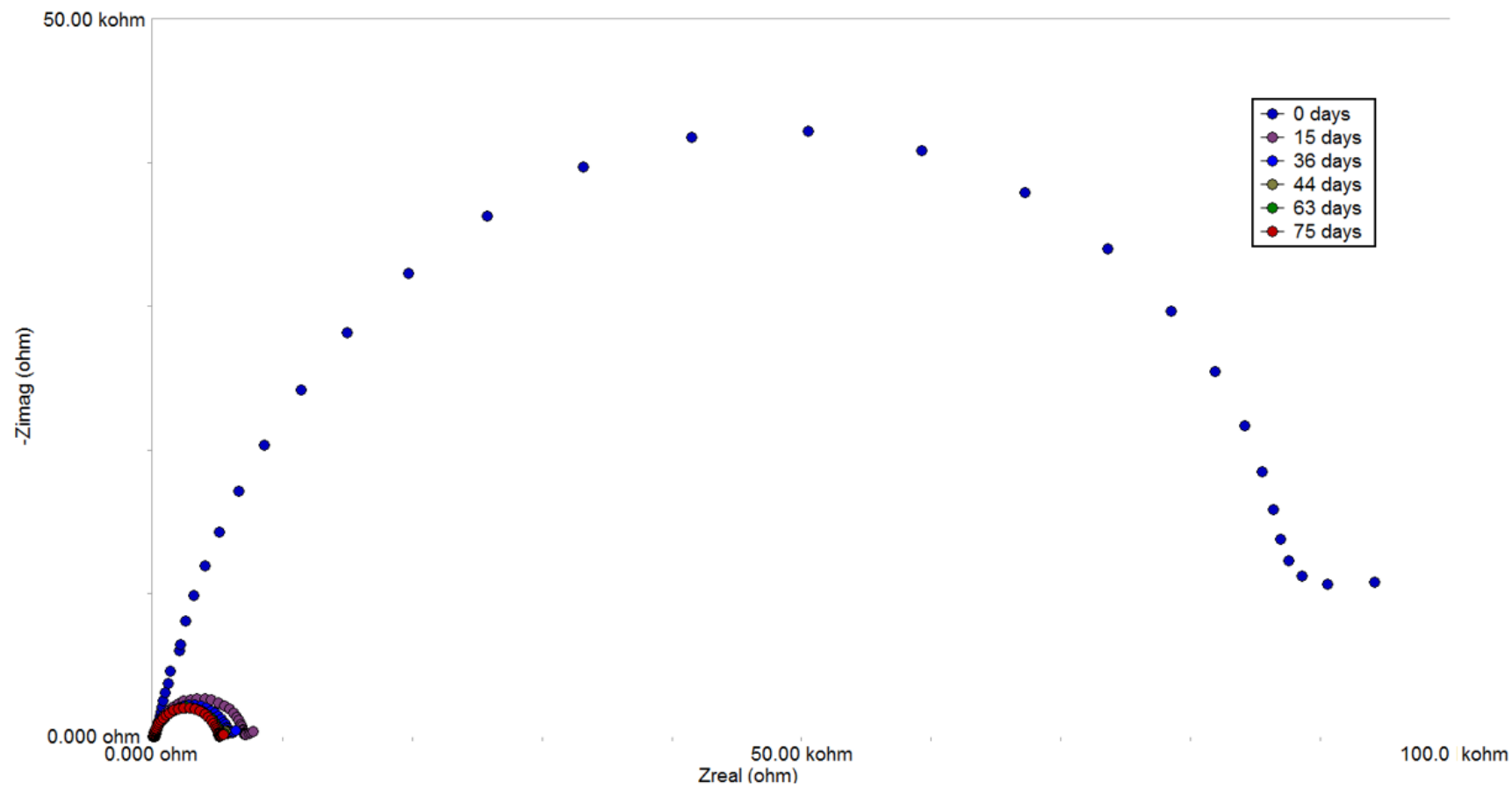


Figure 5-23: 'A Gamma' - Nyquist plot continuous exposure over 75 days

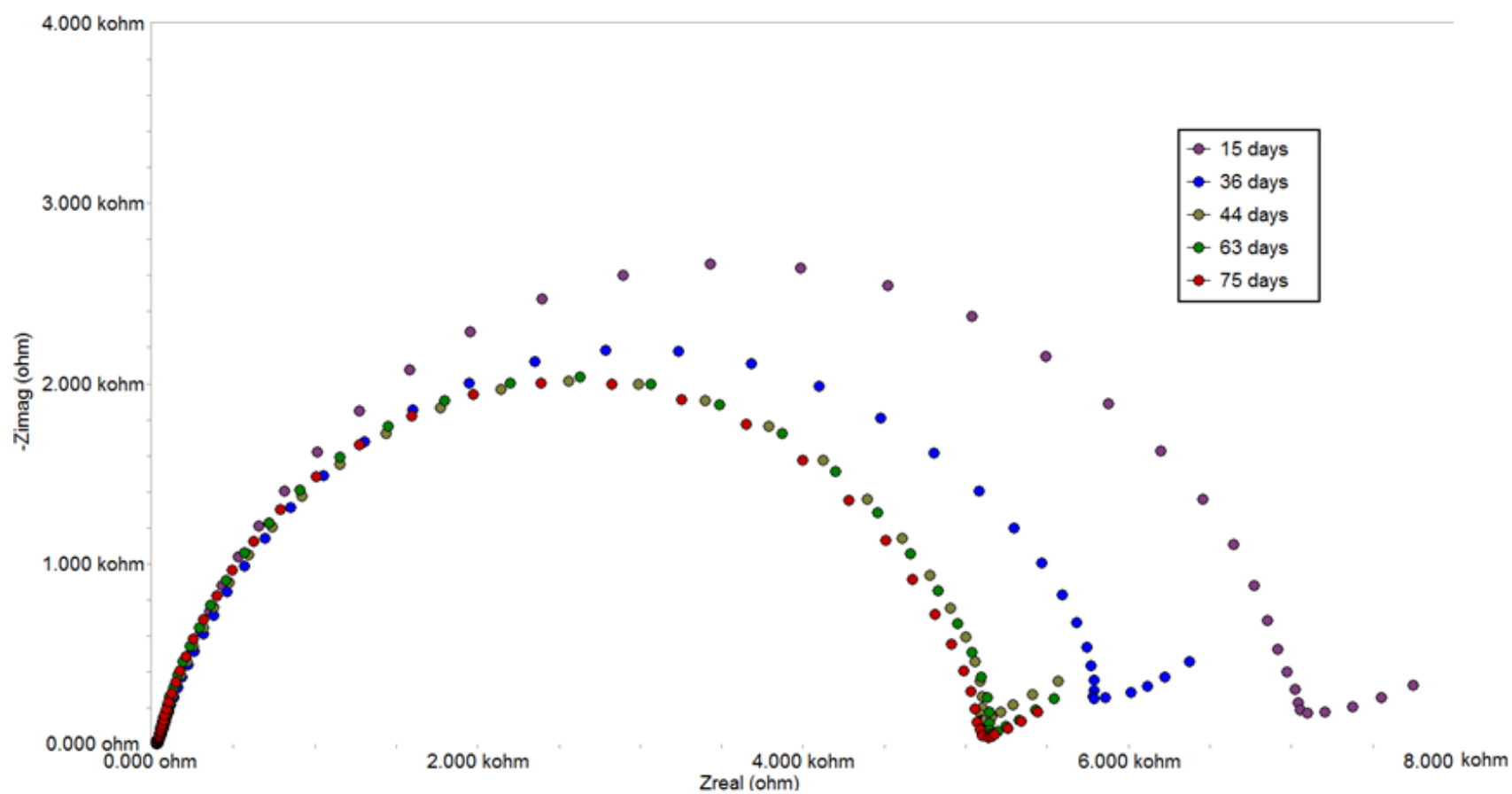


Figure 5-24: 'A Gamma' - Nyquist plot continuous exposure over 60 days (after the 15th day)

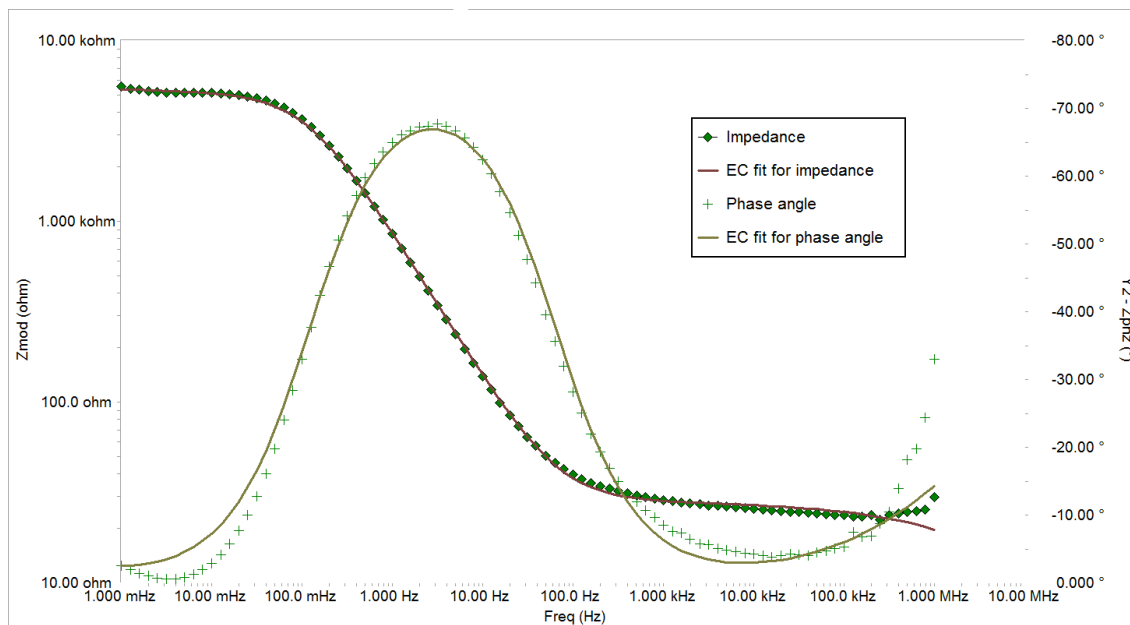


Figure 5-25: Bode plot after 83 days of exposure fitted using circuit 'B'

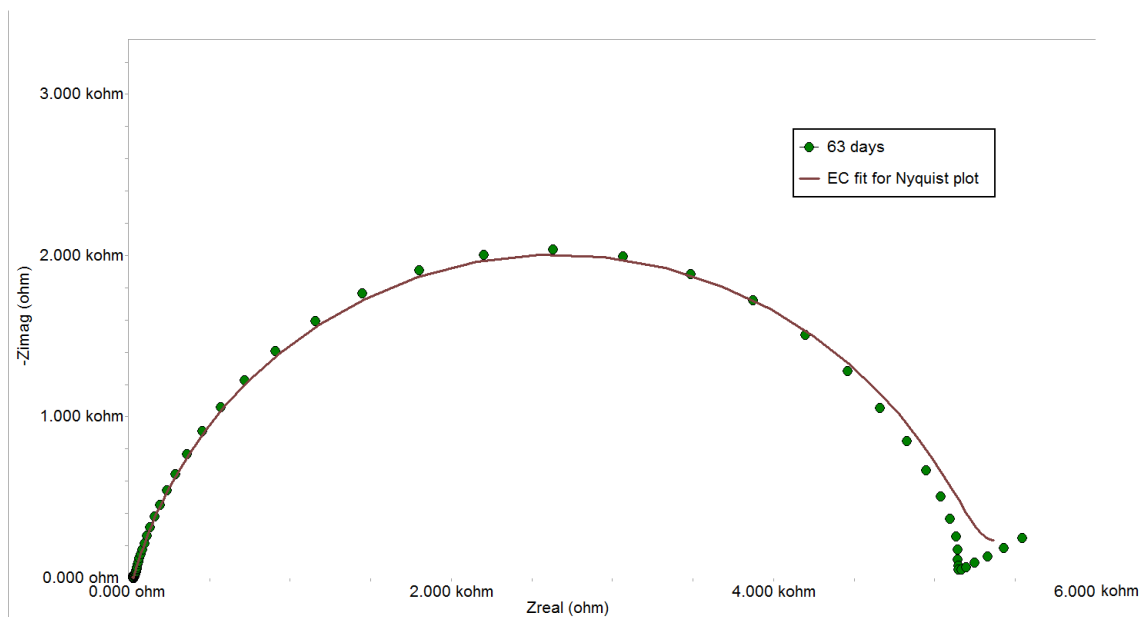


Figure 5-26: Nyquist plot after 63 days of exposure fitted using circuit 'B'

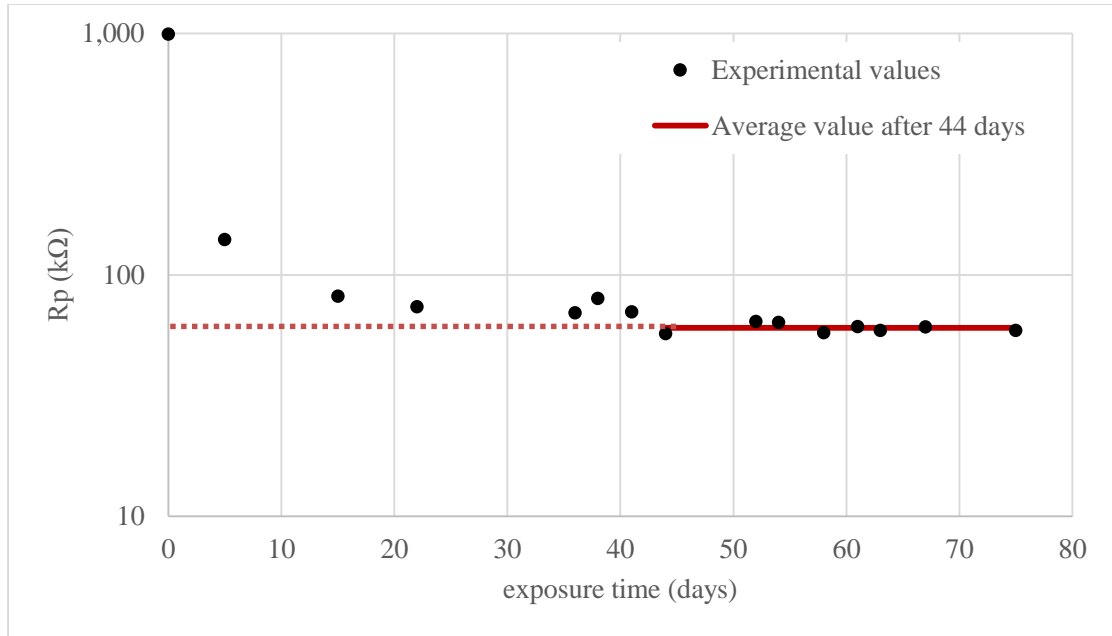


Figure 5-27: Time dependence of resistance R_p for 'A Gamma'

5.2.2 Summary

The equivalent electric circuit model 'B' shown in Figure 5-28 was applicable for samples 'A Gamma', 'H Beta', 'I Beta' and 'F'. Two time constant provided a better fit in both the Bode and Nyquist plots for all the samples. The two time constant accounts for the barrier properties and the metal interface and the corrosion product film formed in the defect regions for the damaged coating or the whole metal surface for the non-coated sample. The polarization resistance was assumed to be the sum of the resistance in parallel with the first CPE and the resistance in parallel with the second CPE in series with the Warburg element.

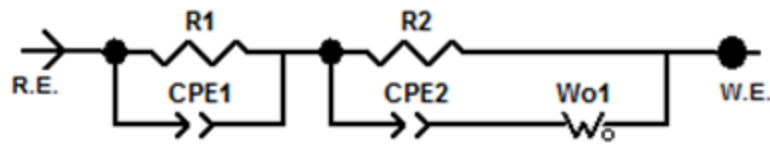


Figure 5-28: Circuit 'B'

The resistance for all the samples was significantly lower than the intact coating. For the minor defect the resistance was in the order of $10^7 \Omega \text{ cm}^2$ while for the major defect, the resistance was in the order of $10^5 \Omega \text{ cm}^2$ as shown in Figure 5-29. This indicates that the type of defect significantly affects the corrosion rate. 'H Beta' and 'I Beta' samples, where the polymer was partially removed at the defect, had a higher R_p than the 'A Gamma' sample where the coating was completely removed at the defect. However, even damaged coating still provide protection for the substrate since the resistance for a non-coated metal is in the order of $10^3 \Omega \text{ cm}^2$. The use of Warburg impedance proves the existence of solution contact with the substrate since it refers to the metal diffusion. The Warburg element proved that corrosion took place in samples 'I Beta' and 'H Beta', in which the damage was minor and primary observations didn't imply the exposure of the substrate to the solution.

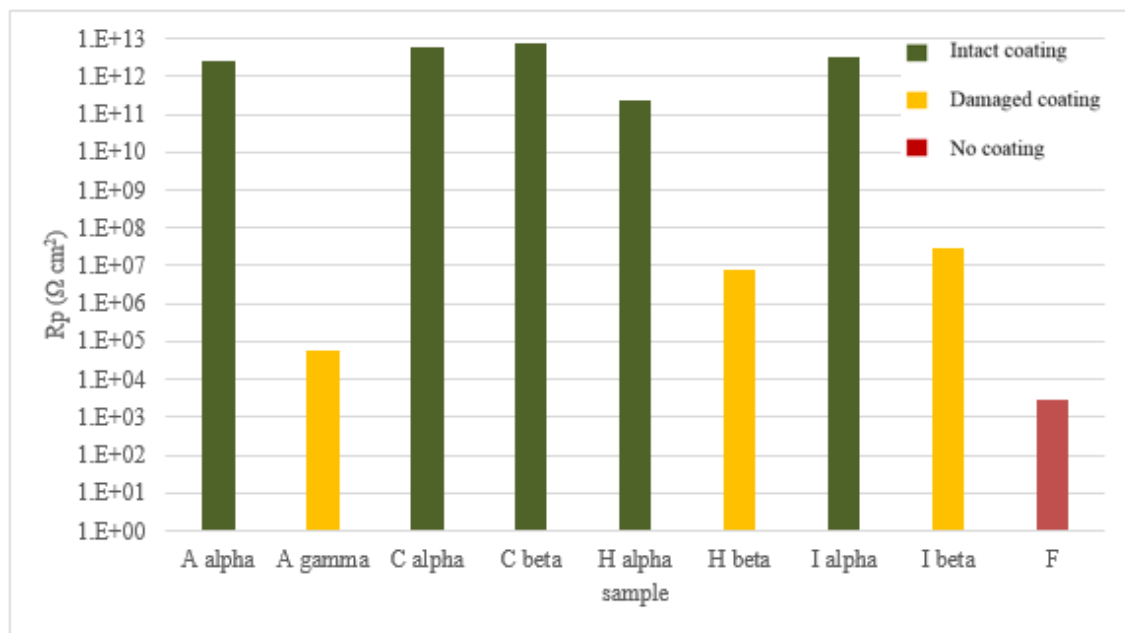


Figure 5-29: Average polarization resistance for all the tested samples

6 CONCLUSION

EIS technique proved to be a powerful tool to study the corrosion resistance of coated steel. Impedance analysis allowed continuous testing of samples exposed to corrosive environment. The designed corrosion cell was practical and efficient as well. Two different impedance models were determined. The first was for the intact polymer coated carbon steel and it consists of a solution resistance in series with a resistor in parallel with a constant phase element (CPE). High impedance of orders higher than $10^{11} \Omega \text{ cm}^2$ were obtained in the low frequency region indicating a high corrosion resistance and absence of corrosion reaction. Effective capacitance was determined from the CPE for these samples and were used to determine the coating water uptake, which was found to be negligible for intact coatings. It was also proven that the thickness of the coating have an effect on the corrosion protection since samples with higher thickness have shown higher polarization resistance. The second model was applicable for the damaged coatings. The equivalent circuit for this model included an addition of an impedance element consisting of a resistor in parallel with a CPE and Warburg element in series to the model for the intact coating. This two time constant model accounted for the barrier properties and the metal interface and the corrosion products accumulated in the defect region. The use of Warburg element indicates the existence of metal diffusion. The drop of impedance from $10^{11} \Omega \text{ cm}^2$ for the intact coating to $10^7 \Omega \text{ cm}^2$ for the damaged coating proves the existence of corrosion. The type of the damage affects the corrosion rate but follows the same impedance model. Lower impedance values in the low frequency range were obtained for the major defect.

7 FUTURE WORK

Further work is needed to understand the dependence of the polarization resistance on the coating thickness and type. Preliminary results in this research work suggested that powder polymer coating is more effective than the liquid polymer coating. However, further investigation is required to determine the best coating type. The resistance of the coating to mechanical damage should be taken into consideration as well as the cost of polymer and the coating technique. Furthermore, it is important to study the coating behavior in extreme conditions that simulate Qatar gas pipelines which are exposed to sour gas at high temperature and high pressure. A sour gas laboratory is currently under construction in Texas A&M University at Qatar and it will be equipped with autoclaves that will allow testing corrosion samples at these extreme conditions.

REFERENCES

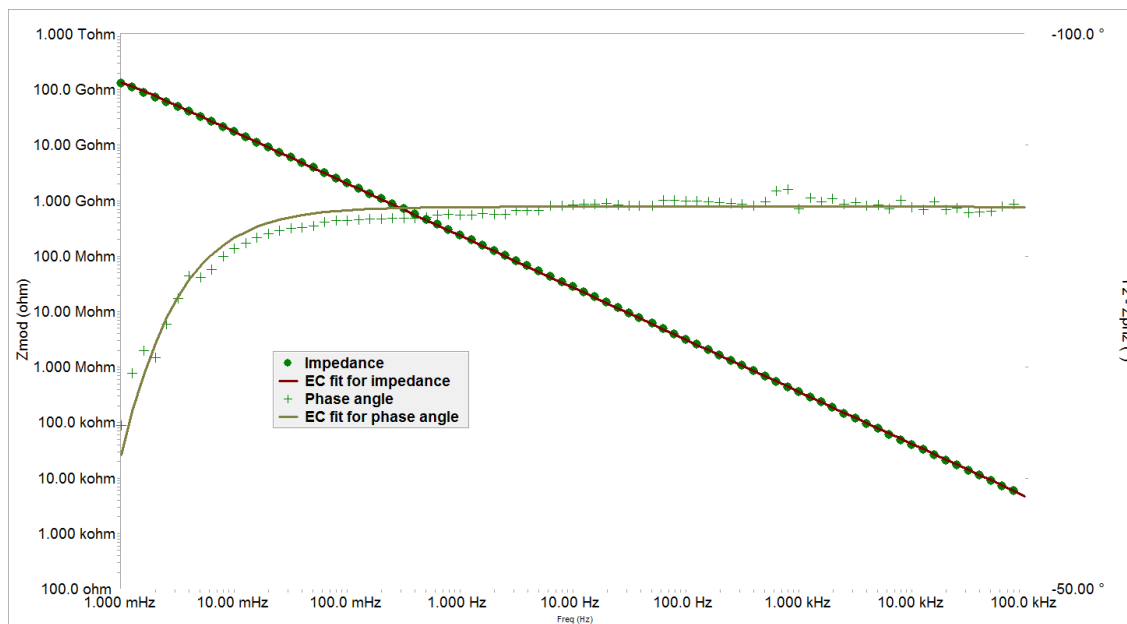
1. Zhang Y, Pang X, Qu S, Li X, Gao K. Discussion of the CO₂ Corrosion Mechanism between Low Partial Pressure and Supercritical Condition. *Corros Sci.* 2012;59:186-197. doi:10.1016/j.corsci.2012.03.006.
2. Stansbury EE, Buchanan RA. *Fundamentals of Electrochemical Corrosion*. ASM International; 2004.
3. ASM. *Metals Handbook*. Ninth. ASM; 1987.
4. Dawson J, Bruce K, John DG. *Corrosion Risk Assessment and Safety Management for Offshore Procession Facilities*. Manchester; 2001. <http://www.hse.gov.uk/research/otopdf/1999/oto99064.pdf>.
5. Davis JR. *Corrosion - Understanding the Basics*. ASM International; 2000. https://app.knovel.com/web/toc.v/cid:kpCUB00002/viewerType:toc/root_slug:corrosion-understanding. Accessed February 25, 2015.
6. Landolf D. *Corrosion And Surface Chemistry of Metals*. First. EPFL Press; 2007:540.
7. Kendig M, Scully J. Basic Aspects of Electrochemical Impedance Application for the Life Prediction of Organic Coatings on Metals. *Corrosion*. 1990;46(January):22-29.
8. Hattori M, Nishikata A, Tsuru T. EIS Study on Degradation of Polymer-Coated Steel under Ultraviolet Radiation. *Corros Sci.* 2010;52(6):2080-2087. doi:10.1016/j.corsci.2010.01.038.
9. Yabuki A, Okumura K. Self-healing Coatings Using Superabsorbent Polymers for Corrosion Inhibition in Carbon Steel. *Corros Sci.* 2012;59:258-262. doi:10.1016/j.corsci.2012.03.007.
10. Scholz F. *Electroanalytical Methods Guide to Experiments and Applications*. Second. Springer; 2010.
11. ASTM Standard G102, 2004 (2010), "Calculation of Corrosion Rates and Related Information from Electrochemical Measurements," ASTM International, West Conshohocken, PA, 2010, DOI: 10.1520/G0102-89R10, www.astm.org.
12. Mansfeld F. Tafel Slopes and Corrosion Rates from Polarization Resistance Measurements. *Corrosion*. 1973;29:397-402. <http://corrosionjournal.org/doi/abs/10.5006/0010-9312-29.10.397>.
13. Hirschorn B, Orazem ME, Tribollet B, Vivier V, Frateur I, Musiani M. Constant-Phase-Element Behavior Caused by Resistivity Distributions in Films. *J Electrochem Soc.* 2010;157(12):C452. doi:10.1149/1.3499564.
14. Brug GJ, Van Den Eeden ALG, Sluyters-Rehbach M, Sluyters JH. The Analysis of Electrode Impedances Complicated by the Presence of a Constant Phase Element. *J Electroanal Chem.* 1984;176:275-295.

15. Castela AS, Simões AM. Assessment of Water Uptake in Coil Coatings by Capacitance Measurements. *Prog Org Coatings*. 2003;46(October 2002):55-61. doi:10.1016/S0300-9440(02)00190-X.
16. Moreno C, Hernández S, Santana JJ, Guzmán JG, Souto RM, González S. Characterization of Water Uptake by Organic Coatings Used for the Corrosion Protection of Steel as Determined from Capacitance Measurements. *Int J Electrochem Sci*. 2012;7:7390-7403.
17. Sykes JM. A Variant of the Brasher–Kingsbury Equation. *Corros Sci*. 2004;46(3):515-517. doi:10.1016/j.corsci.2003.10.001.
18. Rosero-Navarro NC, Pellice SA, Durán A, Aparicio M. Effects of Ce-containing Sol–gel Coatings Reinforced with SiO₂ Nanoparticles on the Protection of AA2024. *Corros Sci*. 2008;50(5):1283-1291. doi:10.1016/j.corsci.2008.01.031.
19. Zhao J. Corrosion Protection of Untreated AA-2024-T3 in Chloride Solution by a Chromate Conversion Coating Monitored with Raman Spectroscopy. *J Electrochem Soc*. 1998;145(7):2258. doi:10.1149/1.1838630.
20. Jianguo L, Gaoping G, Chuanwei Y. EIS Study of Corrosion Behaviour of Organic Coating/Dacromet Composite Systems. *Electrochim Acta*. 2005;50(16-17):3320-3332. doi:10.1016/j.electacta.2004.12.010.
21. Fedrizzi L, Rodriguez FJ, Rossi S, Deflorian F, Maggio R Di. The Use of Electrochemical Techniques to Study the Corrosion Behaviour of Organic Coatings on Steel Pretreated with Sol – gel Zirconia Films. *Electrochim Acta*. 2001;46:3715-3724.
22. Verdian MM, Raeissi K, Salehi M. Electrochemical Impedance Spectroscopy of HVOF-sprayed NiTi Intermetallic Coatings Deposited on AISI 1045 Steel. *J Alloys Compd*. 2010;507(1):42-46. doi:10.1016/j.jallcom.2010.07.132.
23. Liu XP, Zheng TL, Xiong JP. Corrosion Resistance of Polyurea Polyaspartic Ester Coating in 3.5% NaCl by EIS. *Int J Electrochem Sci*. 2013;8:11588-11595.
24. Mouanga M, Berçot P. Comparison of Corrosion Behaviour of Zinc in NaCl and in NaOH Solutions; Part II: Electrochemical Analyses. *Corros Sci*. 2010;52(12):3993-4000. doi:10.1016/j.corsci.2010.08.018.
25. Orazem ME, Tribollet B. *Electrochemical Impedance Spectroscopy*. John Wiley & Sons, Inc; 2008.
26. Dhoke SK, Khanna AS. Electrochemical Impedance Spectroscopy (EIS) Study of Nano-alumina Modified Alkyd Based Waterborne Coatings. *Prog Org Coatings*. 2012;74(1):92-99. doi:10.1016/j.porgcoat.2011.11.020.
27. Martínez I, Andrade C. Application of EIS to Cathodically Protected Steel: Tests in Sodium Chloride Solution and in Chloride Contaminated Concrete. *Corros Sci*. 2008;50(10):2948-2958. doi:10.1016/j.corsci.2008.07.012.

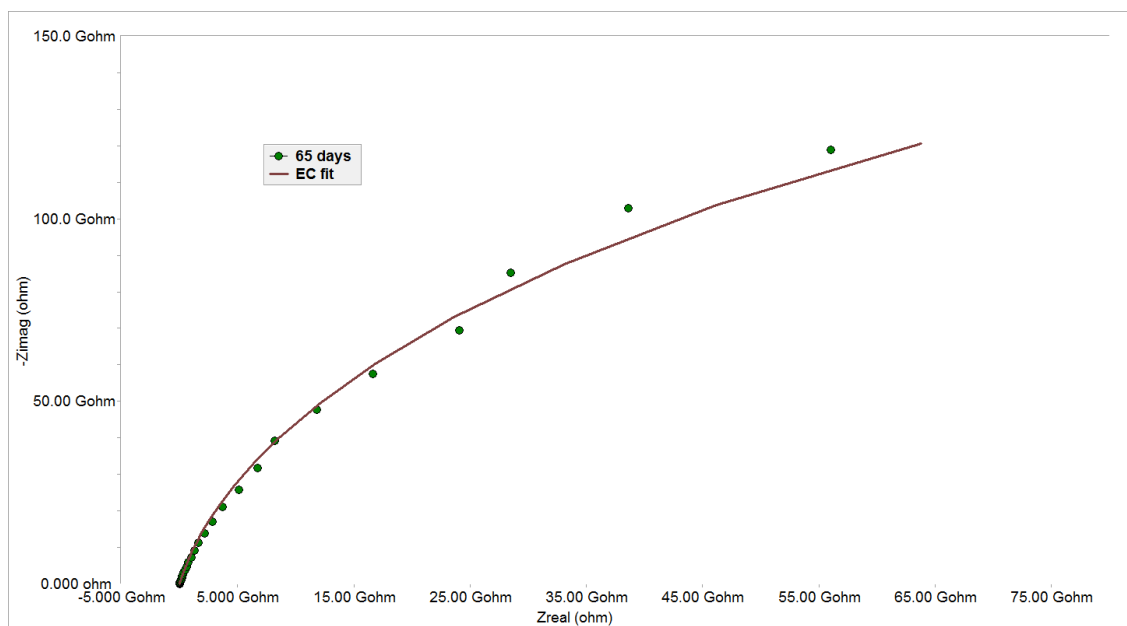
28. Ramezanzadeh B, Attar MM, Farzam M. Corrosion Performance of a Hot-dip Galvanized Steel Treated by Different Kinds of Conversion Coatings. *Surf Coatings Technol.* 2010;205(3):874-884. doi:10.1016/j.surfcoat.2010.08.028.
29. Liu C, Bi Q, Matthews A. EIS Comparison on Corrosion Performance of PVD TiN and CrN Coated Mild Steel in 0.5 N NaCl Aqueous Solution. *Corros Sci.* 2001;43(10):1953-1961. doi:10.1016/S0010-938X(00)00188-8.
30. Youssef KMS, Koch CC, Fedkiw PS. Improved Corrosion Behavior of Nanocrystalline Zinc Produced by Pulse-current Electrodeposition. *Corros Sci.* 2004;46(1):51-64. doi:10.1016/S0010-938X(03)00142-2.
31. Optical Profiler Basics. Zygo. <http://www.zygo.com/?/met/profilers/opticalprofilersabout.htm>. Accessed January 13, 2015.
32. ISO Standard 16773-2, 2007, "Paints and Varnishes - Electrochemical Impedance Spectroscopy (EIS) on High-impedance Coated Specimens - Part 2: Collection of Data," NSAI, Ireland, Dublin, 2007, DOI: ISO 16773-2:2007:E, www.standards.ie.

APPENDIX

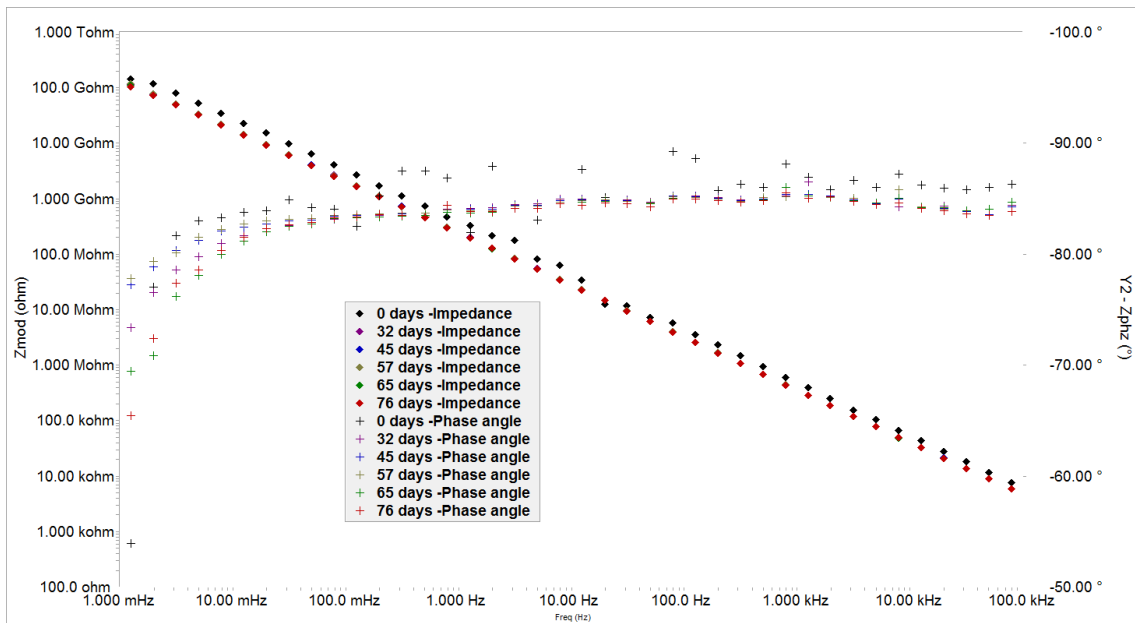
'C Alpha' EIS results



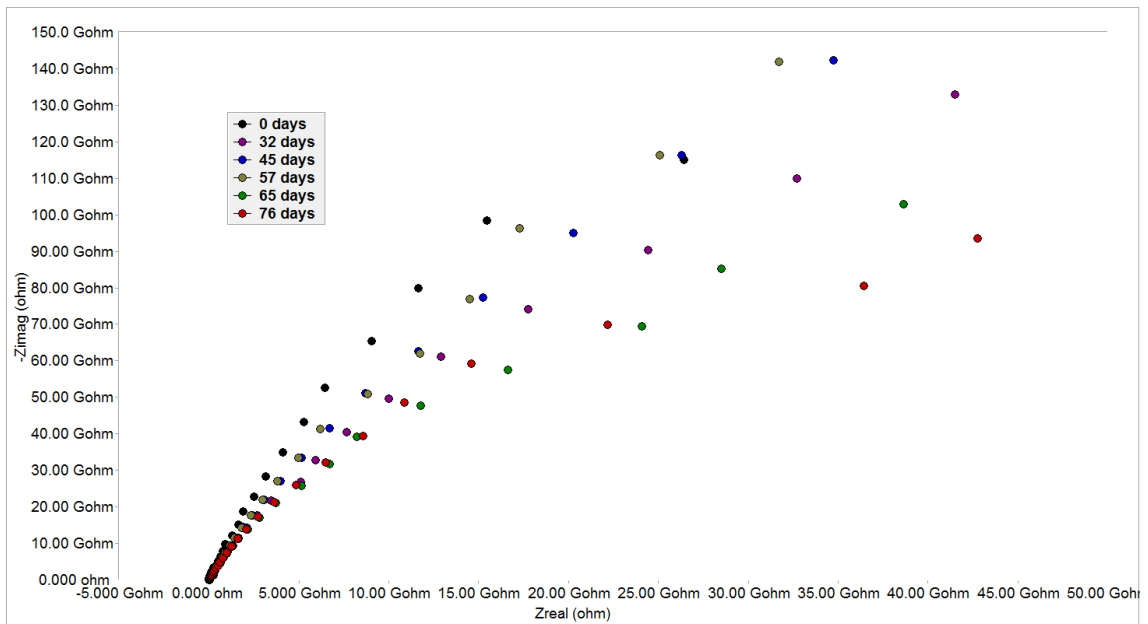
'C Alpha' Bode plot after 65 days fitted using circuit 'A'



'C Alpha' Nyquist plot after 65 days fitted using circuit 'A'

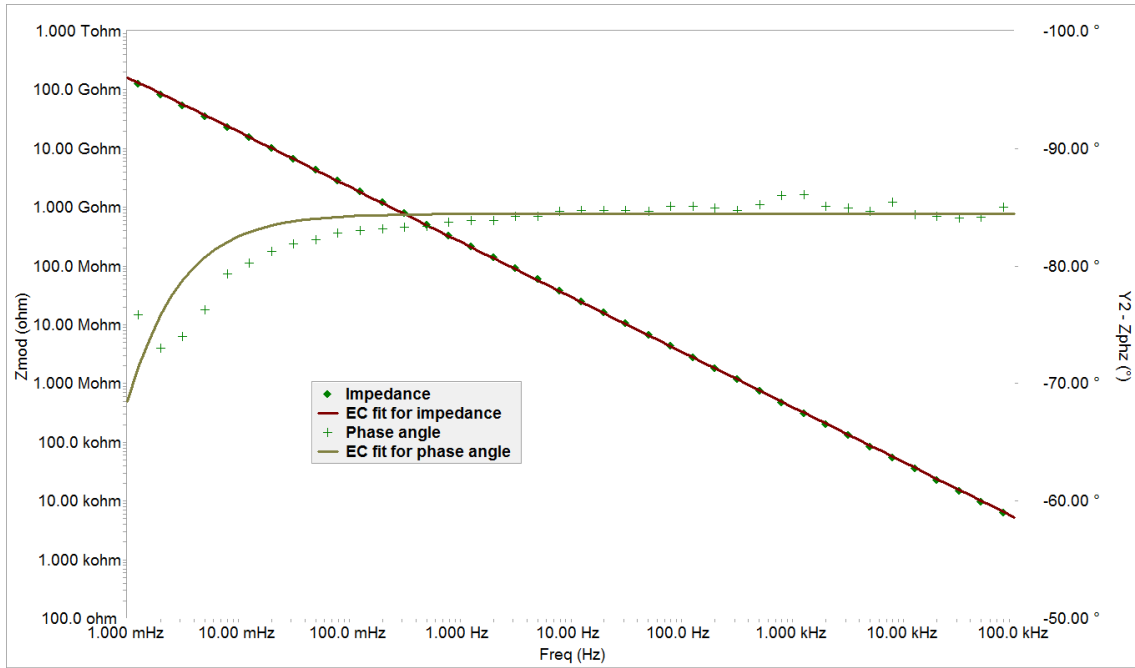


'C Alpha' Bode plot for continuous exposure over 76 days

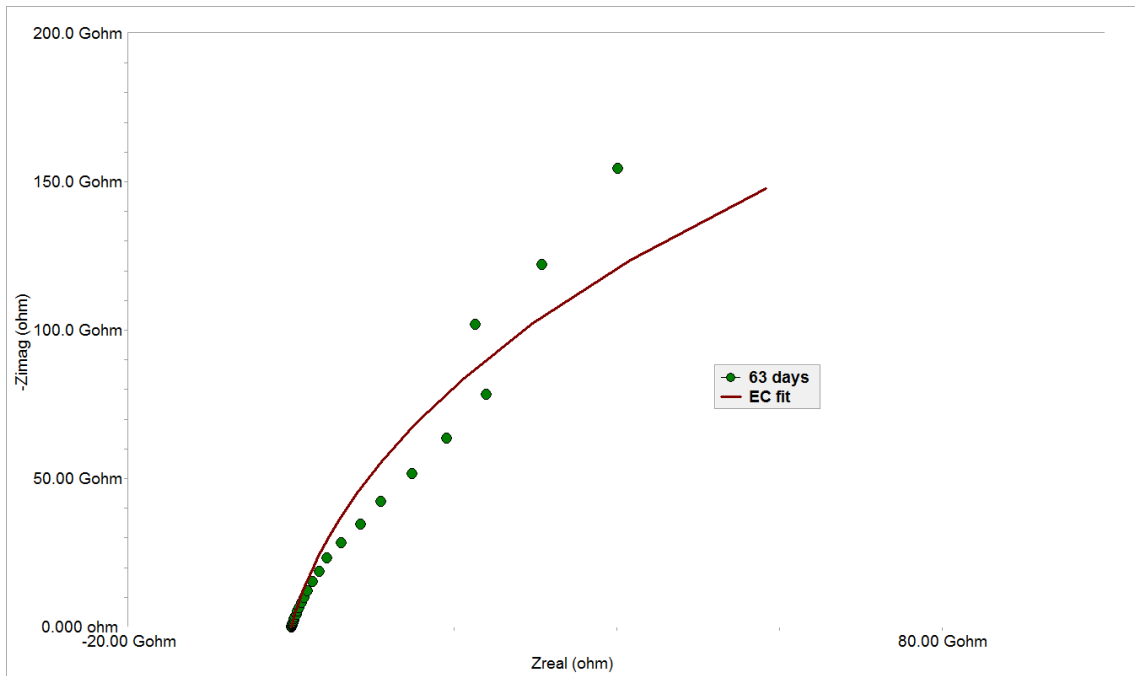


'C Alpha' Bode plot for continuous exposure over 76 days

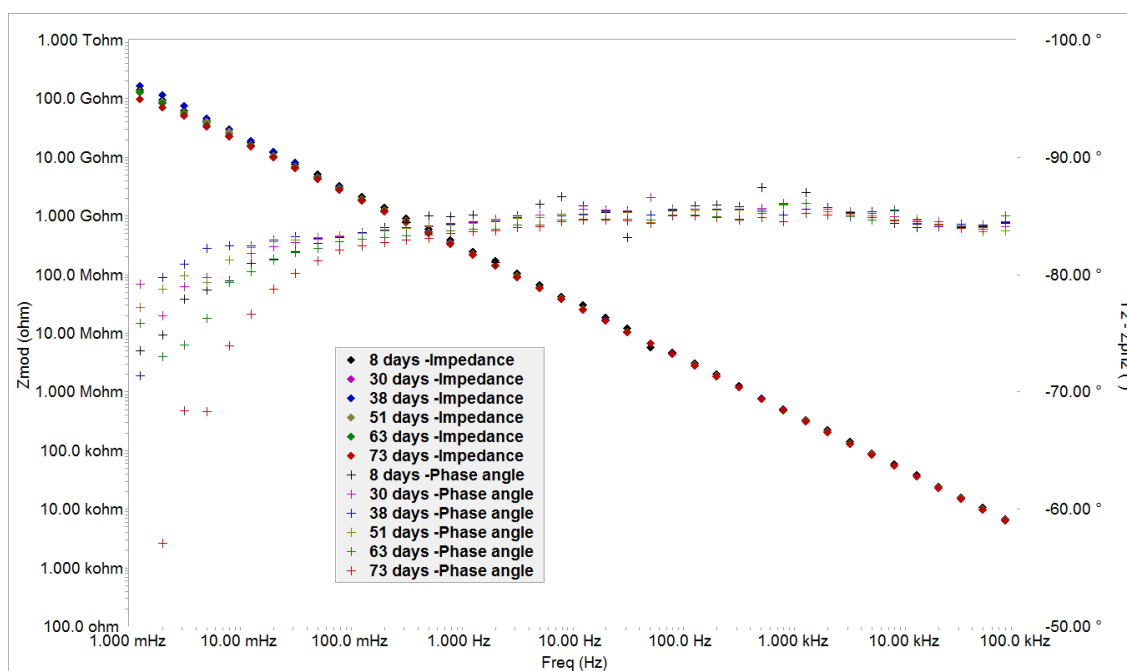
'C Beta' EIS results



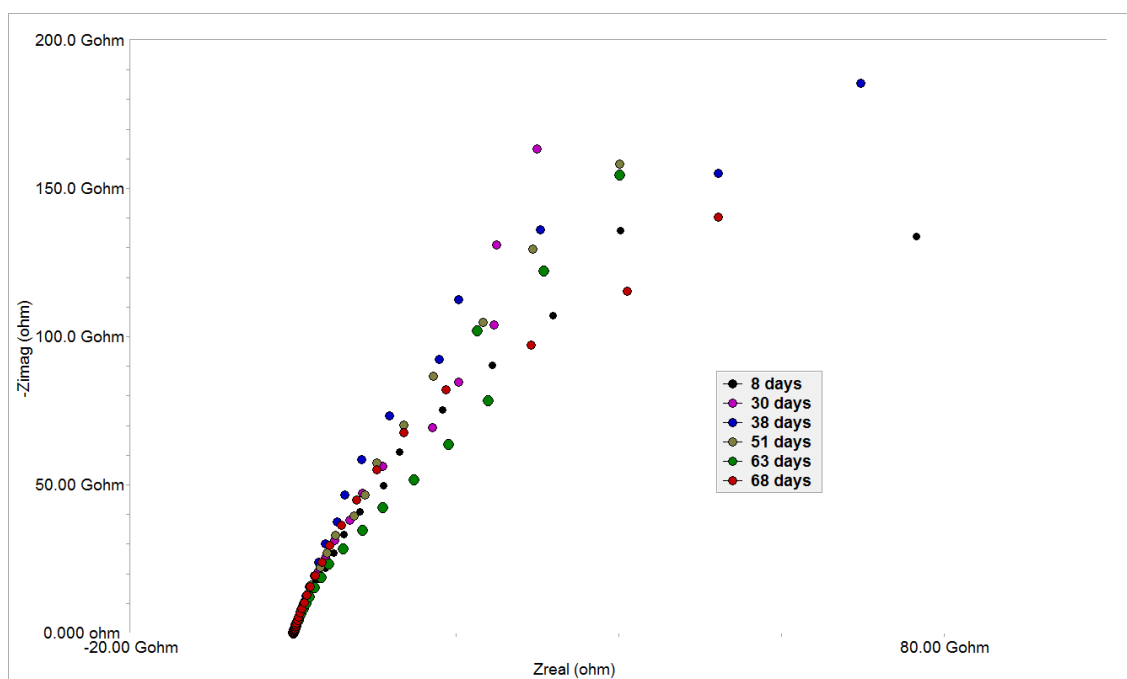
'C Beta' Bode plot after 63 days fitted using circuit 'A'



'C Beta' Nyquist plot after 63 days fitted using circuit 'A'

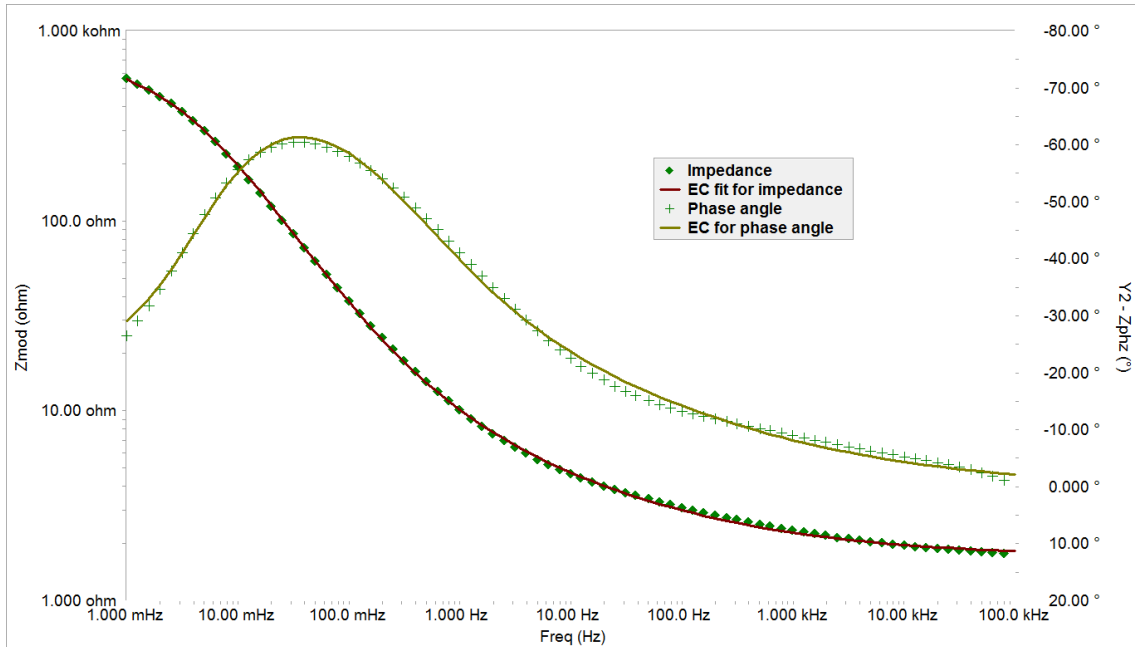


'C Beta' Bode plot for continuous exposure over 68 days

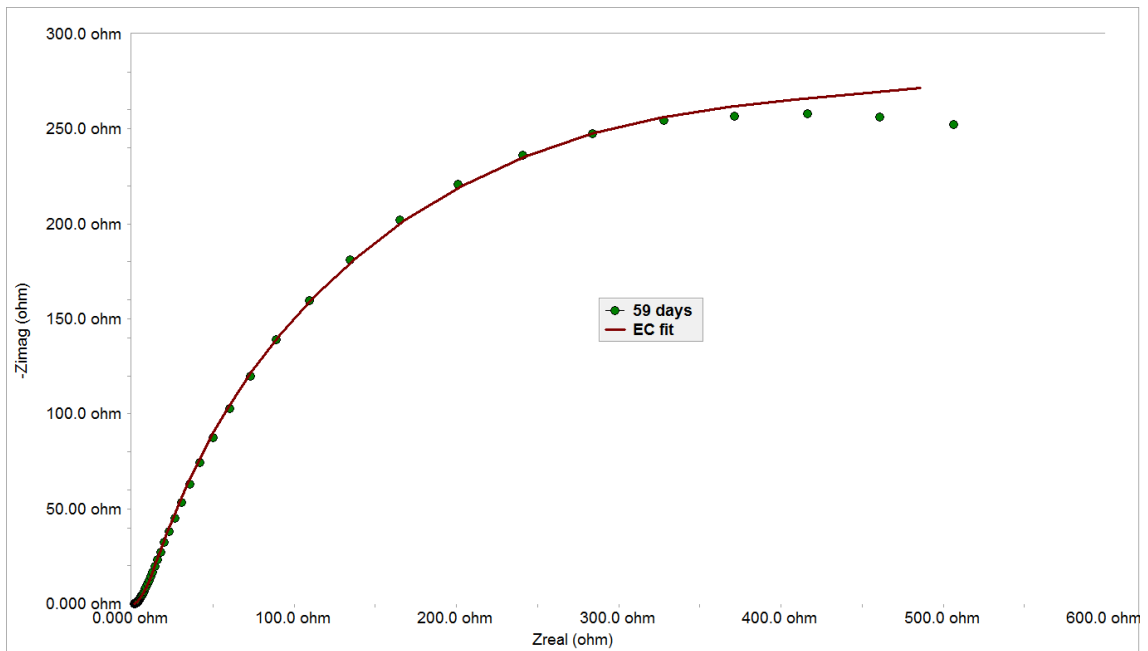


'C Beta' Nyquist plot for continuous exposure over 68 days

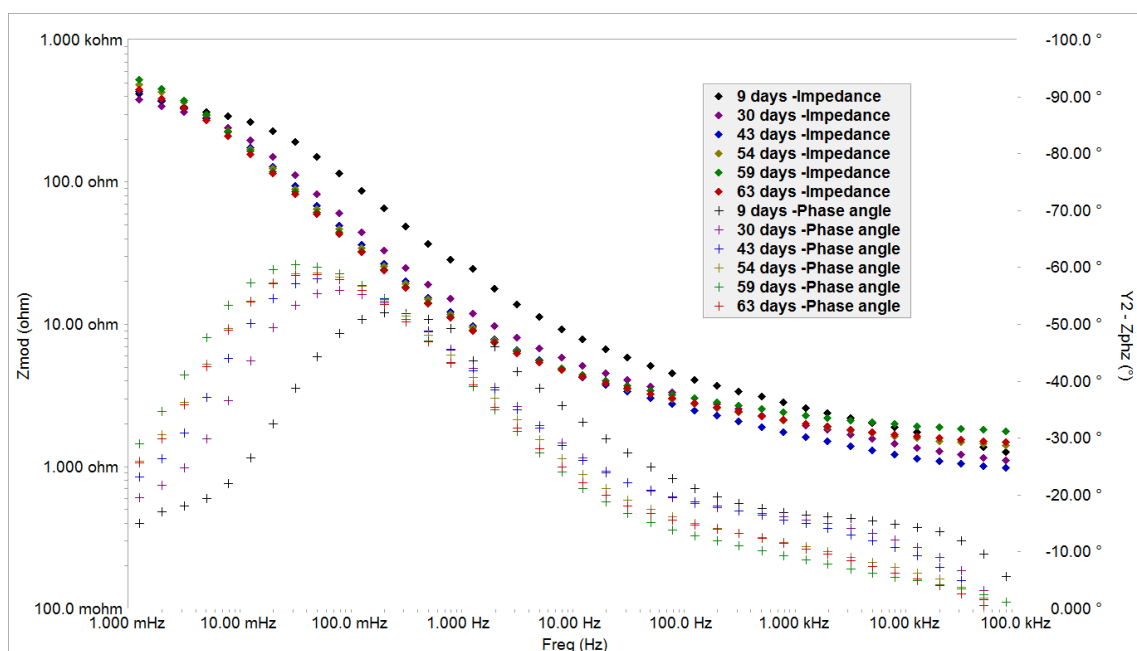
'F Alpha' EIS results



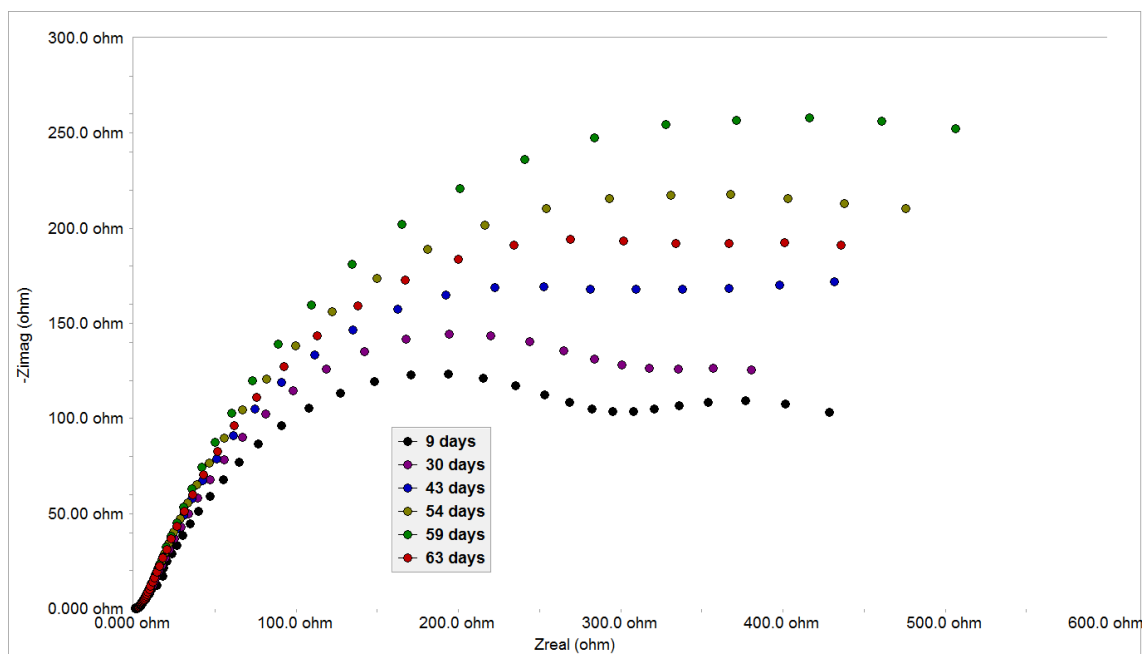
'F Alpha' Bode plot after 59 days fitted using circuit 'B'



'F Alpha' Nyquist plot after 59 days fitted using circuit 'B'

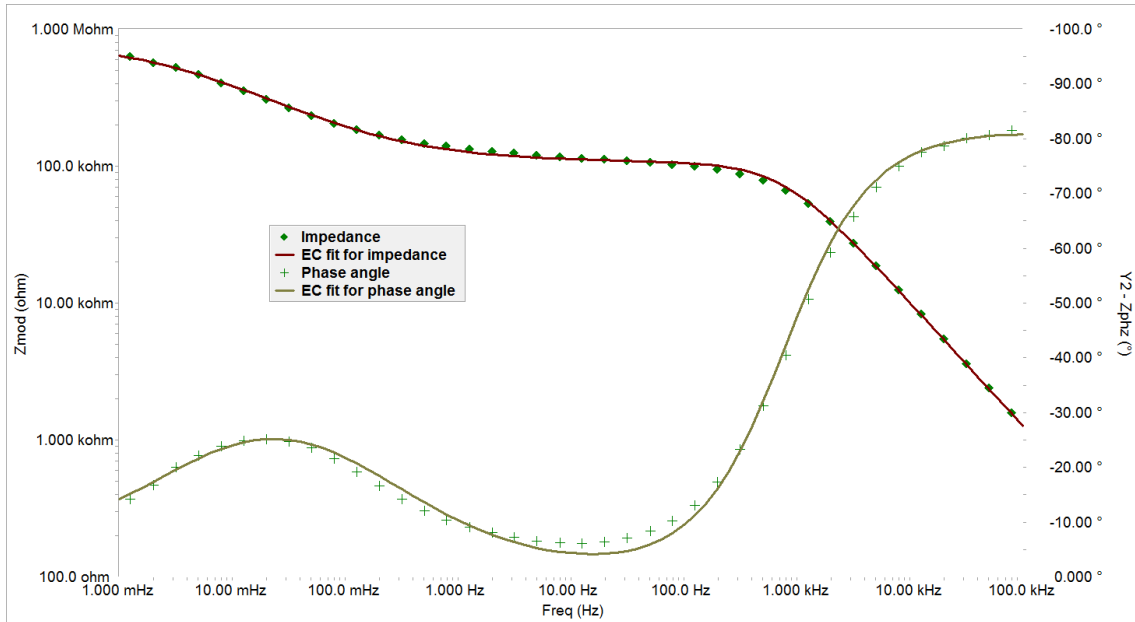


'F Alpha' Bode plot for continuous exposure over 63 days

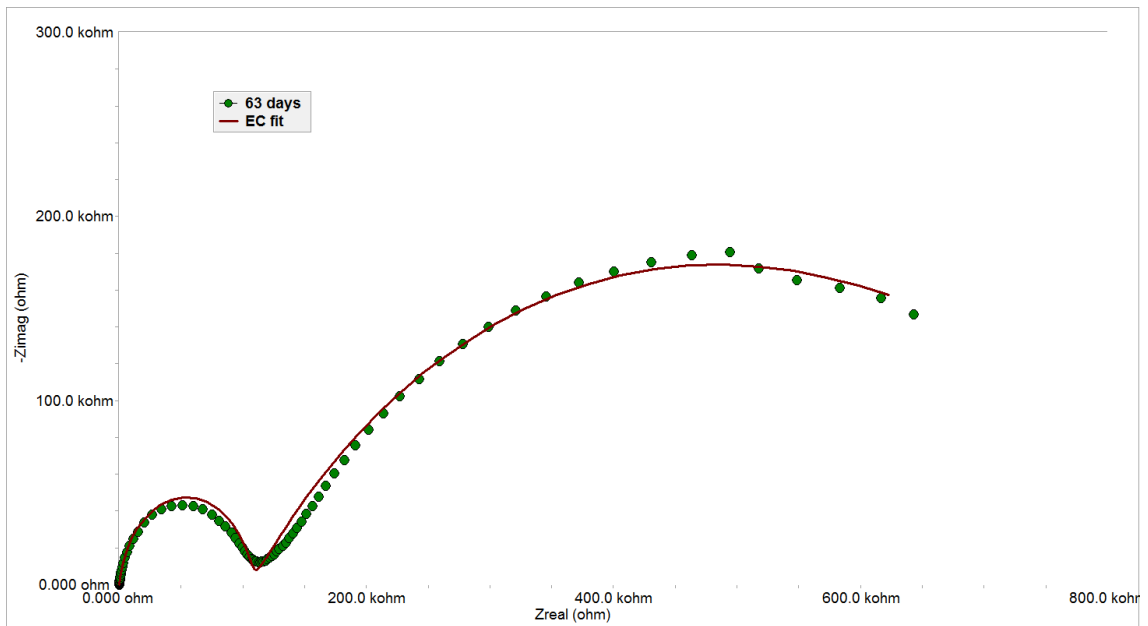


'F Alpha' Nyquist plot for continuous exposure over 63 days

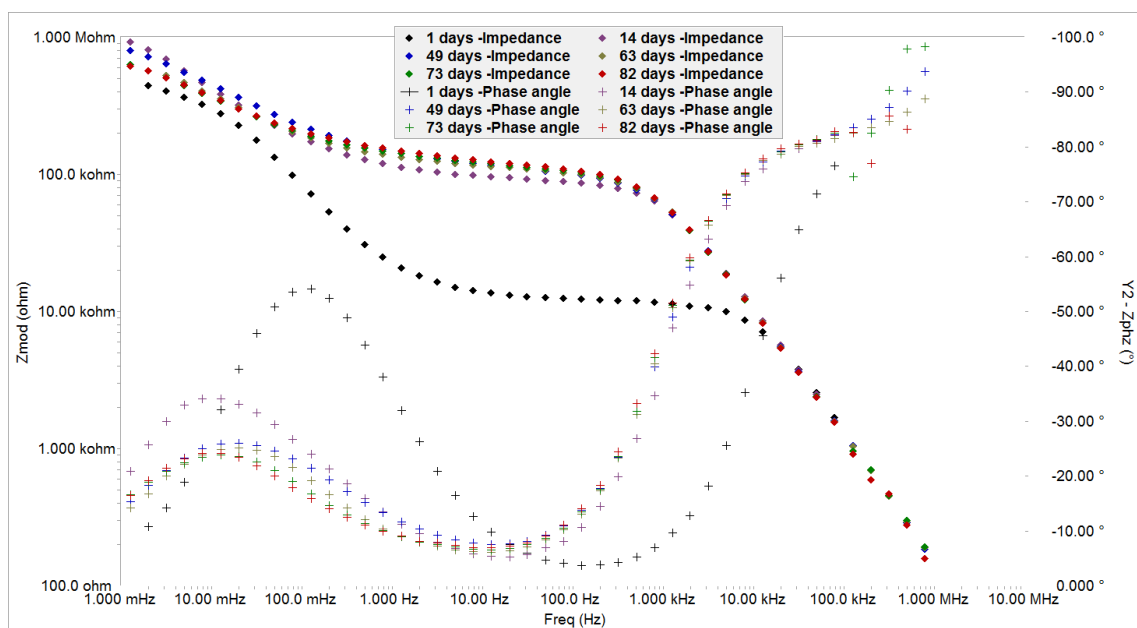
'H Beta' EIS results



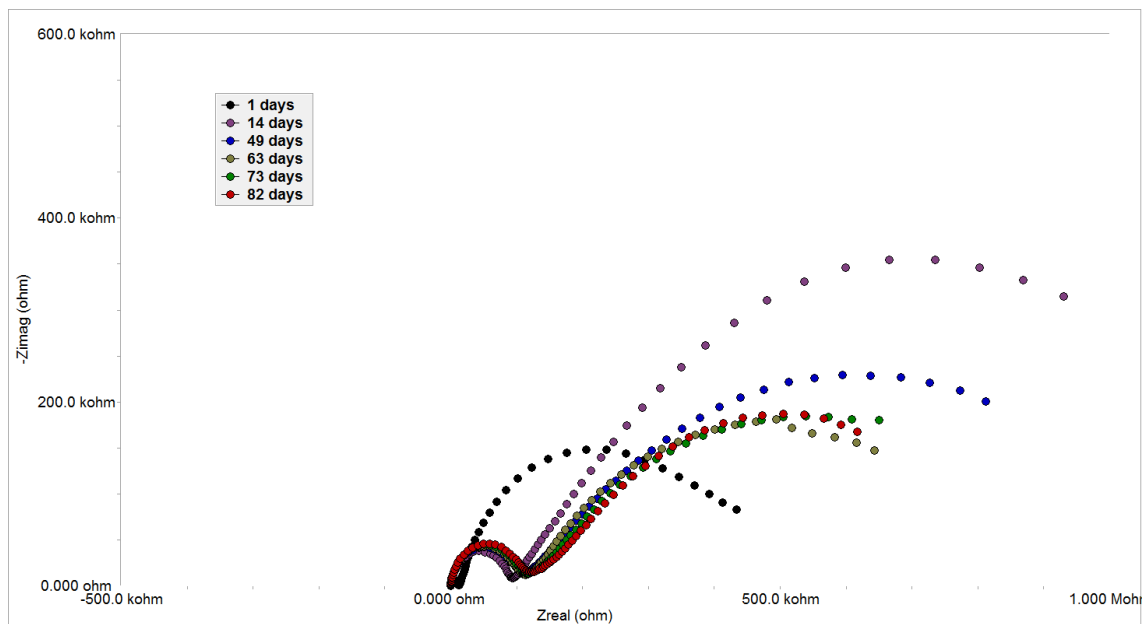
'H Beta' Bode plot after 63 days of exposure fitted using circuit 'B'



'H Beta' Nyquist plot after 63 days of exposure fitted using circuit 'B'

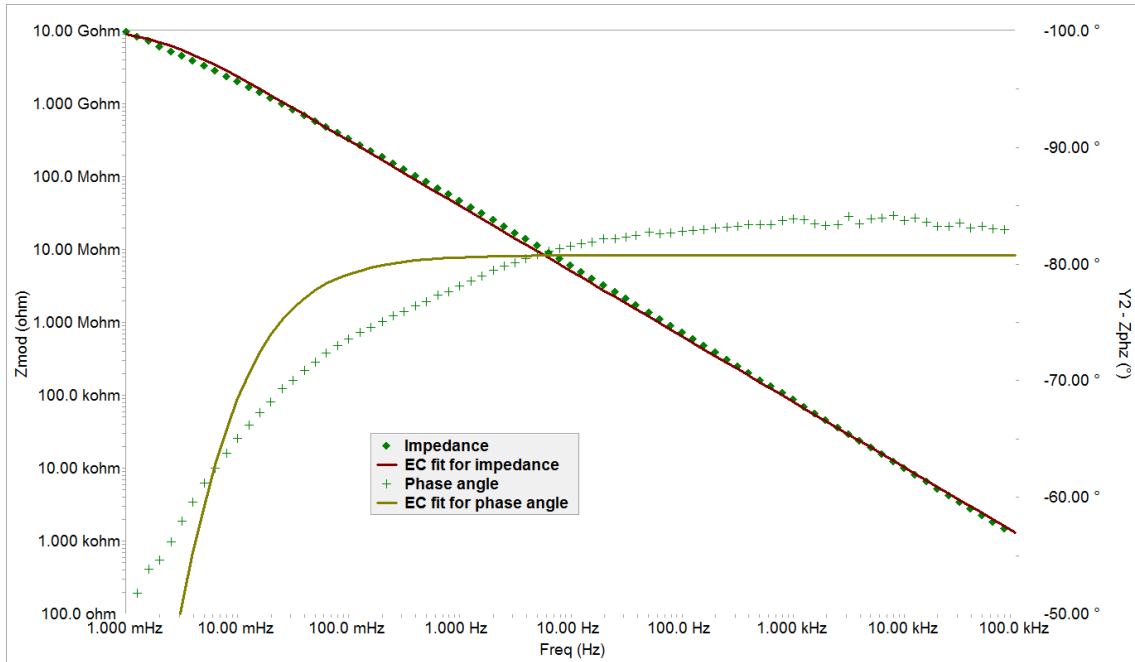


'H Beta' Bode plot for continuous exposure over 82 days

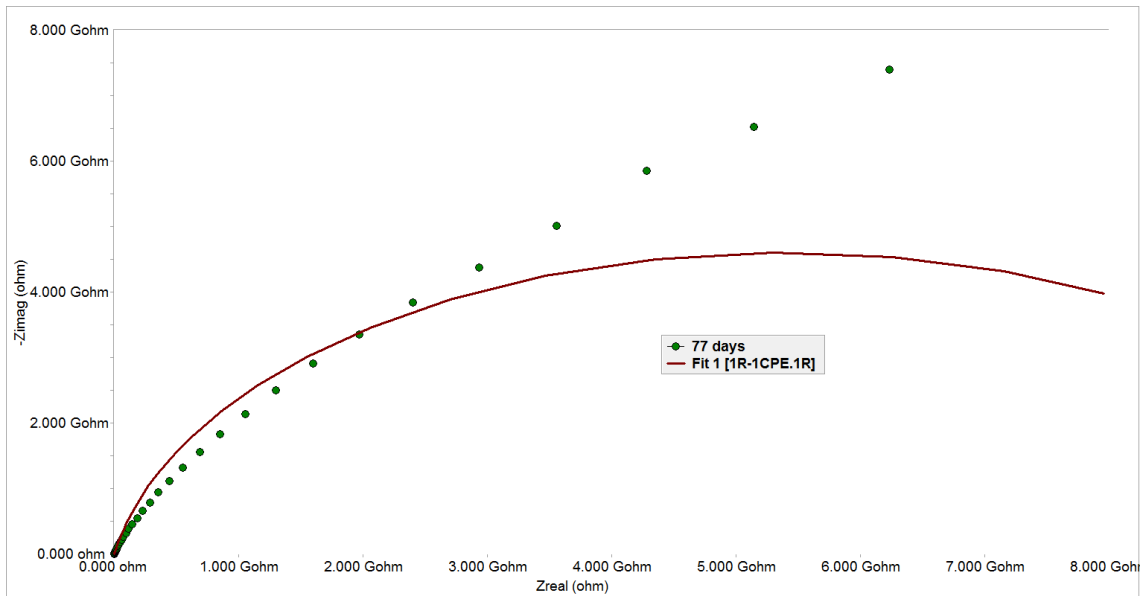


'H Beta' Nyquist plot for continuous exposure over 82 days

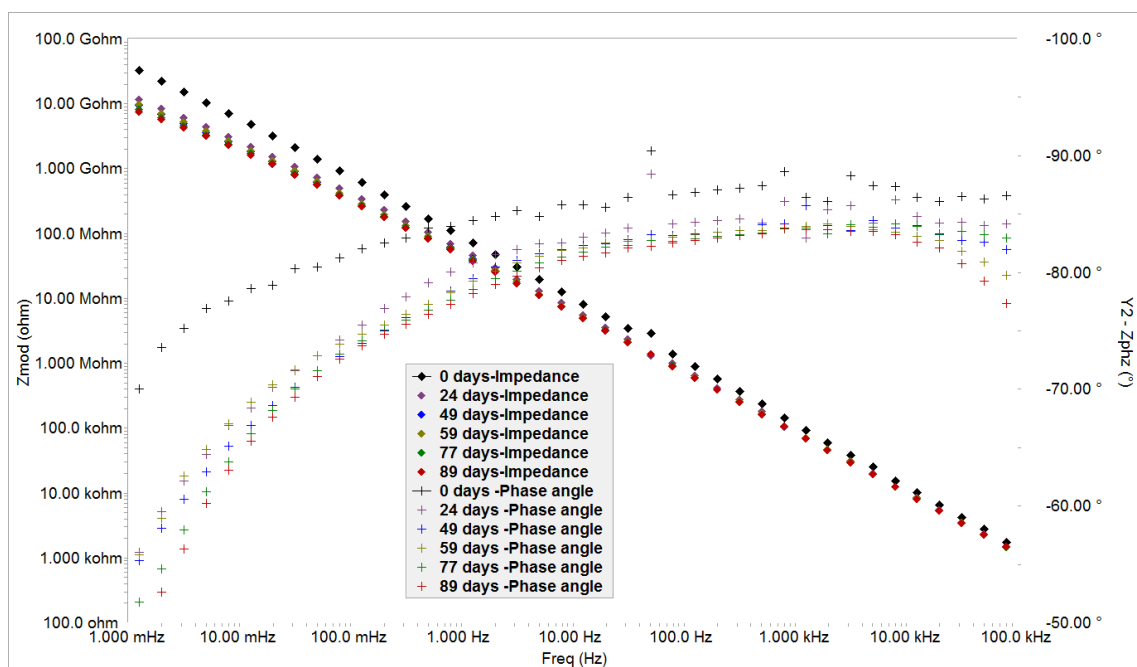
'H Alpha' EIS results



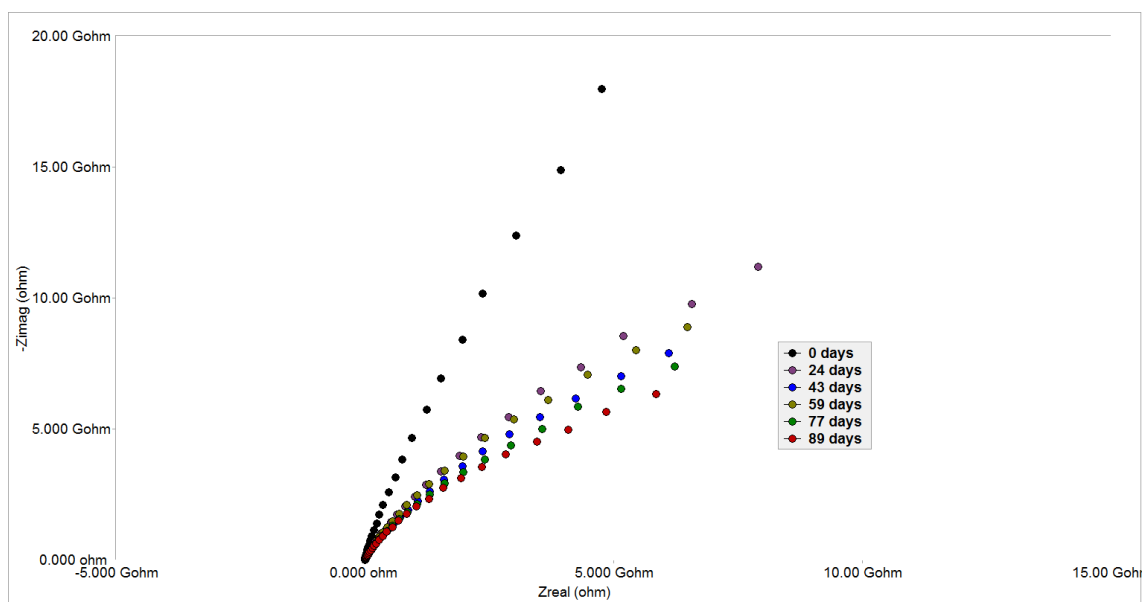
'H Alpha' Bode plot after 77 days of exposure fitted using circuit 'A'



'H Alpha' Nyquist plot after 77 days of exposure fitted using circuit 'A'

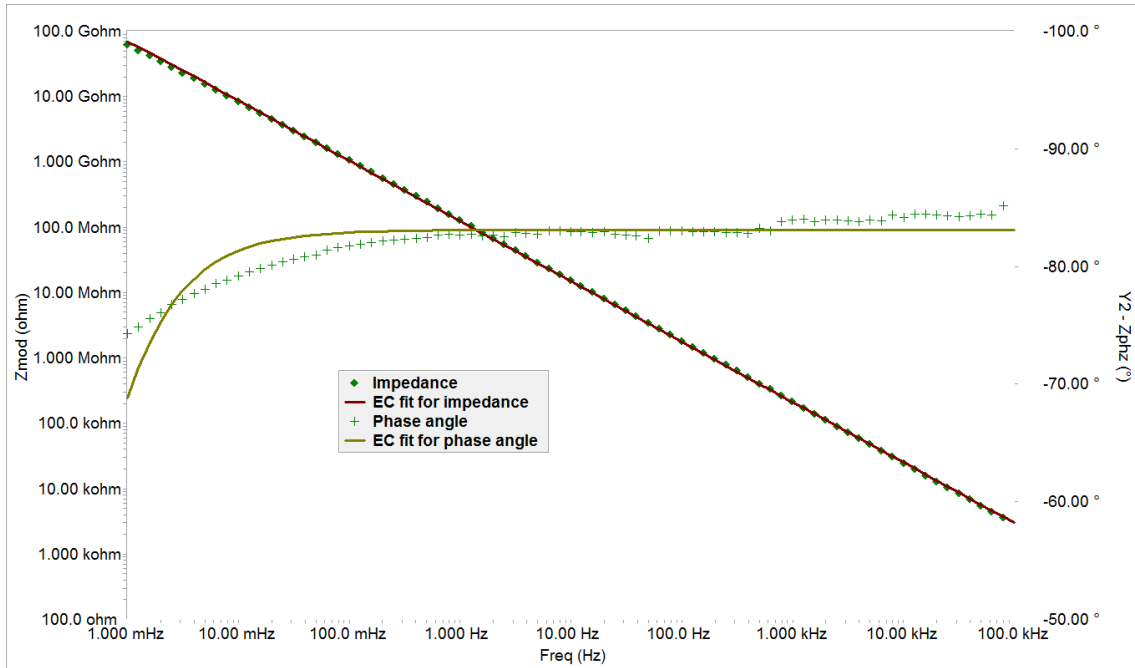


'H Alpha' Bode plot for continuous exposure over 89 days

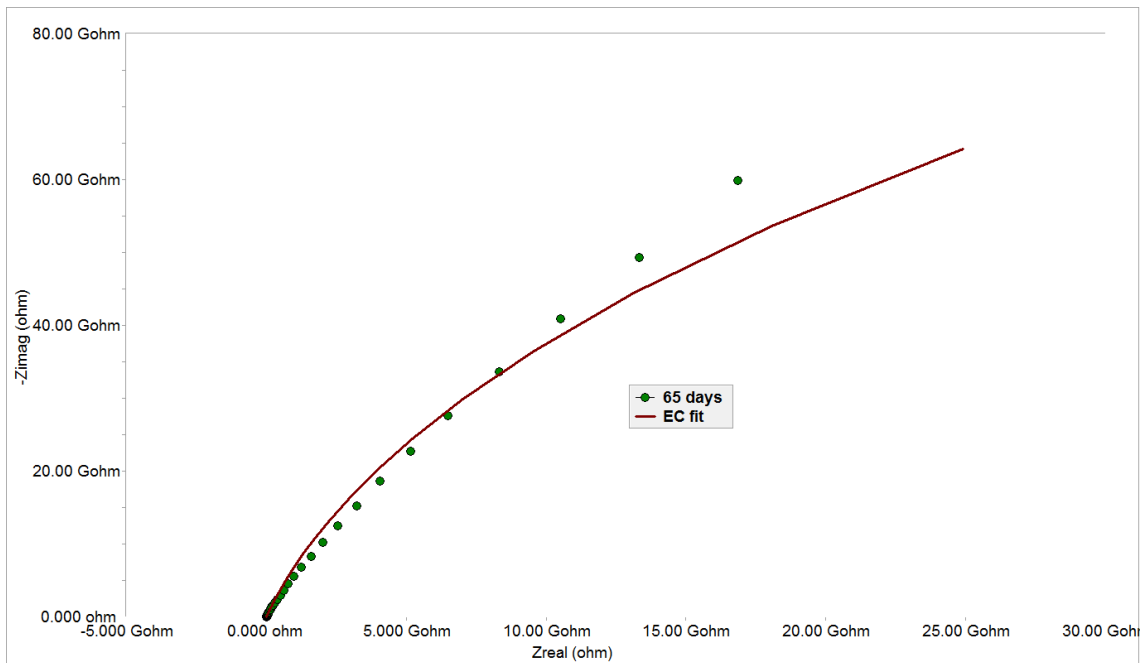


'H Alpha' Nyquist plot for continuous exposure over 89 days

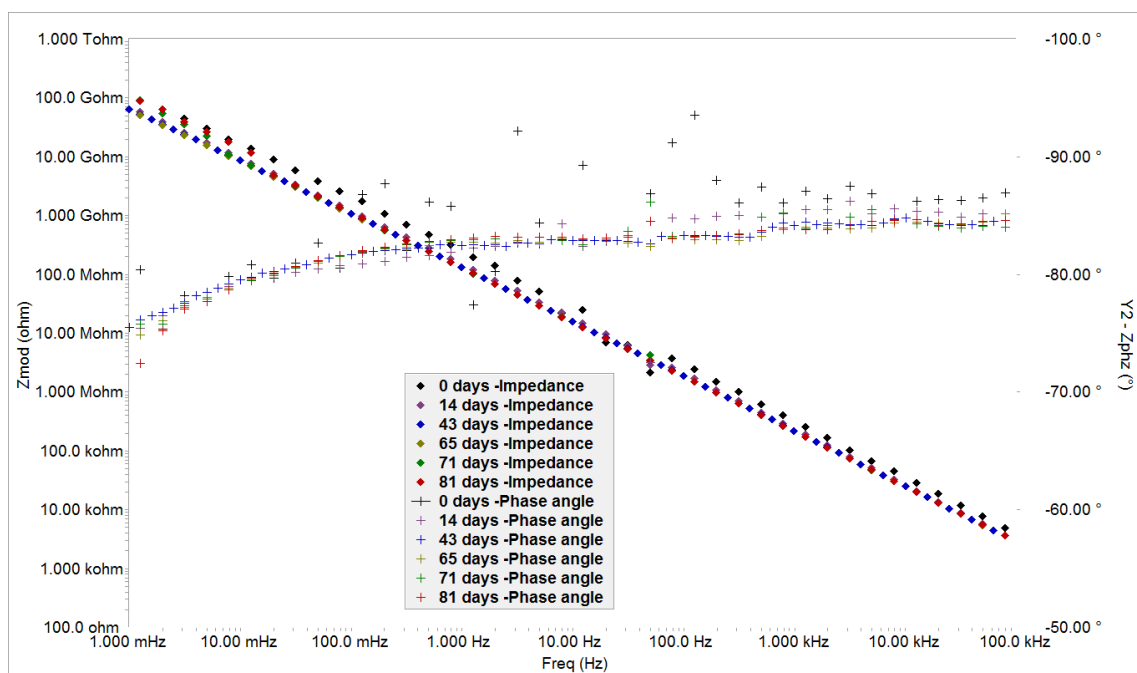
'I Alpha' EIS results



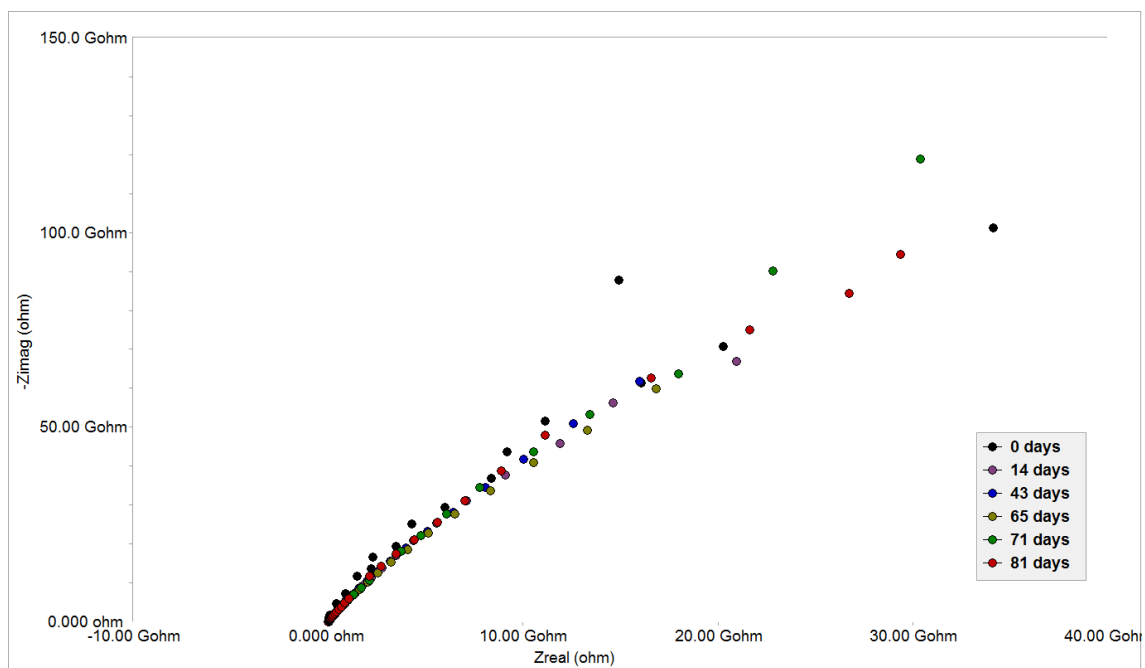
'I Alpha' Bode plot after 65 days of exposure fitted using circuit 'A'



'I Alpha' Nyquist plot after 65 days of exposure fitted using circuit 'A'

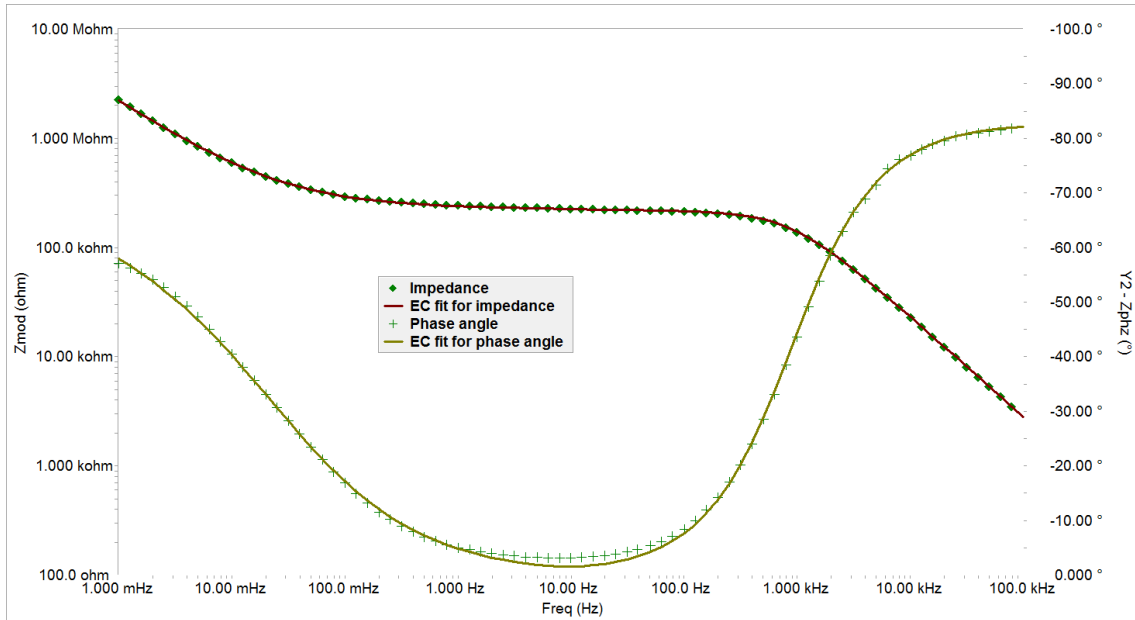


'I Alpha' Bode plot for continuous exposure over 81 days

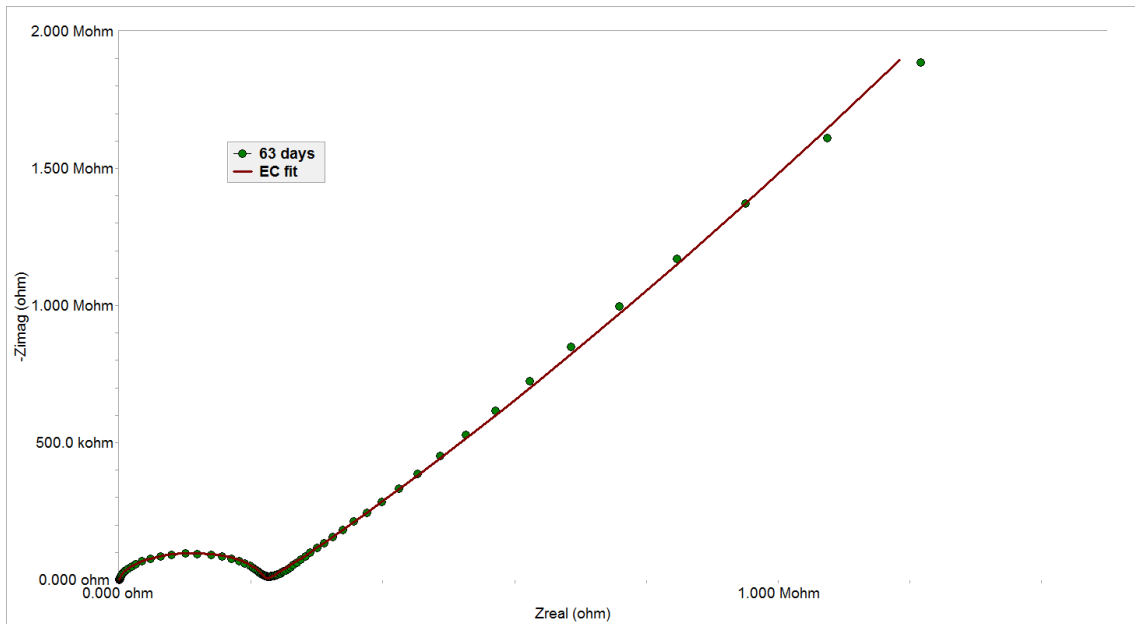


'I Alpha' Nyquist plot for continuous exposure over 81 days

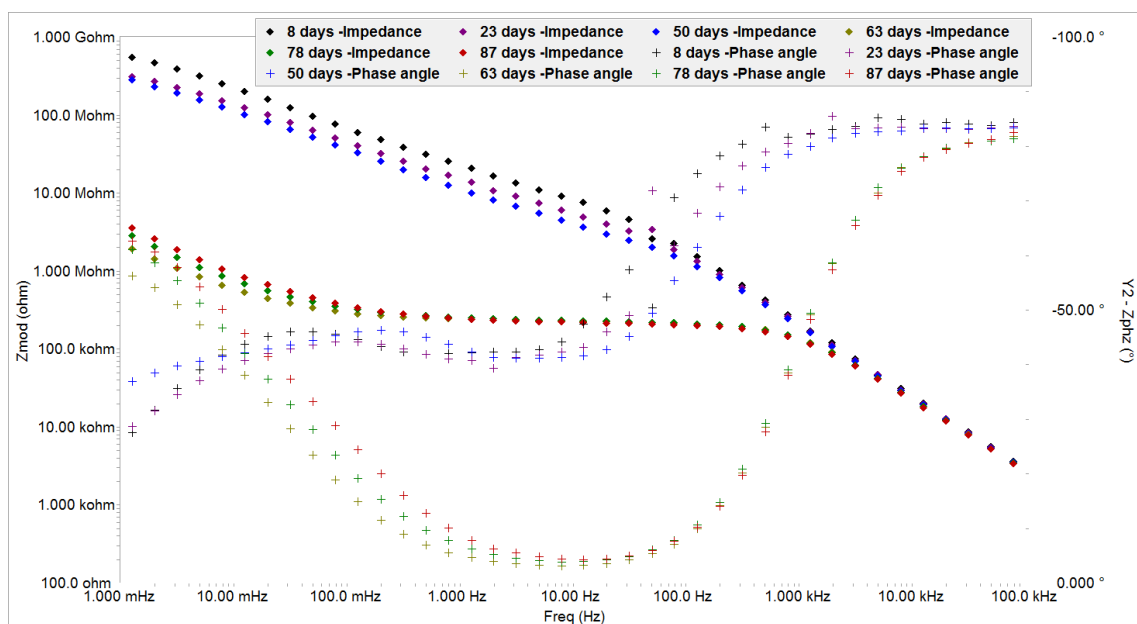
'I Beta' EIS results



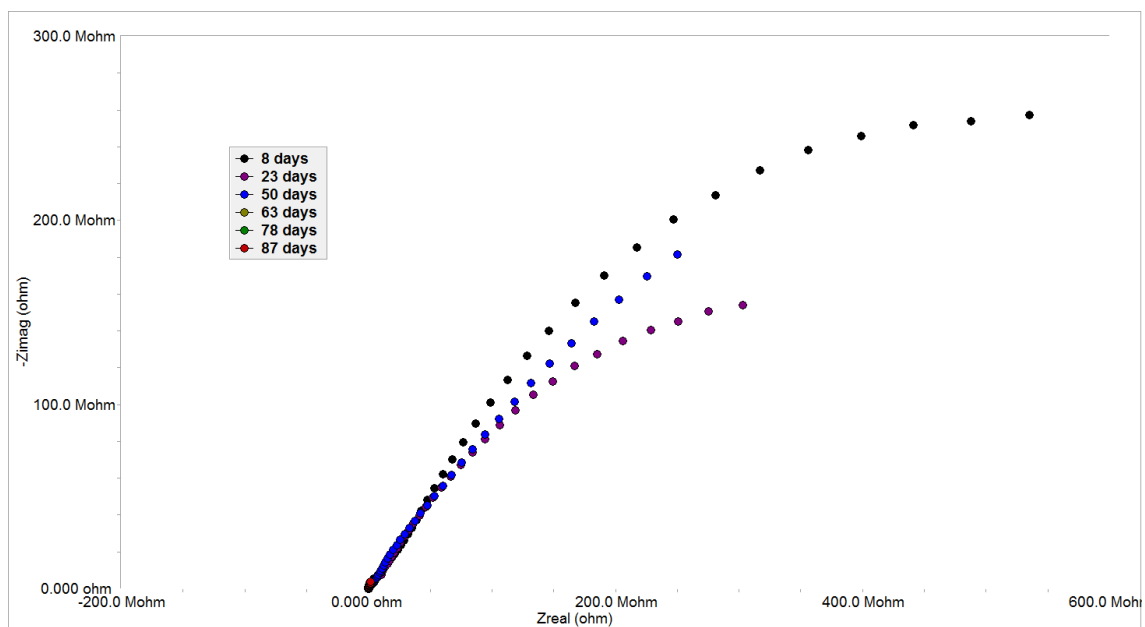
'I Beta' Bode plot after 63 days of exposure fitted using circuit 'B'



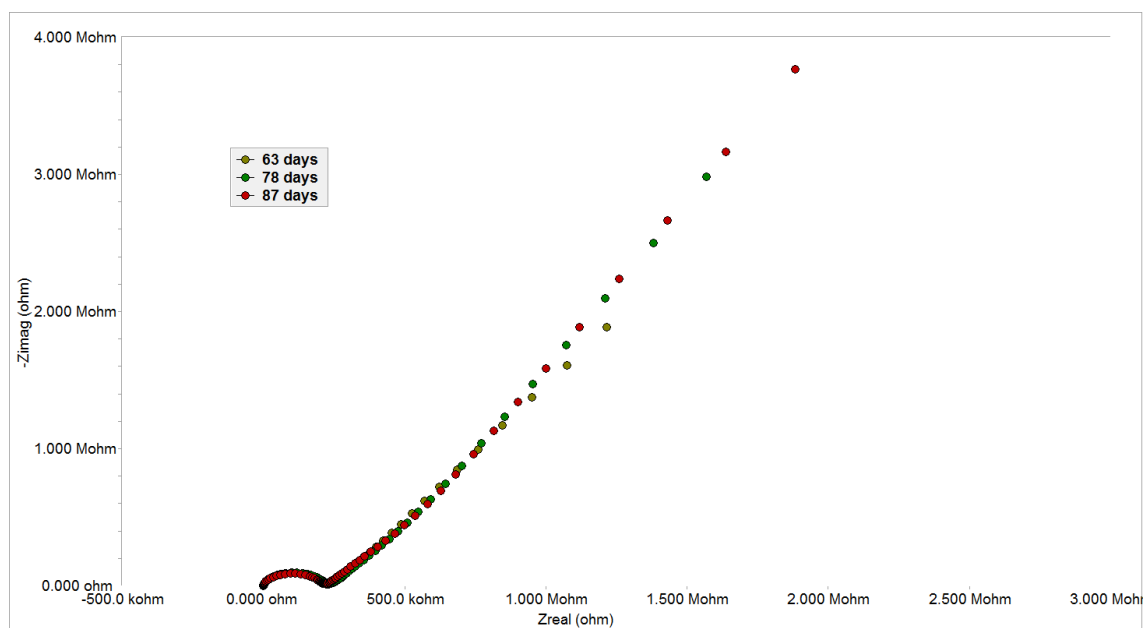
'I Beta' Nyquist plot after 63 days of exposure fitted using circuit 'B'



'I Beta' Bode plot for continuous exposure over 87 days



'I Beta' Nyquist plot for continuous exposure over 87 days



'I Beta' Nyquist plot for continuous exposure over 24 days after day 63